POLITECNICO DI TORINO

Master's Degree in Environmental and Land Engineering

Politecnico di Torino

Master's Degree Thesis

Runoff modelling using QSWAT+ to assess the contribution of piped network stormflow in the Haaganpuro semi-urban catchment

Supervisors

Prof. Pierluigi CLAPS

Prof. Teemu KOKKONEN

Candidate

Antonino MERLO

DECEMBER 2023

To the World,

May someday
the stream of life of each human being
flow into an equal channel of opportunities

Summary

Water-related problems have always represented a tough challenge for human beings throughout history. Their wide collection of issues, ranging from water quality degradation to stormwater management in urban catchments, reflects the controversial power of this fundamental resource, vital for human life and in some cases destructive if not well controlled. Especially, in a context where the climate fluctuations and the development of urban areas are increasing their impacts on both streamflow and water quality, water management solutions are acquiring much more importance day by day. In particular, the rising in the frequency of extreme rainfall events justifies the need for an improvement in the actual stormwater management systems of the cities. In this perspective, hydrological modelling assumes a relevant role since it constitutes a powerful instrument in understanding how rivers and channels act in a watershed and in simulating runoff processes, a crucial part for planning stormwater management solutions. This study focuses on the implementation of the Soil and Water Assessment Tool (SWAT) which is a continuous time, semi-distributed small watershed to river basin-scale model to simulate streamflow from the Haaganpuro catchment, an urban brook located in the city of Helsinki, Finland. The purpose of this simulation was to separate how large a share of runoff originates from areas drained with a stormwater piping system as compared to more natural park areas. The catchment delineation was performed with the support of the QGIS software, while the input data (including weather data) were uploaded through the SWAT+ Editor to allow flow simulation. The model was calibrated for the months between June-August 2017 and validated for September-November of the same year using observed daily streamflow imported on the SWAT+ Toolbox, a software mainly implemented to perform sensitivity analysis, calibration and more. The most sensitive parameters were identified through a sensitivity analysis which showed that the ones related to HRUs (Hydrologic Response Units) and soil were the most significant, calibrated manually to establish their variation range and then automatically to find their optimal value. Simulated daily surface runoff was estimated applying the Curve Number method while model performance was assessed through the Nash-Sutcliffe Efficiency (NSE) and the percent bias (PBIAS) which respectively give insights on how the model is able to

resemble measured values and how much they are under or overestimated. At first, the calibration focused only on a specific section of the Haanganpuro catchment named Lansi-Pakila, an urban neighbourhood in the North-East of the basin whose calibrated parameters are assumed to be representative of all the other built-up areas. Then, the analysis was shifted to the more natural zones with the purpose of identifying some reasonable calibration values to be compared with the urban ones. In this way, two sets of parameters were derived, one for urban areas and one for forested/park areas. These sets were then used to modify the input files of the SWAT+ Editor in order to run the final runoff simulation for the decade 2012-2022 (the study period of this thesis) and split the contribution of the two different domains to streamflow. The results were finally compared to the findings of other studies, understanding in this way their reasonability and enhancing the relevance of the SWAT model for water resources management and controls.

Table of Contents

List of Tables

List of Figures

Acronyms

SWAT
Soil and Water Assessment Tool

HRU
Hydrologic Response Unit

LSU
Landscape Unit

NSE
Nash-Sutcliffe Efficiency

PBIAS
Percent bias

MSE
Mean Squared Error

RMSE
Root Mean Square Error

SCS
Soil Conservation Service

NRCS
Natural Resources Conservation Service

SWRRB
Simulator for Water Resources in Rural Basins

SSURGO

Soil Survey Geographic Database

SMEAR

Station for Measuring Ecosystem-Atmosphere Relations

ROTO

Routing Outputs to Outlet

ARS

Agricultural Research Service

CREAMS

Chemicals, Runoff, and Erosion from Agricultural Management Systems

GLEAMS

Groundwater Loading Effects of Agricultural Management Systems

EPIC

Environmental Policy Integrated Climate

CN

Curve number

MUSLE

Modified Universal Soil Loss Equation

DEM

Digital Elevation Model

FAO

Food and Agriculture Organization of United Nations

CFSR

Climate Forecast System Reanalysis

PET

Potential Evapotranspiration

PM

Penman-Monteith

HA

Hargreaves

MRM

Muskingum Routing

VSR

Variable Storage Routing

FAST

Fourier Amplitude sensitivity analysis

RBD-FAST

Random Balance Designs Fourier Amplitude sensitivity analysis

DMIM

Delta Moment-independent Measure

DDS

Dynamically Dimensioned Search

SYKE

Finnish Environmental Institute

Chapter 1

Introduction

Water is the force that moves the whole World. It flows through each field of life, travelling from the generation of climatic phenomena to the development of plant roots, from the creation of life to the sustenance of animals and humans, from the production of adverse events to their management and control. Every human being is affected by the presence of water during a lifetime, whether in a positive or in a negative way. It symbolically represents the cradle of civilization and constitutes one of the main factors in the future preservation of the human race.
Everything comes from water and everything ends without it. The current times are putting a consistent pressure on this last topic. The constant rise in the World's average temperature, the increase in the frequency of extreme weather events, and the continuous discharge of industrial residuals in water bodies are just some examples of contributors to the acceleration of the impoverishing process that is involving this fundamental natural resource. The themes of water scarcity, water quality degradation, floods, water war are more and more mentioned nowadays, and reflect the difficulties that the countries are facing in managing these problems. The United Nations World Water Development Report 2023 points out a decline of about 20 % in the availability of water resources in the years between 2000-2018 which is determining, together with a constant spreading of freshwater pollution, the development of an endemic nature of the water stress topic [1]. Concerning this issue, the same study shows how about one third of the World's population (approximately 933 million people) lived under water stress conditions in the year 2016 [1]. Its tendency does not seem to decrease and a study conducted by He et al. (2021) projects an involvement of about one third to nearly half of the global urban population (1.7–2.4 billion people) in the water scarcity issue by 2050 [2].
Consequentially, the combination of water scarcity and rise in water demand (mainly due to the growth of population and the expansion of urban settlements), together with a much bigger seasonal variability in water availability related to climate change, is damaging water supply and is putting a greater stress on the

depletion of groundwater resources that, over the years, have been more and more exploited and subjected to pollution. In fact, water quality degradation is another rising theme, mainly due to an increasing process of urbanization, agricultural runoff and industrial chemicals release, together with emerging pollutants such as microplastics and pharmaceuticals.
From these concerns, it is clear how the need for water management solutions is assuming an increasingly important role, not only to guarantee the provision of sanitized freshwater to the people, but also to protect the fauna and the flora of water bodies. These ones usually represent elements that need to be monitored not only from a water quality point of view, but also from an extreme events point of view. In fact, over the years, the number of flooding events has significantly increased, mostly due to climate change, leading to huge impacts on infrastructures, humans and crops. This increment is strictly linked to a higher frequency in the occurrence of storm events of stronger intensity which, in turn, are related to higher atmospheric moisture content, caused by a larger evaporation empowered by an average overall increase in global temperature. Also, human-related actions such as deforestation, land use changes that are altering the drainage systems and are enlarging the extent of impermeable areas, determine the generation of larger amount of runoff and, consequentially, less water absorption, causing the development of higher water levels that are difficult to manage, especially in an urban context. From here arises the necessity of improving the existing stormwater drainage systems of the cities and to find solutions able to face the new challenges that the current tendency of water issues is posing on society.
In this perspective, hydrological modelling plays a fundamental role since it constitutes a powerful tool to manage water resources, predict the way through which they are affected by climate change, simulate water storage, water fluxes and chemicals transportation processes, quantify streamflow and runoff volumes, and create a solid base for the consequent sizing of water collection and drainage networks. The computation of these outputs is allowed by a simplified but coherent reproduction of the real world which can be achieved only through the use of real meteorological data and a model calibration to replicate reality as close as possible.
The history of hydrological modelling can be traced back to the 1850s when Mulvany (1850) pioneered a technique for calculating the time of concentration, a pivotal component of the rational method used in contemporary urban drainage design to determine peak discharge [3]. Nonetheless, the realm of hydrological modeling has undergone substantial evolution in the interim. Progress has been achieved in data acquisition and processing, conceptual and theoretical frameworks, integration with related disciplines, computational and analytical tools, and the refinement of models and their associated outcomes [3]. The beginning of computer revolution in the 1960s led to the development of numerical, statistical and stochastic hydrologic methods which, then, evolved in the distributed ones through which it was possible

to replicate hydrological phenomena at a more detailed spatial granularity [3]. Always in those years, it is allocated the birth of the Curve Number method, introduced by the Soil Conservation Service (SCS) (now known as the Natural Resources Conservation Service (NRCS)) for the estimation of runoff coming from small watersheds and widely used still nowadays [4]. The 1980s saw the birth of physically-based models, expanding, in this way, the possibilities of exploration to the simulation of the movement of water through the soil and the unsaturated zone, which then, in the 1990s, was enlarged to incorporate the analysis of the interactions between surface water and groundwater and the consideration of changes in the land use [5] [6].
Among the various hydrological models born from the collection of the efforts and the innovations briefly discussed above, there is the Soil and Water Assessment Tool (SWAT) which, developed in the early 1990s, is a process-based, continuous-time and semi-distributed river basin model designed to evaluate the impacts of land use and management decisions on water resources, sediments and non-point pollution sources in large watersheds [7]. The software was developed by the USDA Agricultural Research Service (ARS) and Texas A&M University as a results of their 30 years of research in the field of hydrological modelling, and represents a direct outgrowth of the SWRRB model (Simulator for Water Resources in Rural Basins) [8]. In the following years, the model has undergone through a series of updates which are visible in the five official versions that have been developed in the last 30 years: SWAT2000, SWAT2005, SWAT2009, SWAT2012, and SWAT+. The latter is the one implemented in this thesis and places itself as a reconstructed version of SWAT by using similar equations to estimate the various hydrological components, but presents a more flexible spatial representation of the processes and the interactions within a catchment [9].
In this study, a SWAT+ model was applied to the Haaganpuro river basin, a semi-urban catchment located in the city of Helsinki, Finland that occupies an area of about 10.8 km^2 and is famous for its trout population which places a crucial attention on its preservation and safeguard, especially considering the urban location of the river. In the most recent years, the whole country of Finland has experienced a rising trend in the development of flooding phenomena which are expected to increase even more in the next 30 years, mainly due to climate change, as reported by the Finnish Climate Change Panel [10]. These flooding events are already causing consistent losses for the Finnish government in financial terms. For example, in 2013, spring floods resulted in a total damage of 5 million euros, while, the previous year, the cost to face flood damages was around 10 million euros [11]. Focusing on the capital, Helsinki, where the studied catchment is placed, in 2023, torrential rainfall resulted in floods that affected several buildings and a metro station, leading to the accumulation of standing water in various areas of the city [12]. Even the coast of the Helsinki metropolitan area has been experiencing an

increase in the risk of flooding. According to the report of the Finnish Climate Change Panel, extreme weather events could result in an annual damage of about 4 million euros for the cities of Helsinki and Espoo and, in the absence of mitigation measures, this cost could escalate by a range of 16 to 120 percent by 2050, with the potential for even more substantial increases by 2100 [10].
However, the city of Helsinki is already taking several measures to prevent floods and minimize their impact on people and urban life. Among these, the city has developed a dedicated guide named "The instructions on Prevention and Control of Floods by the City of Helsinki", published in 2013, which clarifies how to react in the case of a flood, provides the instructions to prevent and control flooding phenomena, and suggests possible measures that citizens can take to protect their property from flooding, especially for the ones that live in the most exposed areas [13]. Furthermore, the city has formulated a climate adaptation strategy, with a special focus on addressing the issue of rainwater pooling on streets after heavy rainfall. The strategy involves a storm-water management approach that prioritizes managing water at its source, rather than redirecting it to different areas of the city [14]. This approach aims to either facilitate water absorption by the soil and vegetation or, as a minimum, reduce its flow velocity before it enters the drainage system [14]. As a part of the achievement of the purposes exposed in the strategy, the city has started to plant trees in anticipation of flood events, heatwaves, and other consequences related to the climate crisis, and is ensuring the continuous operation of its functions and services (like schools, hospitals, etc...) even during a flood situation [13] [14].
In the described perspective of dealing with the water levels generated by rainfall events in the urban areas of the capital, this thesis places itself as a contextualized study since it copes with the computation of the amount of surface runoff produced by selected precipitation events occurred in the Haaganpuro basin, which covers various urban districts of Helsinki. In fact, the objective of this analysis was to compute the surface runoff coming from different regions of the watershed in order to separate the share of runoff generated by urban areas and the one produced by more natural park areas. In this way, it was possible to evaluate the contribution of piped network stormflow in the catchment and to make a comparison with the results obtained in other studies conducted in Southern Finland or in regions with similar climate conditions, in order to assess the efficiency of the constructed SWAT model in computing runoff values. These ones were calculated for the years between 2012 and 2022, only considering the months from May to November and skipping winter months due to a lack in the observations used to calibrate the model and the consequent necessity to build a proper snow model. Specifically, the model was calibrated and validated for the period June-November 2017, after a sensitivity analysis was performed to identify the most sensitive parameters for streamflow. In fact, the two implemented observed datasets both consider streamflow and refer

to different places in the catchment. The first one concerns the urban district of Lansi-Pakila and was used for the calibration of all the urban areas in the basin since it was considered as representative of the urban flow. The second one is relative to the flow at the catchment's outlet (defined as the point through which the water, coming from all the channels and their respective regions, flows) and was used to calibrate the rest of the areas, always taking into account the urban areas calibration previously performed.
All the calibration and sensitivity analysis procedures were carried out through the use of a dedicated tool named "SWAT+ Toolbox", while the runoff simulations were performed through the SWAT+ Editor, part of the QSWAT+ software which operates through a QGIS interface on which a plugin connected to SWAT+ is added. The application of QGIS allowed to delineate the watershed and its channels, thanks to the consideration of a digital elevation model (DEM) and a outlet shapefile reporting its position, and to create the so called "Hydrological Response Units (HRUs)" that are the smallest elements of a basin through which SWAT is able to predict the loadings of water, sediments and nutrients according to similar characteristics of land use, soil and slope. These are gathered together in a single HRU and need to be provided to allow their creation.
In the following sections, all these operations will be described step by step, starting from an overview of the data used and the sources from which they were taken, going through a description of the methods used to setup the SWAT+ model (from watershed delineation to model calibration and validation) and ending with a report and a discussion of the results based on which the presented conclusions, limitations and possible improvements are elaborated.

Chapter 2

Materials

2.1 Study area

The model was set up for the Haaganpuro catchment, located in the city of Helsinki, Finland. The basin occupies an area of approximately 10.8 km^2 while its route has an extent of 11.6 km [15]. The river, whose old name was Mätäpuro, is mainly an urban stream, entirely located in the Helsinki area, which originates from the city's Central Park near Maununneva, a subdivison of the Kaarela district, flows through the residential area of Pirkkola and continues its run following the side of the Hämeenlinnanväylä (or Highway 3), the highway connecting Helsinki to Vaasa passing through Hämeenlinna and Tampere, where it is partially pipelined (for about 25 % of its length [16]) under the Metsäläntie bridge. Then the stream reappears in the area of Etelä-Haaga, finally reaching the sea in the neighbourhood of Pikku Huopalahti [17]. A side stream, named Maunulanpuro and known for carrying a more abundant water amount than the main bed, starts from Maunula Suursuo and meets the Haaganpuro stream in Pirkkola [17].
One of the most relevant aspects of the studied catchment is its trout population. Some of it tends to spend its life entirely in the river while the other is prone to migrate to the Baltic Sea based on the different survival behaviour. In both cases, a lot of attention has been reserved to this trout population, especially in the perspective of the progressive extinction of the species that is affecting the Gulf of Finland and in the context of the increasing emissions caused by the surrounding urban settlements (like sewage outflows and sludge discharges from construction and borehole sites) that are placing the need for water quality restoration techniques in order to preserve the nature of the stream, which is also home to many other water species that can be seen based on the different seasons [17] [18]. For all these reasons, in the recent years, Haaganpuro has been known as Finland's most urban trout stream and has become a hot spot for urban activism with the aim of

safeguarding and enhancing the center of Helsinki's urban nature.
As it is possible to see from figure 2.1, the catchment's elevation ranges from -3 m to 91 m with most of the higher elevation bands concentrated in the North, while the Southern part is manly composed of plain area. The map reports both the actual and the simulated borders of the basin. The latter were delineated through the QSWAT+ Editor as a first step in the model setup. Major insights about this watershed delineation phase will be given in a specific paragraph under the next chapter. For the moment, the analysed figure is used just to give an idea of its geographical location in the Helsinki area. The reasons why the SWAT generated catchment was also reported in this section is that the channels represented in the map are also obtained through the software and therefore refer to the simulated basin.

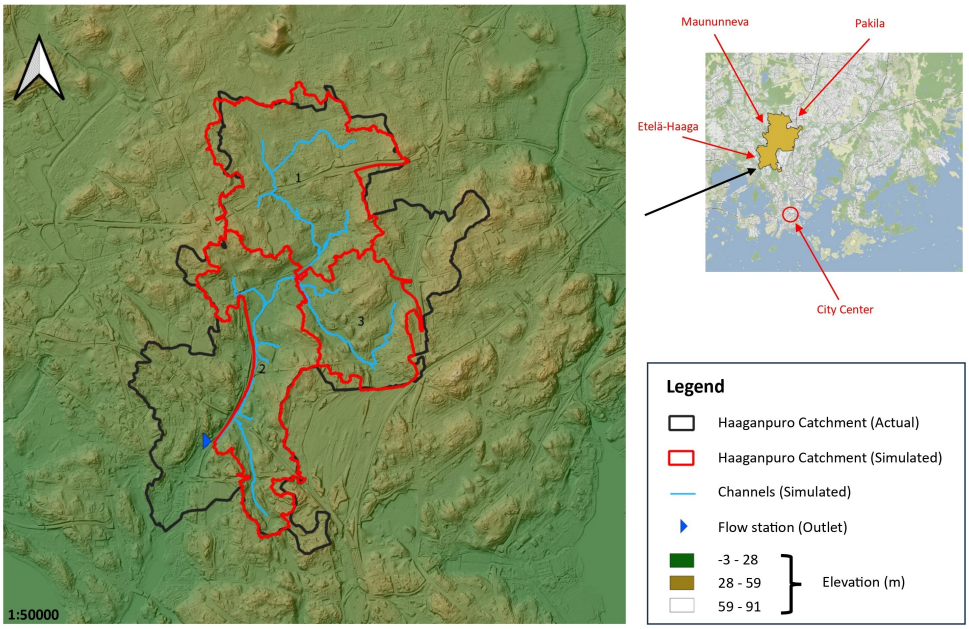

Figure 2.1: Geographical location of the Haaganpuro Catchment in the Helsinki area

As previously stated, Haaganpuro is classified as an urban catchment being its total extent completely located in the Helsinki area. Specifically, the urban areas (buildings, roads, etc..) account for 27.32 % of its land use coverage, while the natural parts (including both forests and grasslands) account for 65.87 % giving proof about how nature is a consistent part of the city territory (figure 2.2). Concerning soils, the relative map (figure 2.3) clearly shows the predominance of the infill, moraine, clay, silt and sand soil types. In particular, it is interesting to notice how moraine and infill are predominant in the North section of the basin

whereas the South is mainly constituted of bedrock and clay layers (figure 2.3). The data used to derive the land use and soil maps reported in figures 2.2 and 2.3 will be described in the next paragraph related to the description of their sources.

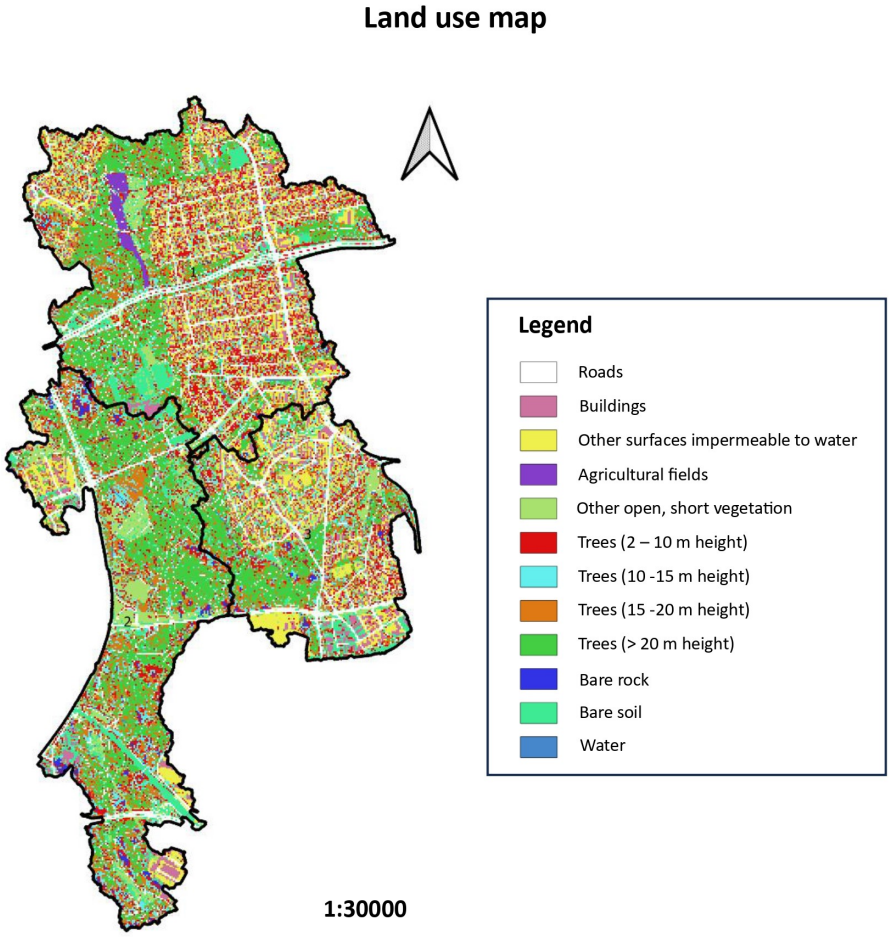

Figure 2.2: Land use map

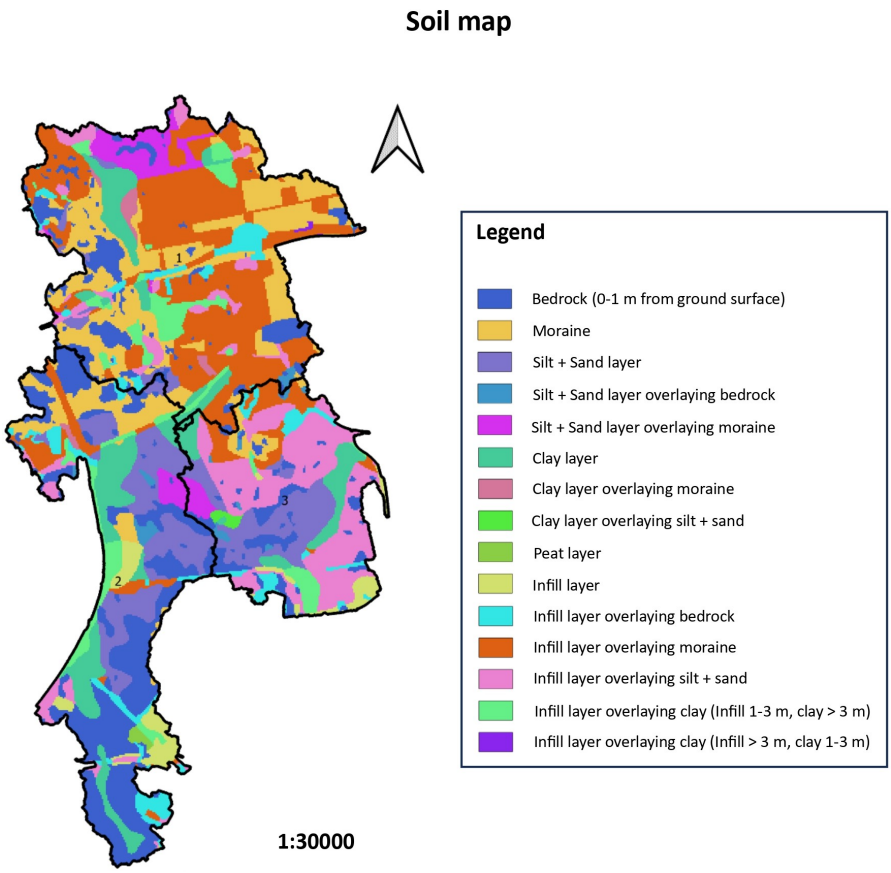

Figure 2.3: Soil map

Concerning climate, the region of the Haaganpuro basin, as well as the whole city of Helsinki, is subjected to a humid continental climate characterized by large seasonal differences, ranging from cold winters, during which the average temperature is a few degrees below 0 °C, to mild/warm summers [19]. The city receives an annual precipitation of approximately 600 to 700 millimeters (23.6 to 27.6 inches), and snow blankets the ground from December to April, with the highest peaks between late February and mid-March, when the snow cover reaches a thickness of about 20 to 25 cm (8 to 10 inches) [20]. The driest season is spring, with precipitation reaching a maximum of 100 mm over three months, while the wettest period goes from June to January, with a chance greater than 25 % to have a wet day in the considered period [19] [21]. In particular, referring to rainfall, the month with the most days of rain is October with 8.9 days on average, which is also the one with the highest rainfall amount, with an average value of 2.2 inches (approximately 56 mm) [21]. This last fact is shown in figure 2.4 which reports the cumulative precipitation recorded within a rolling 31-day window, centered on each day of the year.

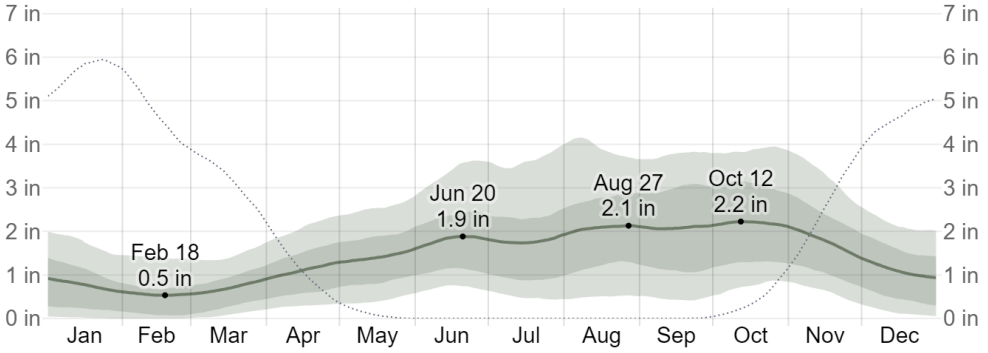

Figure 2.4: The average rainfall (solid line) accumulated over the course of a sliding 31-day period centered on the day in question, with 25th to 75th and 10th to 90th percentile bands. The thin dotted line is the corresponding average snowfall [21]

The graph gives a further confirmation of the fact that the wettest months are especially the summer and autumn ones, with the second, third and fourth highest mean rainfall amounts registered in the months of August, September and July respectively. These are also the months when thunderstorms occur most frequently in Helsinki, with a peak during summer months around July [22]. In general, in the Southern and central part of Finland, thunderstorm events occur on average 12 days during the period from May to September, with the most days concentrated in July [22].
The provision of these basic notions about climate in the analyzed region is fundamental to link the obtained runoff results to the weather data used to build the SWAT model, referring specifically to precipitation data. This connection will be better understood in the next sections, especially in the one related to the discussion of the results. For now, a general description of the climate was provided to have a clearer vision of the context in which this thesis is operating.

2.2 Data sources

The input files needed to built the SWAT model include a digital elevation model (DEM), an outlet shapefile, a land use map, a soil map, meteorological data (precipitation, air temperature, relative humidity, wind speed, solar radiation) and two observed flow datasets, one for the outlet of the catchment and one for the Lansi-Pakila urban drained area. All input files, together with their sources, are listed in table 2.1.
The digital elevation model (DEM) was derived from the website of the Finnish National Survey with a spatial resolution of 2 x 2 m. The land use map was built

starting from the coverage data provided by the SMPA 2016 Helsinki Alaluokka map by assigning to each SMPA code a SWAT land use category (table 2.2). The soil map was generated from the City of Helsinki Map Service and converted to the SWAT format by transforming each soil code in the corresponding SWAT soil name (table 2.3). These conversions to the SWAT land use and soil codes are done by means of two lookup tables, one for land use and one for soil, constructed to make the associations between the original name and the one through which SWAT recognizes the specific land use and soil considered. Their setup will be better described in the next chapter. In this section, only the SWAT codes will be reported. However, it is worth to mention that, for the conversion of the soil layers in the respective SWAT format, the SWAT names implemented and reported in table 2.3 are derived from the Soil Survey Geographic Database (SSURGO) which is basically a list of soils together with their hydraulic, geotechnical and geological properties. These data were necessary to generate the "usersoil" file through which SWAT is able to associate each original soil name to the one reported on the lookup table. In the case of land use, there was no need to have a vehicle between the model and the lookup table since the SWAT land use codes are already incorporated in the software.

Concerning weather, the dataset includes measured values for the following variables: precipitation, air temperature (max and min), relative humidity, wind speed and solar radiation. For all of them, the values are considered at a daily timestep and were provided by the Finnish Meteorological Institute. Two weather datasets were generated: the first one for the period June-November 2017 was used for the calibration of the model since the measured flow data were available only for the mentioned time interval, the second one for the period 2012-2022 considering only the months between May and November (winter months were excluded due to the lack of observed flow data that were needed for the calibration of the temperature-index snowmelt method incorporated in the QSWAT+ Editor). The data for all the variables were measured from the Kaisaniemi weather station, except for the solar radiation ones that were extracted from the Kumpula weather station. As already mentioned, the observed flow data were available only for June-November 2017 and referred to the channel that functions as the catchment's outlet and to the Pakila urban area located in the North-East of the basin. These data are also considered at a daily time step and were retrieved from the measurements performed by the Aalto University's Water and Environmental Engineering department.

Data	Source	Description
DEM	Finnish National Survey	Digital elevation model with 2 x 2 m resolution
Land use	SMPA 2016 Helsinki Alaluokka	Land use map
Soil	City of Helsinki Map Service	Soil map
Weather	Finnish Meteorological Institute	Daily data for June-November 2017, daily data for 2012-2022 covering May-November for each year
Streamflow	Aalto University: WAT department	Observed streamflow for June-November 2017 for catchment's outlet and Pakila urban drained area

Table 2.1: Model input data and their sources

SMPA code	SMPA description	SWAT code	SWAT description	(%) Basin
121	Buildings	UINS	Institutional	13.44
130	Other surfaces impermeable to water	UTRN	Transportation	13.88
211	Agricultural field	AGRL	Agricultural Land-Generic	0.26
212	Other open, short vegetation	RNGE	Range-Grasses	24.59
221	Trees (2-10 m height)	FRST	Forest-Mixed	25.37
222	Trees (10-15 m height)	FRST	Forest-Mixed	25.37
223	Trees (15-20 m height)	FRST	Forest-Mixed	25.37
224	Trees (>20 m height)	FRST	Forest-Mixed	25.37
310	Bare rock	SWRN	South Western Range + Bare Rock	20.25
410	Bare soil	SWRN	South Western Range + Bare Rock	20.25
510	Water	WATR	Water	2.21

Table 2.2: Land use categories and corresponding SWAT land use codes

Soil code	Map Service soil name	SWAT soil name	Description
2	Ka	Typic Cryochrepts	Bedrock (0-1 m from ground surface)
3	Mr	Arches	Moraine
6	S+H	Pinal	Silt + Sand layer
7	s+h/Ka	Horsley	Silt + Sand layer overlaying bedrock
8	s+h/Mr	Fluvaquents	Silt + Sand layer overlaying moraine
11	Sa	Campanile	Clay layer
13	sa/Mr	Arents	Clay layer overlaying moraine
14	sa/S+H	Oktibbeha	Clay layer overlaying silt + sand
20	Tv	Winginaw	Peat layer
24	Tä	Udorthents	Infill layer
25	tä/Ka	Quiensabe	Infill layer overlaying bedrock
26	tä/Mr	Udalfic Arents	Infill layer overlaying moraine
27	tä/S+H	Roxal	Infill layer overlaying silt + sand
28	tä/Sa	Davidson	Infill layer overlaying clay (Infill 1-3 m, clay > 3 m)
29	Tä/sa	Yadkin	Infill layer overlaying clay (Infill > 3 m, clay 1-3 m)

Table 2.3: Soil layers and corresponding SWAT names

2.3 Weather stations

Before going directly through the Methods section dedicated to the model setup and the calibration procedures, it is better to give some insights about the two weather stations (Kaisaniemi and Kumpula) from which the implemented meteorological data were derived.

2.3.1 Kaisaniemi

The Kaisaniemi weather station (figure 2.5), with an elevation of 4 m above sea level, is the official meteorological station of the city of Helsinki and is located in the university's botanical garden in the Kaisaniemi park (60°10´N, 24°56´E) [23]. It is the oldest Finnish weather observation station as it was founded in 1844 and has been in place since 1969 after being relocated in 1958 [23]. The observatory buildings were completed in 1841 in the former Kaisaniemi park on the site of Säätalo, next to the current Kaisaniemi school. According to the original plan developed by the architect Carl Ludvig Engel (known for being the designer of the Helsinki Cathedral and the buildings surrounding the Senate Square), the observatory was supposed to be built in Katajanokka but its location was moved and the construction drawings were stripped down to a simpler form after Engel's death (1840) [24]. Regular observations started in 1844 and was initially conceived as a magnetic-meteorological measurement station. Towards the end of the 19th century magnetic measurements were left out, enhancing the focus in the direction of meteorology [25]. The weather station was moved to the university's botanical garden in 1962 and to its current location in 1969 and has not been moved since that time. It was automated in 2001 and manual measurements officially ended in 2008 [24].
Concerning its functioning, the weather automat continuously collects values of temperature, relative humidity, precipitation, visibility, cloud cover and air pressure. In particular, temperature is measured through an automatic device (figure 2.7a) with which the values are obtained starting from changes in the electrical resistance of the platinum resistor (Pt-100). The sensor is inside a cylindrical radiation shield. It also contains an electronic humidity sensor (HMP35). According to international observation standards, the sensors have a distance of 2 m from the ground. [24]
An automatic rain gauge VRG101 (figure 2.7b) is used to collect precipitation. Rainfall values are retrieved from the results of weighing the water accumulated in the tank (30 l) which must be emptied twice a year. Freezing of the rain tank is prevented with environmentally non-toxic chemicals and electric heating. There is also a slatted wind shield around the tank, which reduces the turbulence of the wind around the collection container, allowing a more precise collection of the falling material. During winter, the station is also able to measure snow depth by

Figure 2.5: General overview of the Kaisaniemi weather station [24]

means of an automatic gauge (figure 2.7c) which is able to measure the distance from the top surface of the snow cover accumulating in the sanded area to an ultrasonic sensor, located at the end of the slanting boom, based on the snow travel time. The device is ponded to prevent splitting and has a measurement accuracy of $\pm$ 1 cm. [24]
For cloud altitude calculation, a cloud altimeter is adopted (figure 2.7d). The device sends laser beam pulses (with wavelength of 905 nm) invisible to the human eye up into the clouds, from which they are reflected back to the device. Based on the passing time, it is possible to calculate the heights of the clouds. The changes in cloud reflections from hour to hour can also be used to estimate the total cloudiness of the sky. The measurement range is 0 - 7.5 km. The station is also equipped with a prevailing weather measurement device (figure 2.7e) able to estimate the amount of moisture and the other components blocking visibility by measuring the scattering of pulses of infrared light. Additional information are given about the type of snow and the rainfall intensity. [24]
Wind speed and direction are always derived from the anemometer located on the roof of Säätalo (figure 2.6). The device is composed of a sensor that produces measurements based on the folding of tubes as a reaction to the transition of ultrasound signal transmitted in pairs. About the time the sound travels from one tube to another, wind direction and speed can be calculated. [24]

The weather information obtained through the analysed devices is then transferred via modem in real time to the weather database of the Finnish Meteorological Institute where it is delivered to the meteorologists, to the internet and for international distribution. The modem consists of a data collection, processing and transmitter unit (figure 2.7f) which transmits data via a GSM phone connection. Inside the protective cabinet of the device there is a pressure sensor for automatic measurement of air pressure [24].

Figure 2.6: Traditional (left) and modern (right) anemometer. The latter is the one used in the Kaisaniemi weather station [24]

(a) *Temperature measuring device*

(b) *Rain gauge*

(c) *Snow depth gauge*

(d) *Cloud altimeter*

(e) *Prevailing weather measuring device*

(f) *Data collection, processing and transmitter unit*

Figure 2.7: Measurement devices of the Kaisaniemi weather station [24]

2.3.2 Kumpula

The Kumpula meteorological measurement site is known for being the settlement of one of the SMEAR III towers located in the city of Helsinki, part of the Station for Measuring Ecosystem-Atmosphere Relations (SMEAR) network of research stations in Northern Europe. The Kumpula SMEAR III tower is placed near the University of Helsinki campus while the other is on the roof of the University's Physicum Building. The operations at the SMEAR III station of Helsinki started in autumn 2004 [26] with the objective to expand the atmospheric measurements to urban areas where the human impacts on measurements are meaningful. Therefore, the station was conceived as an extension to the other SMEAR stations that were already functioning in Finland at that time (figure 2.8a): the SMEAR I located in in Värriö (67°46´N, 29°36´E), Eastern Lapland [27], and the SMEAR II located in Scots pine forest near Hyytiälä Forestry field station in Southern Finland (61°51´N, 24°17´E) [28].

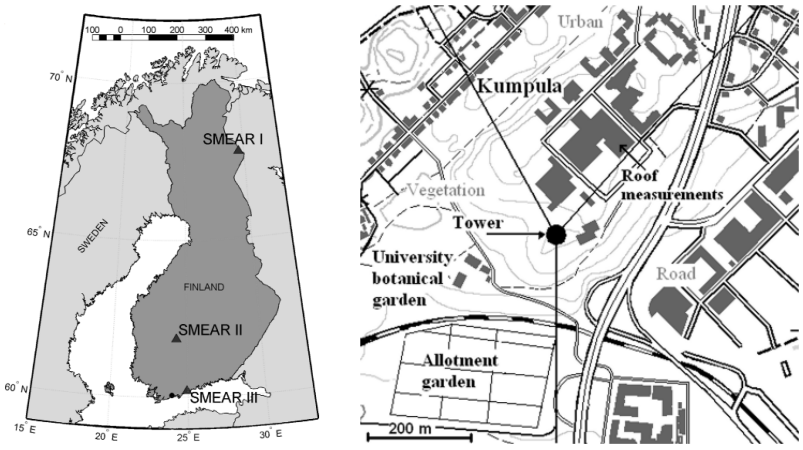

(a) *Location of the SMEAR stations in Finland*

(b) *Schematic map of the Kumpula site*

Figure 2.8: Finnish SMEAR network and Kumpula SMEAR III station [26]

In this thesis, the focus is reserved only to the Kumpula SMEAR III station (figure 2.8b) since it represents the source of the implemented solar radiation data, as stated in paragraph 2.2. The station is run by the Finnish Meteorological Institute and the Departments of Physical Sciences, Chemistry and Forest Ecology of the University of Helsinki and the site has a distance of about 5 km North-East from the city center [29]. The micrometeorological measurements are carried out through a 31 m high triangular lattice tower (figure 2.9) placed on a rocky hill, 26 m above sea level (60°12´N, 24°58´E) which is used to collect data related to solar radiation, vertical profiles of temperature and wind, turbulent fluxes of water, heat,

momentum, carbon dioxide, implementing the eddy covariance technique on the top of the tower near which it is also located an air-conditioned measurement container, including a variety of instruments for aerosol particle and gas concentration [26] [29]. In the site, a weather station is also present on the top of a University of Helsinki building at a height of 50 meters. The surrounding area mainly consists of buildings, roads, parking lots, forests and low vegetation [29]. Nearby, it is located the building of the Finnish Meteorological Institute.
Concerning the instruments used for the measurement of turbulent fluxes, the eddy covariance setup includes an ultrasonic anemometer which measures all three wind components and sonic temperature and whose data logger is connected to an open path infrared gas analyzer to measure carbon dioxide and water vapour mixing ratios, allowing in this way synchronization and the storage of raw data for the calculation of turbulent fluxes [26]. Measurement frequency of the EC measurements is 10 Hz [29]. Since May 2005, the Kumpula tower is also equipped with a PT-100 Platinum Resistance Thermometer for air temperature measurement, while total solar radiation and PAR (photosynthetically active radiation) are detected with a net radiometer and photodiode sensor (CNR1 + PAR lite), respectively, starting from July 2005 [26]. All these devices have a time resolution of one minute. Air pressure and relative humidity are measured with a barometer and platinum resistance thermometer and thin film polymer sensor respectively, both with a time resolution of four minutes [26].

Figure 2.9: Measurement tower of the Kumpula station [30]

Chapter 3

Methods

3.1 Soil and Water Assessment Tool (SWAT)

The Soil and Water Assessment Tool (SWAT) is a process-based, continuous-time and semi-distributed river basin model designed to evaluate the impacts of land use and management decisions on water resources, sediments and non-point pollution sources in large watersheds [7]. It regularly operates on a daily time step and is mainly used to perform continuous simulations over a long time period. The first version of SWAT was released in the 1990s and it was conceived as a direct outgrowth of the SWRRB model (Simulator for Water Resources in Rural Basins), following its combination with the ROTO model (Routing Outputs to Outlet) which was developed to overcome the limitation related to the SWRRB model regarding the subdivision of a watershed in a maximum of ten subbasins and the fact that the model routed water and sediment transported out of these subbasins directly to the catchment outlet [31]. In particular, the ROTO model overcame the subbasin limitation by linking multiple SWRRB runs together and provided a reach routing approach that, even it was effective, suffered the need for a large computer storage related to the size of the input and output of multiple SWRRB files and the necessity to perform each SWRRB run independently before uploading the files on the ROTO model [32]. This is the main reason why the two models were merged together, giving birth to the first version of SWAT (SWAT94.2) which maintained all the features that made SWRRB a valuable model while allowing the simulation of more extended areas.
The development of SWAT is a continuation of USDA Agricultural Research Service (ARS) modeling experience that covers a period of over 30 years. The model includes the contribution of several ARS models as it is shown in figure 3.1:

- The Chemicals, Runoff, and Erosion from Agricultural Management Systems (CREAMS), the Groundwater Loading Effects of Agricultural Management

Systems (GLEAMS) and the Environmental Policy Integrated Climate model (EPIC) which allowed the incorporation of components such as hydrology, pesticide transport and crop growth [33] [34] [35] [36];

- Routing components (including reservoir, pond, wetland, point source, and septic tank effects), improved sediment routing and submodels and in-stream kinetics provided by the QUAL2E model [37] [38];
- the CFARM model for the development of a carbon cycling routine, the Green-Ampt infiltration method and other alternative hydrological submodels and enhanced management modules related to expanded irrigation options, tile drainage, representation of grassed waterways and filter strip [37] [39] [40].

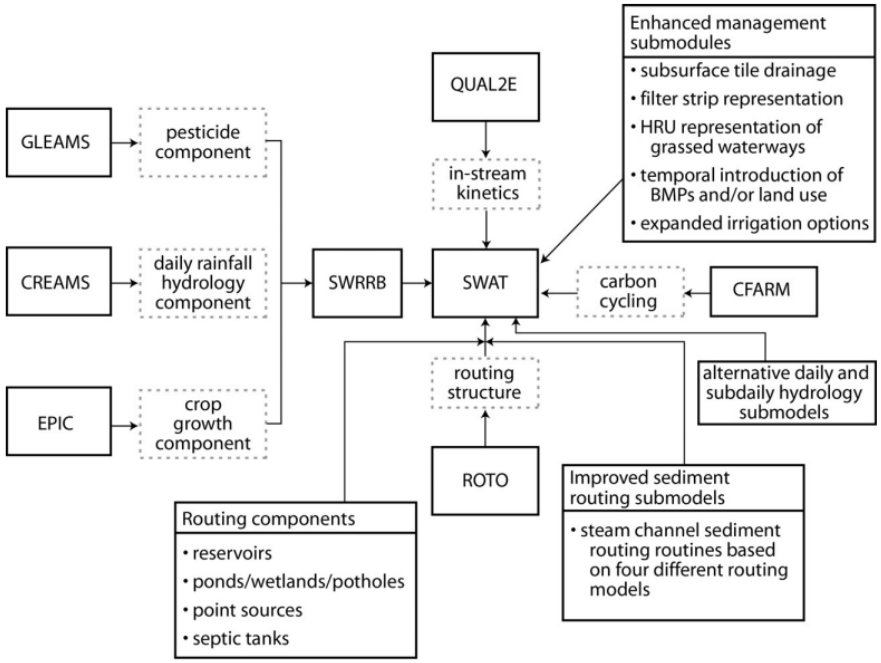

Figure 3.1: Development of SWAT and incorporated models [7]

The peculiarity of SWAT is that it allows the simulation of a large number of physical processes in a catchment based on some major model components such as temperature, hydrology, weather, land management, soil, plant growth, nutrients, bacteria, pesticides and pathogens. In SWAT, a river basin can be subdivided according to two approaches:

- Into different subbasins, which are then subdivided into hydrologic response units (HRUs) which are the smallest spatial units of the model where response

of similar land use, soil and slope within a subbasin are lumped together based on user-predefined thresholds [41].

- Into only subbasins distinguished by dominant characteristics related to soil, land use and management [7].

The driving force that controls all the simulated processes is the water balance since it affects plant growth and all the movements of nutrients, pesticides, pathogens and sediments. Concerning hydrology, its simulation is separated in the land phase, which defines the water amount and the loadings of nutrients, sediments, pesticides to the main channel in each subwatershed, and in the routing phase, which refers to the movement of water, sediments, etc.. through the channel network of the catchment to the outlet [42]. The simulated hydrologic cycle (figure 3.2) must accurately reproduce what really happens in the watershed in order to validly predict the movement of each model component.

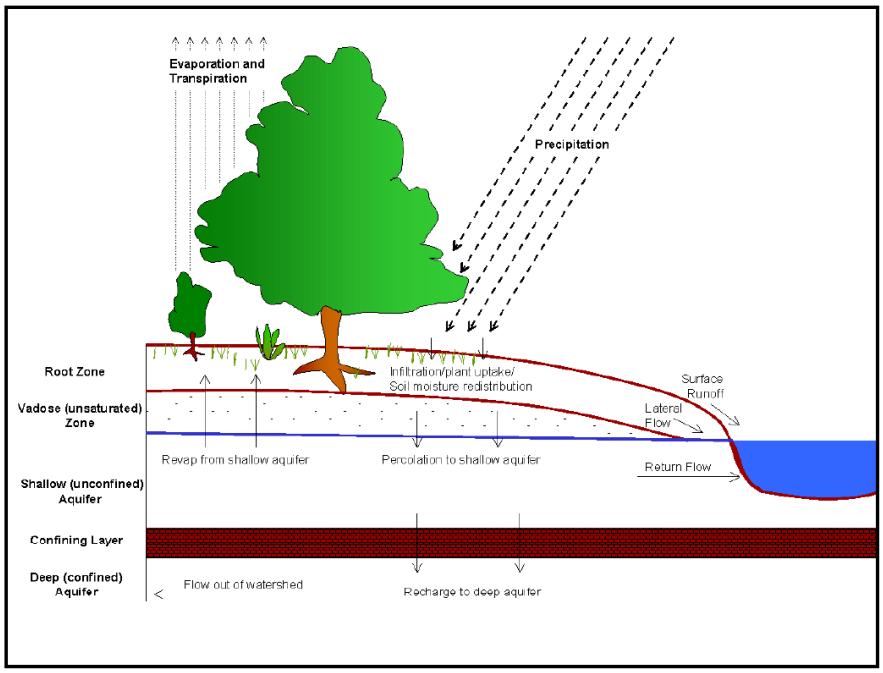

Figure 3.2: Overview of the simulated hydrologic cycle [32]

SWAT is able to replicate the hydrologic cycle by using the water balance equation:

$$SW_t = SW_0 + \sum_{i=1}^{t} (R_{day} - Q_{surf} - E_a - w_{seep} - Q_{gw}) \tag{3.1}$$

where SW_t and SW_0 are the final and initial soil moisture content (mm H_2O), t is the time in days, R_{day} is the precipitation amount on day i (mm H_2O), Q_{surf}

is the amount of surface runoff on day i (mm H_2O), E_a is the contribution of evapotranspiration on day i (mm H_2O), w_{seep} is the water amount entering the vadose zone from the soil profile on day i (mm H_2O), and Q_{gw} is the amount of return flow on day i (mm H_2O) [32]. In this perspective, the subdivision of the catchment in subwatersheds helps to enhance accuracy and to describe the water balance in a better way since the mentioned subdivision allows to simulate differences in evapotranspiration for different crops and soils and to predict runoff for each HRUs independently which is then routed to calculate the total runoff at the catchment outlet.
Figure 3.3 presents a summary of all the processes involved in the land phase of the hydrologic cycle. A more detailed description of all the processes and the relative inputs is given in the SWAT Theoretical Documentation. However, in order to enable a better understanding of how SWAT works, a brief description of some key points related to the land phase will be provided.

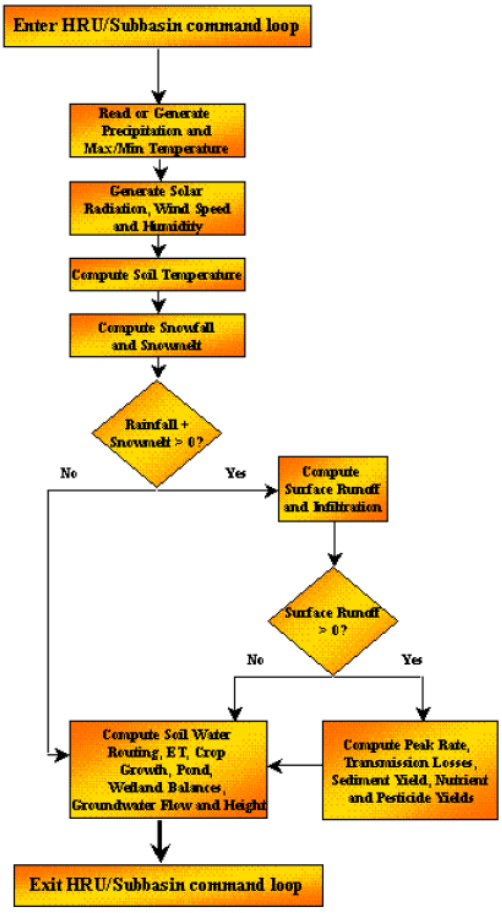

Figure 3.3: Sequence of processes used in the land phase [32]

Climate is one of the main drivers of the hydrologic cycle since it provides moisture and energy inputs that play a fundamental role in its control. Among the weather variables needed to build a functioning SWAT model there are: maximum and minimum air temperature, daily precipitation, relative humidity, wind speed and solar radiation [32]. Their values can be derived from collections of measured datasets or can be generated during the simulation (in the case of this study, weather data were provided by the Finnish Meteorological Institute, as said in the previous chapter dedicated to the materials used in this thesis). Snow is calculated when temperatures drop below freezing and soil temperature is considered due to its influence on both water movement and the decay rate of residue within the soil [7].
As rainfall comes down, it can be intercepted by the vegetation cover or go directly to the soil surface. In this last case, water can infiltrate into the soil layers or flow over the soil surface as runoff which determines a short-term stream response and is subjected to a fast movement towards a channel. Instead, the amount of water penetrated into the soil can be stored in it and later evapotranspired, or it can find a way back to the surface-water system thanks to some potential underground pathways reported in figure 3.4.

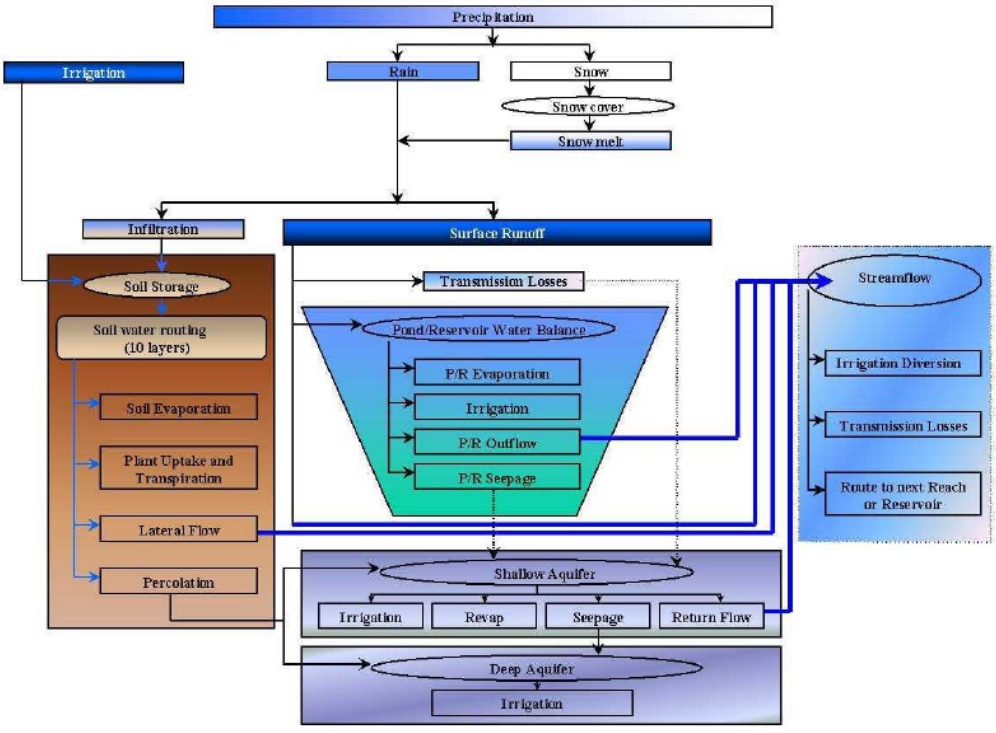

Figure 3.4: Pathways available for water movement in SWAT [32]

Specifically, the hydrologic processes that govern these paths are canopy storage, infiltration, redistribution, evapotranspiration, lateral subsurface flow, surface runoff, ponds, tributary channels and return flow. Focusing on surface runoff, which is the main output of the model analysed in this thesis, SWAT outputs surface runoff volumes and peak runoff rates for each HRUs [32]. The first output is simulated according to two approaches:

- The Curve Number Method
- The Green and Ampt Infiltration Method

The first one was developed by USDA Natural Resources Conservation Service and is based on the use of the curve number (CN), an empirical parameter derived from the analyisis of runoff coming from small catchments and hillslope plots monitored by the USDA, which is implemented to efficiently predict the amount of runoff caused by a precipitation event in a specific area based on its land use, hydrologic soil group, treatment and hydrologic condition [43]. The CN is characterized by a non-linear variation with the soil moisture and can assume values between 30 and 100 [32]. Lower values stand for lower runoff potential (the soil is more permeable) while higher values are prone to increase runoff potential. It is used to define the potential maximum soil moisture retention after runoff begins (S) through the following equation:

$$S = \frac{1000}{CN} - 10 \tag{3.2}$$

which then it is used in the runoff equation:

$$Q = \begin{cases} 0 & \text{for } P \leq I_a \\ \dfrac{(P - I_a)^2}{P - I_a + S} & \text{for } P > I_a \end{cases} \tag{3.3}$$

where Q is runoff, P is precipitation and I_a is the initial abstraction or the amount of water before runoff (e.g. infiltration) [43].
To the estimation of surface runoff, it is mainly related the main difference between the daily and sub-daily simulation in SWAT. In fact, in case of a model operating at a daily time step, the Curve Number Method is used [44], while for a sub-daily time step, the Green and Ampt Infiltration Method is adopted [45]. The latter is a physically based model that estimates infiltration as a function of effective hydraulic conductivity and the wetting front matric potential, converting in surface runoff the share of water amount that does not infiltrate [32]. SWAT is also provided with a function that allows runoff estimation from frozen soils (temperature below 0 °C) by determining an increase in runoff in the considered case. In this thesis, the simulations are performed at a daily time step, so from now on, every runoff

calculations will be executed by implementing the Curve Number Method.
Concerning peak runoff rate, estimations are done by means of a modified rational method which is based on the assumption that if there is an instantaneous beginning and an indefinite continuation of a precipitation event, the level of runoff will continue to rise until the so called "time of concentration" t_c which represents the time when the entire subbasin contributes to the flow at the outlet. The peak runoff rate is then calculated considering the daily surface runoff volume, the portion of rainfall collected in a subbasin, and its time of concentration that is predicted by using the Manning's formula studying both overland and channel flow [32].
In order to evaluate transpiration, removal of water and nutrients from the root zone and production of biomass, SWAT implements a single plant growth model to simulate all types of land cover and to define the separation limit between annual and perennial plant [7]. Additionally, SWAT utilizes the Modified Universal Soil Loss Equation (MUSLE) to estimate the sediment load from the landscape [46], simulates the transport and alteration of various types of nitrogen, phosphorus, pesticides, and sediment within the watershed and allows the users to specify the implementation of management practices in each HRU [32].
Once all the loadings of water, nutrients, pesticides and sediment to the main channel are determined in the land phase, the simulation proceeds with the routing phase during which the mentioned loadings are routed through the stream network of the basin by using a computational setting similar to that of HYMO [47]. The transformation of chemicals is also modelled to keep track of mass flow in the stream. A summary of all the routing phase processes performed by SWAT is reported in figure 3.5. Particularly, always considering the purpose of this study (and so by focusing on water), it is important to highlight that during the movement of water downstream, different types of loss may occur. For example, a potential loss can be due to evaporation and transmission through the channel bed or can be related to the removal of water for agricultural purposes [32]. Additional water amount can come from rainfall directly into the channel or from point sources discharges. Anyway, flow is usually routed using a variable storage coefficient method (the one implemented in this thesis) developed by Williams (1969) or the Muskingum routing method.
For more detailed information about SWAT model components, hydrologic processes, model equations, etc... it is suggested to take a look at the SWAT Theoretical Documentation. In this paragraph, only a brief summary of the theory behind the model, with a specific focus on the aspects that mostly interest this study, was given in order to have an idea about how SWAT operates, what led to its development and which are the simulated processes that affect the model outputs.

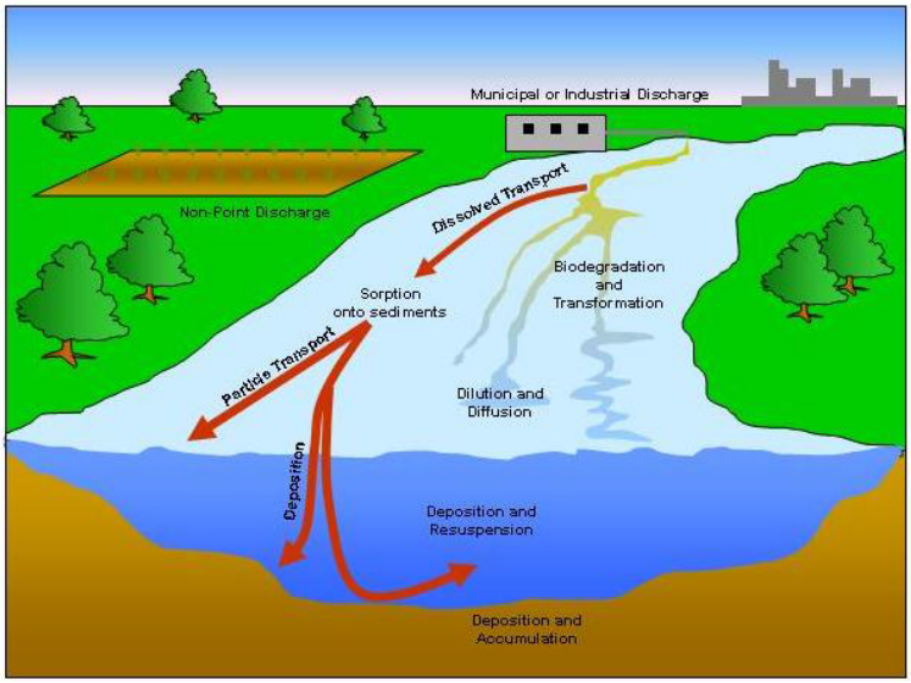

Figure 3.5: In-stream processes modelled by SWAT [32]

3.2 Model setup

This study implements version 2.1.4 of SWAT+ Editor incorporated in QSWAT+ version 2.3.0, a QGIS interface for SWAT+ used for setting up the analysed watershed. To access the SWAT+ Editor through QGIS, a QSWAT+ plugin was added to the interface which then was used for the setup and parameterization of the model. SWAT+ is a completely restructured version of SWAT, which uses similar equation for the estimation of surface runoff, infiltration, evapotranspiration, routing, plant growth, etc... but presents more benefits mainly related to a more flexible spatial representation of the processes and the interactions within a catchment [9] [48]. The need for a revised version of the SWAT model arose from the limitations revealed through its use over the years, which led to numerous additions and modifications in order to facilitate model maintenance, future code modifications and integration of new science [49]. Among the various features added, one in particular is worth of mention: the division of subbasins in "landscape units (LSUs)" [50]. A landscape unit is defined as a collection of HRUs which can be identified as a subbasin, a flood plain or a upland unit, or it could be a grid cell with multiple HRUs [51]. LSUs are not routed but are only used for output, providing simulation results for HRUs, LSUs and the basin. For their definition, two types of files are required: the elements file, that specify the share of each

HRUs within a landscape unit or a basin, and the define file, which assigns each HRUs to a specific LSU [51]. In the context of this thesis, the addition of the LSUs feature played an important role in the extrapolation of the runoff values for urban and forested areas, since the distinction between the two was made based on how large the share of urban and rural HRUs in each LSUs was, as will be better explained later.
In order to really understand how those runoff values were simulated by SWAT, before getting to the results, it is useful to go through the various steps that led to the setup of the model for the Haaganpuro catchment. These include: watershed delineation, HRUs creation and run of the SWAT+ Editor.

3.2.1 Watershed delineation

QSWAT+ performs an automatic watershed delineation which represents the first step in the model setup. The procedure starts with the loading of the DEM file through the QSWAT+ plugin. The digital elevation model is a GeoTiff file with a spatial resolution of 2 x 2 m, based on the European Terrestrial Reference System 1989 ensemble (EPSG:6258) with an accuracy of 0.1 m maximum. The interface that allows the selection of the DEM and reports the other options required in the catchment delineation is shown in figure 3.6.
For channel creation, in this case, the option "burn in existing network" was not set due to the absence of an existing stream network shapefile. Sometimes this option can be functional in order to have a reference for the selection of the channel and stream thresholds, which are normally assigned by default depending on the total area of the DEM. However, since a stream file was not provided (as previously mentioned), the threshold default values were implemented. These thresholds identifies the number of cells or the area required to form a channel or a stream. In fact, a cell will become part of a channel or stream if it receives a minimum number of cells flowing into it, reaching the threshold [49]. The main difference between channels and streams in SWAT is that the latter are sections of the stream network located between significant points such as stream sources and junctions, water gauges, monitoring points, catchment inlets and outlets, whereas channels represent narrower subdivisions and extensions of stream reaches, enabling an accurate position of the watershed components that will constitute the SWAT+ model such as HRUs, LSUs, reservoirs, ponds and point sources [49].
Concerning inlets and outlets, a shapefile containing a main outlet for the Haaganpuro catchment is provided. This outlet coincides with the basin's flow station and is automatically added to the stream network. Other inlets/outlets options refer to the possibility of insert more points in case of multiple inlets/outlets files available, like the "draw inlets/outlets" function (which allows a manual placement of the points on the stream network) and the "select inlets/outlets" option (which enables

to choose just a bunch of points among the available ones). In this study, those options were not used due to the presence of only one outlet file.

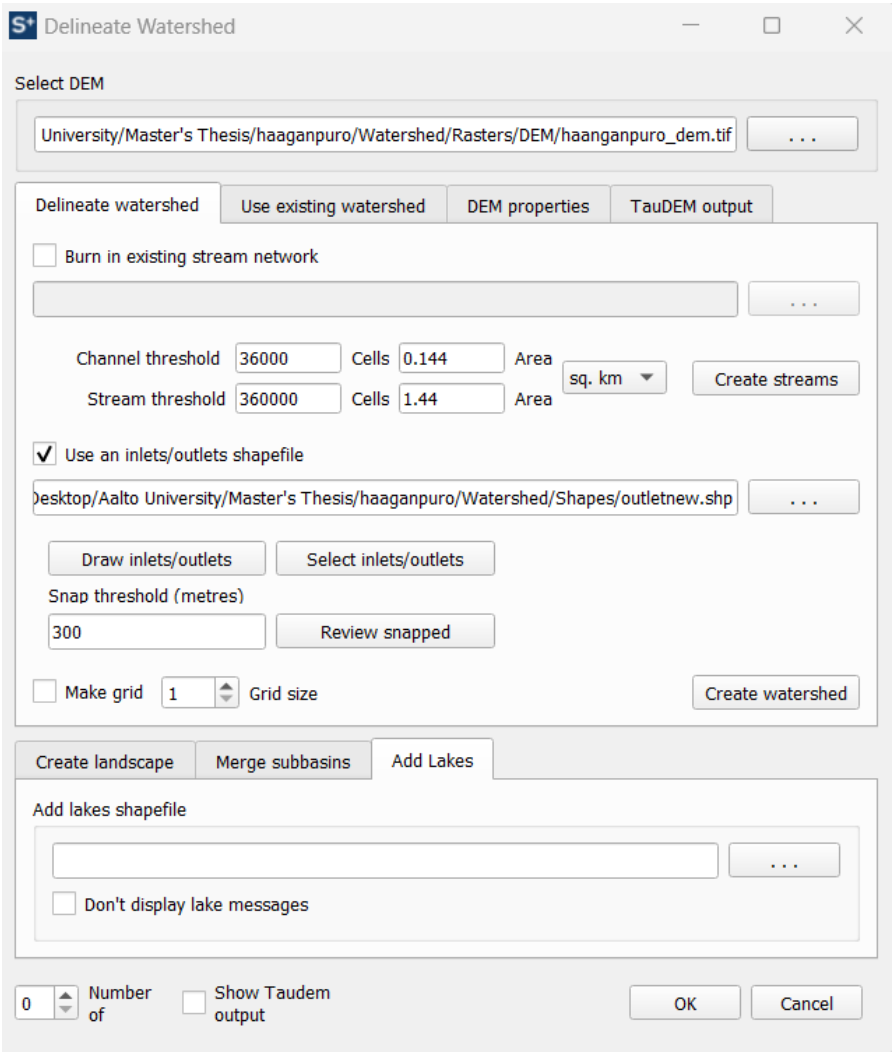

Figure 3.6: Watershed delineation command window in QSWAT+

By clicking "create watershed", the automatic catchment delineation is performed, including the drawing of the stream and channel network and the division of the watershed into subbasins which are identified as areas draining into a stream reach and whose outputs constitute the essential base of this analysis. The result of this phase is reported in figure 3.7. For Haaganpuro, three subbasins were automatically identified within the catchment, while the simulated stream network is composed of a main stream, which resembles the real trend of the Haaganpuro brook in a good way (verification was visually made by comparing the model output to the

river trend reported on Google Maps), and a collection of channels that directly flows into the main bed.

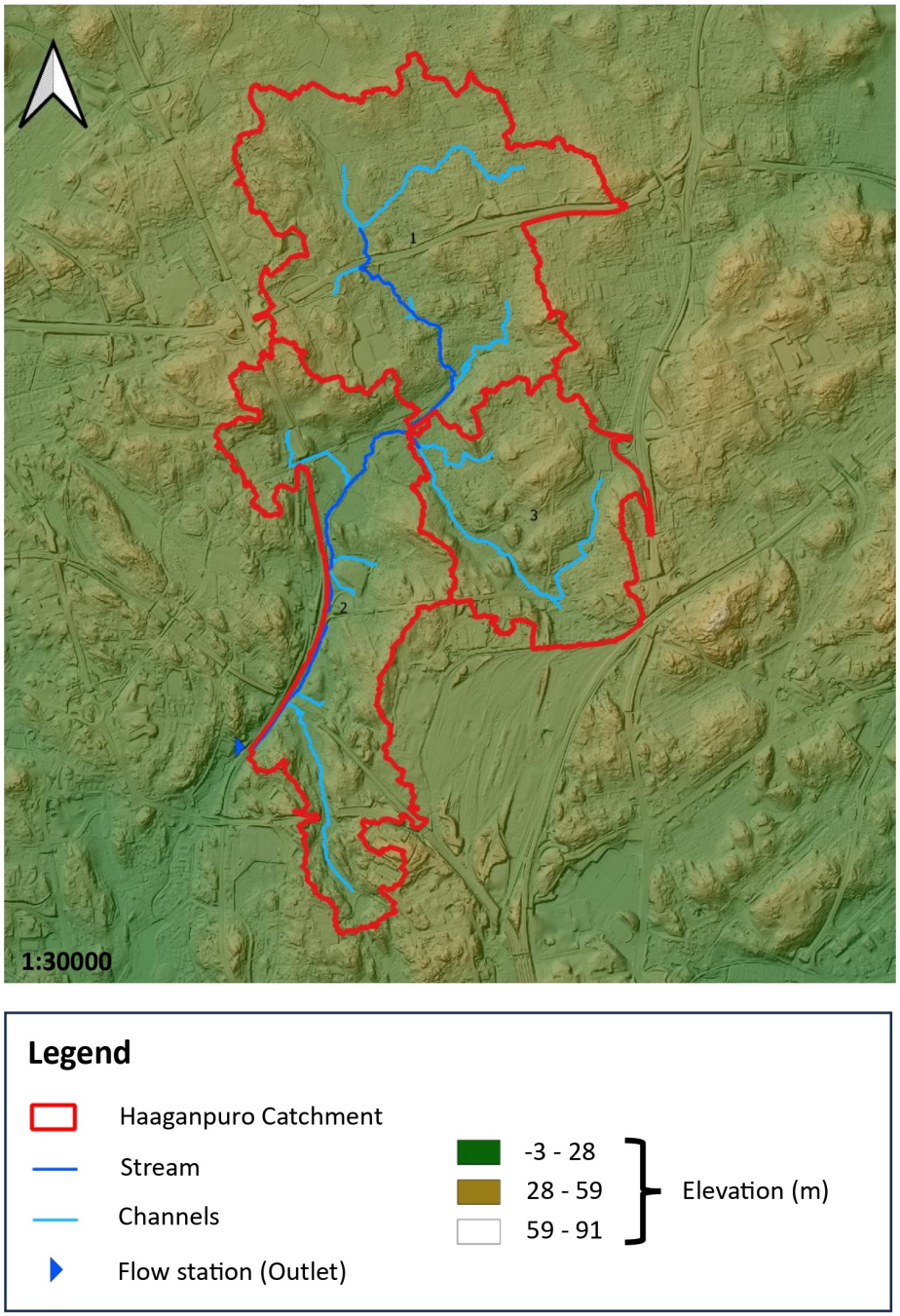

Figure 3.7: Watershed delineation result for Haaganpuro

The simulated Haaganpuro watershed was then overlaid on the shapefile of the original basin for comparison. Figure 3.8 shows how the shape of the simulated catchment resembles pretty well the real one except for the South-West and North-East parts that are not reproduced by the model. In fact, SWAT outputs a total catchment area of 7.2 km^2 out of the original 10.8 km^2, meaning that there is a loss of 3.6 km^2 (approximately 30 %). At the moment, there are no such studies that focus on evaluating whether a loss of area in the watershed delineation phase is acceptable or not. Judgement is mainly based on experience in the field of hydrological modelling and consult with experts. For the purposes of this thesis, the 30 % loss in catchment area was considered acceptable in accordance with the thesis supervisor and due to the fact that the main river is efficiently replicated and that the simulated area covers most of the real one and includes the channels that predominantly contributes to the flow in the main stream (considerations always based on a visual verification through Google Maps).

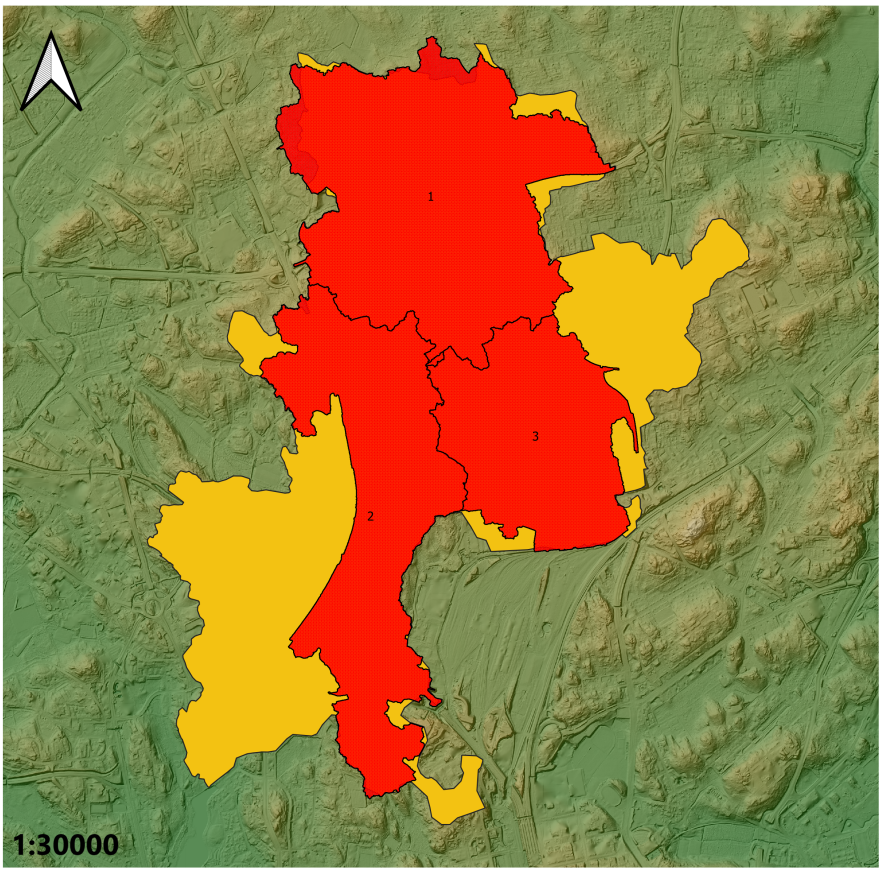

Figure 3.8: Comparison between Haaganpuro original (yellow) and simulated (red) watershed

In the last tab of the watershed delineation command window, reported in figure 3.6, there are three more sections ("create landscape", "merge subbasins", "add lakes"). In the case of this thesis, none of these options were implemented, so their description will be left out.

3.2.2 Creation of HRUs

Once the watershed delineation is completed, it is possible to proceed with the second step: the creation of HRUs. Hydrological response units can be considered as the heart of the SWAT model since they constitute the elements through which it is able to predict the loadings of water, sediments and nutrients from different land areas in a basin [52]. As already said in the paragraph referred to the description of the SWAT tool, the HRUs are the smallest spatial units of the model by means of which the mentioned estimations are done according to similar responses of land use, soil and slope, lumped together in a single HRU [53]. Given their importance, it is necessary to define, with a certain level of detail, their unique characteristics through the provided land use and soil data. The command window for their creation is reported in figure 3.9.
At first, the land use and soil maps are uploaded. They are both GeoTiff files in the same projection as the DEM (required by SWAT) and they must cover the watershed area. If they are bigger than the DEM file, SWAT automatically clips them to avoid having bigger files than necessary [49].
An essential aspect of the analysed command window is the import of a .csv file known as "lookup table" both for soil and land use. This file is required to convert the numeric values found in the land use and soil maps to the respective SWAT land use codes and soil names [49]. The ones used in the implemented lookup tables have already been reported in tables 2.2 and 2.3. As said in the "Data sources" paragraph, this section will focus on their setup. In both the land use and soil lookup tables, in each row two elements are reported: the numeric code present in the map and the corresponding SWAT code/name separated by a comma. Usually, it is possible to use some predefined lookup tables called "global_landuses" and "global_soils" but they are intended to be implemented with the corresponding global maps, which is not the case of this thesis. That is why the lookup tables were prepared manually in advance.
It is necessary to point out that in order to allow soil data to be read by the software, in addition to the soil lookup table, another file named "usersoil", describing soil properties, is needed [49]. Also, for this kind of purposes, a default "global_usersoil" (with data coming from the FAO, Food and Agriculture Organization of United Nations) is available but it was not used due to the same reasons explained above. The "usersoil" file was manually created starting from the Soil Survey Geographic Database (SSURGO) which contains information about soil properties collected

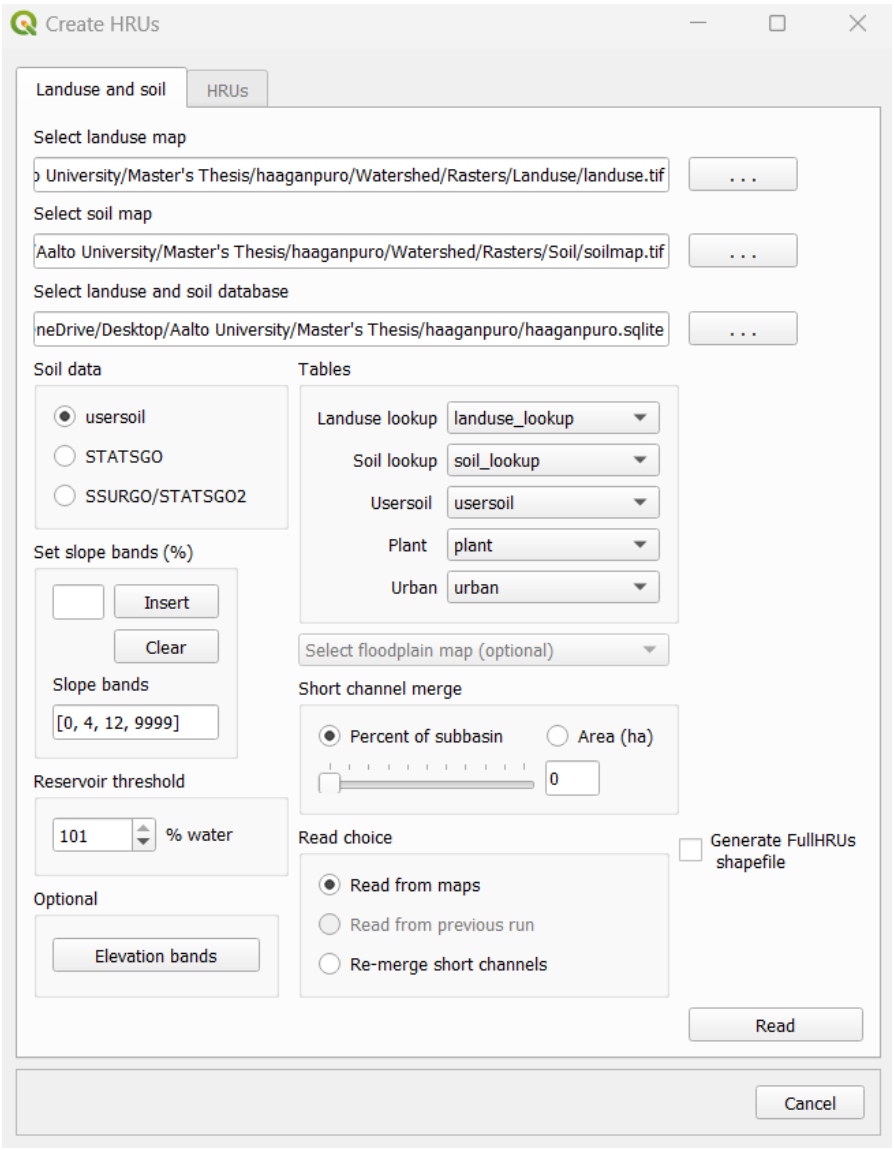

Figure 3.9: HRUs creation command window in QSWAT+

by the National Cooperative Soil Survey of United States that, over the course of a century, analyzed many soil samples in laboratories in order to define each soil type alongside with its properties. In fact, the SSURGO database is composed of rows, each of which reports a specific soil type with its characteristics and its SWAT name. The ones that were more similar to those contained in the soil map provided by the City of Helsinki Map Service were extracted and imported in the manually created "usersoil" .csv file. This one is needed in order to allow SWAT to associate to each soil type its properties of hydraulic conductivity, porosity,

density, grain size, etc... that are essential to calculate the share of water that infiltrates into the soil and the one that flows as surface runoff. Without this file, the software would not be able to clearly distinguish the different types of soil. Figure 3.9 shows that other options for soil data were possible such as STATSGO and SSURGO/STATSGO2 but those can not be implemented in this case since their selection would involve an automatic extraction of soil properties that is valid only for catchments located in the territory of the United States [54].
HRUs are also formed based on slope as well as land use and soil. Normally, a slope analysis would be required, but the amount of work related to it would have exceeded the boundaries of this thesis. For this reason, some intermediate points (e.g. 4, 12) were randomly added in order to separate the HRUs into those that have an average slope in the intervals 0 - 4 % and 4 - 12 % from those with an average slope above 12 %. Also, a full HRUs file was generated in order to visualize the outputs at the HRUs level, which usually have a higher spatial resolution. Lastly, the plant and urban tables were left as default.
At this point, the software starts to read the maps and the tables imported in the form and changes to the QGIS display starts to appear:

- A slope bands map is created based on the selected intermediate points.
- A legend for both the land use and soil maps showing the land use categories and the soil types taken from the respective lookup table.
- Two shapefiles called "Full HRUs" and "Full LSUs" showing the location of HRUs and LSUs within the basin. The landscape units are single regions draining into a channel reach and each of them forms a single polygon [49]. Hydrological response units, instead, are collection of pixels within a LSU that share similar properties of land use, soil and slope (as already explained).

Once the reading from maps process is over, the HRUs tab in the form of figure 3.9 becomes available. This allows the user to generate the "Actual HRUs" shapefile. The tab is shown in figure 3.10. All the options reported are used to filter the "Full HRUs" shapefile by removing certain HRUs that do not have a significant impact on the results, like the very small ones for example. The splitting and exempting land uses functions are implemented to define more precise land uses than the ones provided by the map, but they need to have more details about the possible subcategories of each land use [49]. For example, to split the agricultural land use into precise types of cultivation, it is necessary to known which plants are cultivated in the regions of the basin and which is their percentage on the total area. Since this kind of information is not available in the case of this study, those options were not used. Same discussion for the filtering options reported in the "Single/Multiple HRUs" section that remove insignificant HRUs based on thresholds set according to land use, slope, soil and area. The ones under the

"dominant" category extract a single HRU from the ones present within a landscape unit, while the "filter" categories output multiple HRUs extracted from the total number depending on the percentage limit set on the land use, soil, slope and area properties, or the number limit over the total [49].
In the end, none of the options of the HRUs tab were implemented with the consequence that the "Actual HRUs" shapefile coincides with the "Full HRUs" one.

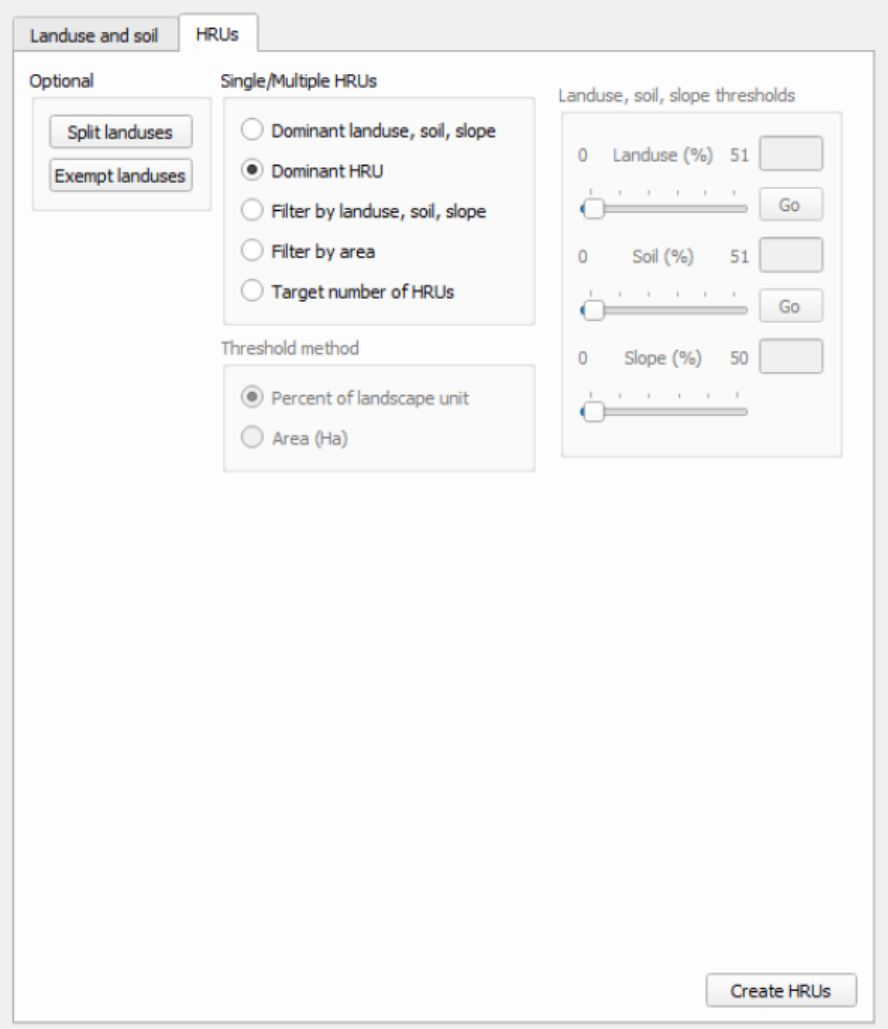

Figure 3.10: HRUs tab of the HRUs creation command window

At this point, the creation of HRUs is fully completed. The software generated a total of 2672 HRUs contained in 33 LSUs draining in the 33 channels plotted by the model. The HRUs and LSUs outputs are respectively reported in figure 3.11 and 3.12.

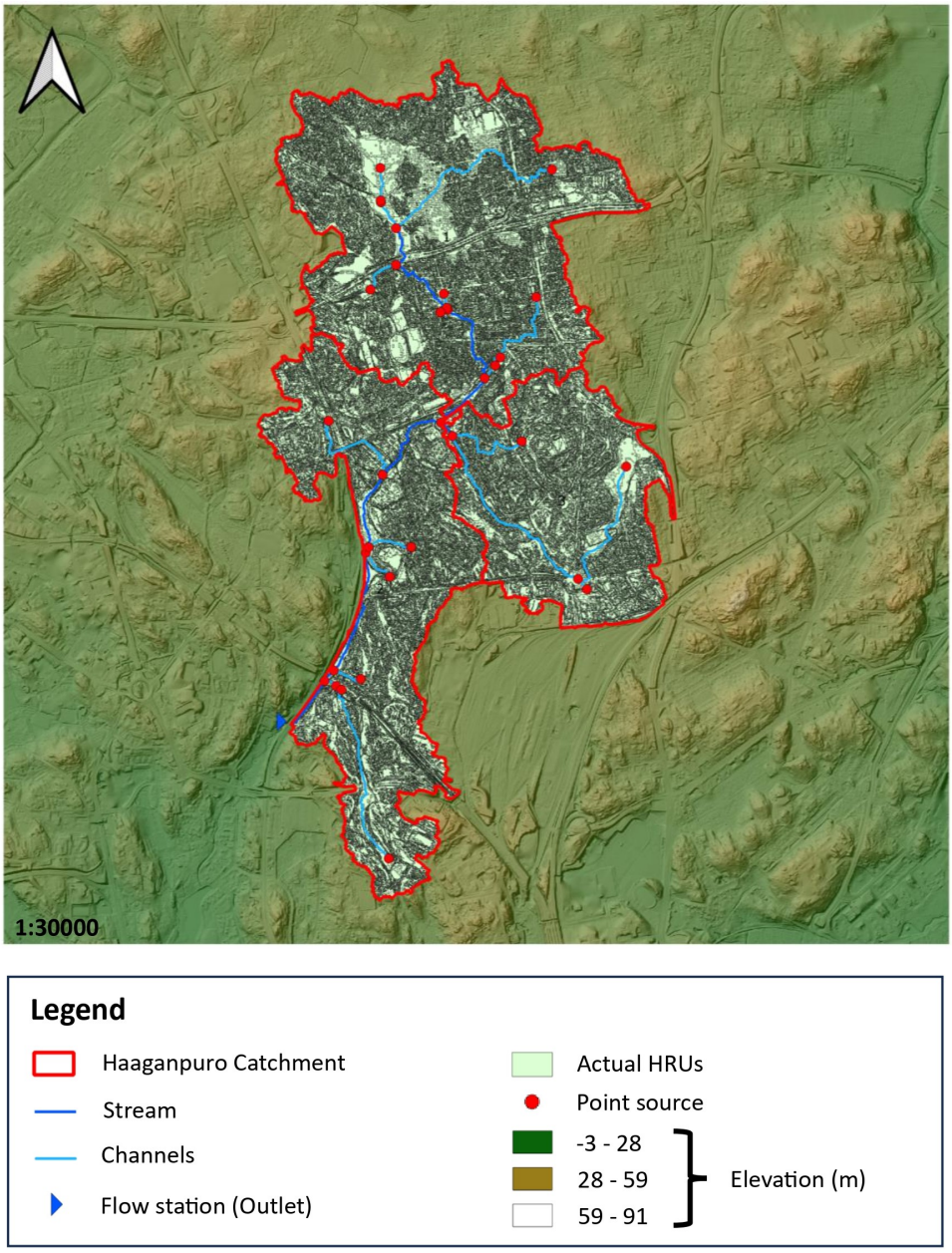

Figure 3.11: Actual HRUs within the Haaganpuro basin

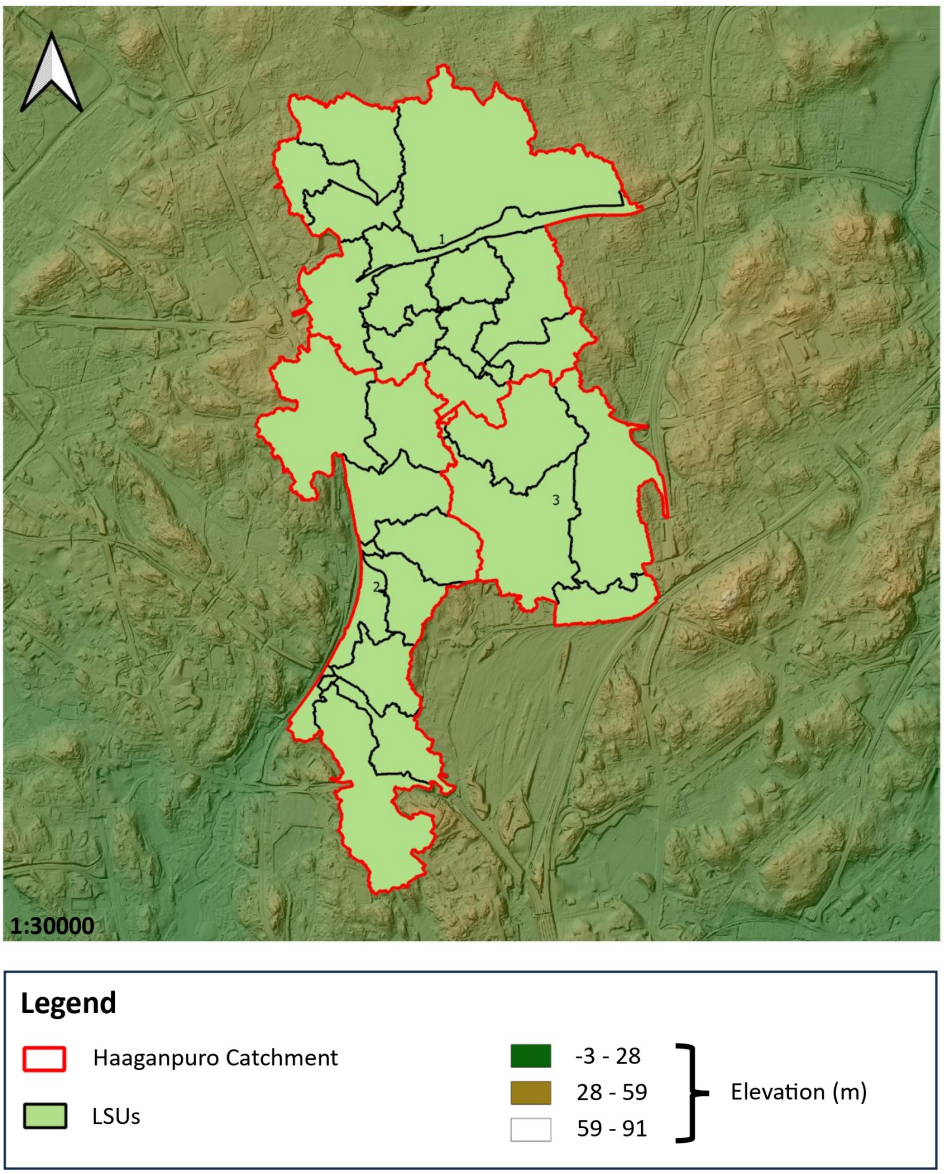

Figure 3.12: Subdivision of Haaganpuro basin into LSUs

3.2.3 Run of SWAT+ Editor

Once the watershed is delineated and HRUs and LSUs are created, the project is imported on the SWAT+ Editor in order to set the rest of the parameters and the inputs needed and finally run the model. Specifically, the interface of the SWAT+ Editor, referred to the editing of the inputs, is shown in figure 3.13.

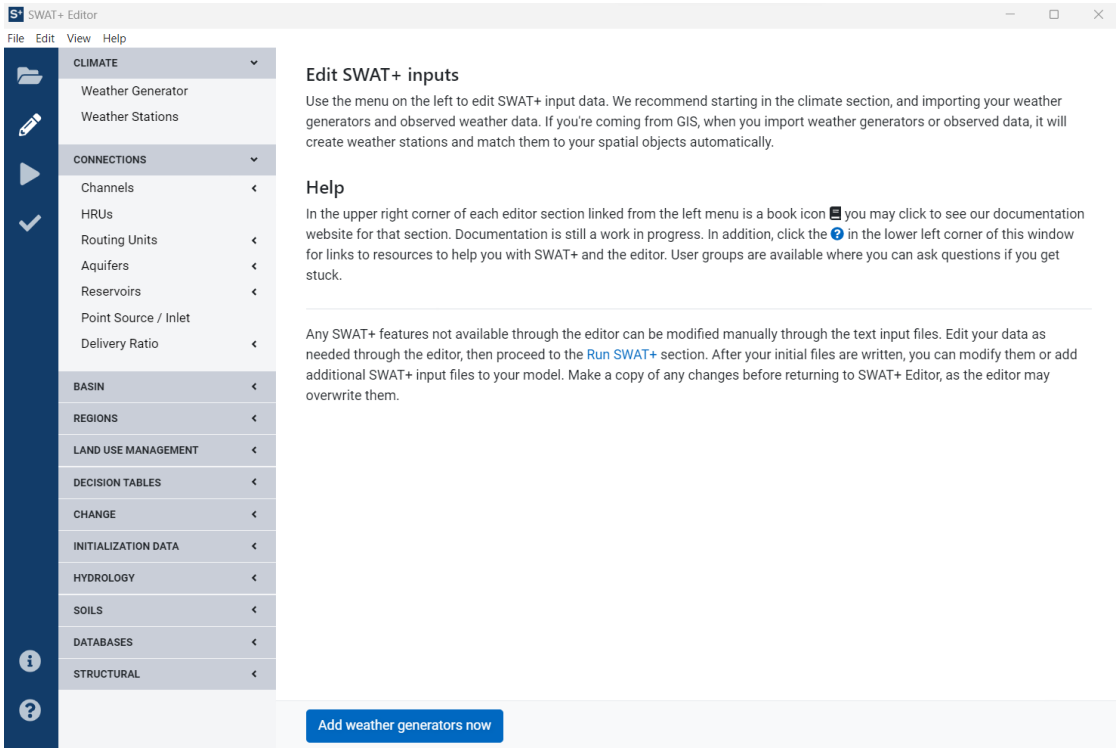

Figure 3.13: Edit SWAT+ inputs interface

Among the various input sections reported in figure 3.13, the one that requires more attention is climate. The parameters values of the other sections are generated automatically during the processes related to watershed delineation and HRUs creation and can be manually modified. Instead, climate data need to be uploaded and represent the last step before running the model. Weather data, and the meteorological stations from which they are taken, have already been described in the previous chapter. Here, the focus is on their implementation.
In the climate section, two files are fundamental: the weather generator (.wgn) input file and the weather data input file. The first one contains the necessary statistical data required to produce daily climate data that are representative for the subbasins [55]. At least 20 years of records are used to calculate parameters in the mentioned file [55]. There are two ways to import the .wgn data file: it can be selected by default along with the CFSR (Climate Forecast System Reanalysis)

world table from the SWAT+ databases, or it can be manually added to the database if the user has its own [56]. In this thesis, the first option was adopted and weather stations were created based on the studied location and the observed weather data provided by the Finnish Meteorological Institute. In this way, weather stations automatically match the spatial connection objects (channels, HRUs, etc..) in SWAT+ [56].
Concerning the weather data file, this is in the SWAT2012/Global Weather Data CFSR website format, meaning that each measurement (precipitation, temperature, solar radiation, relative humidity and wind speed) must have the entry file names reported in figure 3.14.

Measurement	Entry File
Precipitation	pcp.txt
Temperature	tmp.txt
Solar radiation	solar.txt
Relative humidity	rh.txt
Wind speed	wind.txt

Figure 3.14: Entry file names in the SWAT2012/Global Weather Data CFSR website format [56]

Each entry file is a comma-separated list of stations (in case of multiple stations), reporting the station id and name, its latitude, longitude and elevation. Then, each station name should have a corresponding .txt file that in the first line reports the starting day with the format "YYYYMMDD", while in the following lines there are the measurements for each day, one line per day [56]. In the case of temperature, each line contains two values referring to minimum and maximum temperature. Once uploaded, the weather file is automatically converted in the SWAT+ format for which the entry file names are shown in figure 3.15. Every entry file starts with a title line (allowing any text), followed by a heading line, and then an alphabetical list of filenames corresponding to each station [56]. In each station file, there is a title line, followed by a heading line ad data line specifying time and location. Subsequently, measurements for each time step are documented and for temperature they are listed as minimum and maximum temperature [56]. The other input sections were left as they were and, for this reason, are not treated in this discussion. In each of them, it is possible to add or delete rows but this action is suggested only in the case the user is completely sure that a row is respectively useful or worthless, since an erroneous move can cause the model to break [56].

Measurement	Entry File
Precipitation	pcp.cli
Temperature	tmp.cli
Solar radiation	slr.cli
Relative humidity	hmd.cli
Wind speed	wnd.cli

Figure 3.15: Entry file names in the SWAT+ format [56]

Once all the inputs are set, the model can be run. The running model interface is shown in figure 3.16.

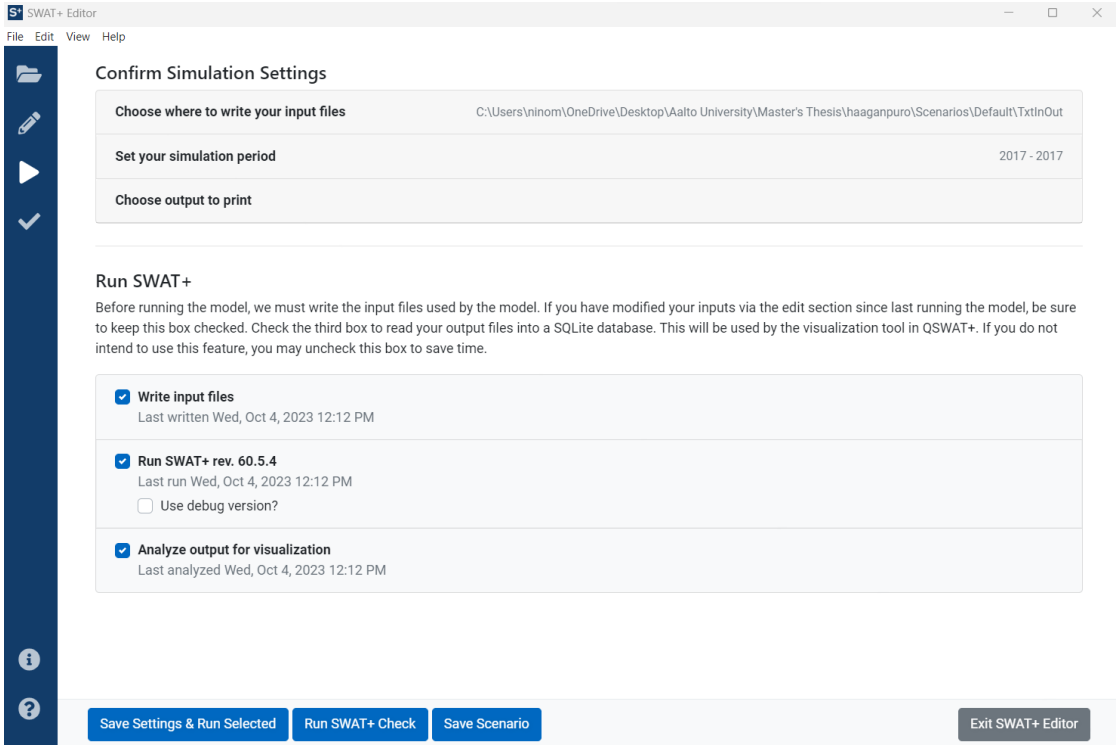

Figure 3.16: Runnig SWAT+ interface

In this form, it is possible to set the directory where to save the input files (that is the same folder of the outputs), define the simulation period and choose which outputs must be printed. Since this thesis is dealing with the analysis of surface

runoff and its share from urban and rural areas in the Haaganpuro basin, all the outputs related to channels and water balance at HRUs, LSUs and basin level have been printed, considering their daily, monthly and yearly variations and their average value. Better explanations about the simulated periods and the obtained results are given in the calibration paragraph and in the results chapter. However, it is worth to mention that, since the observed data provided refers to June-November 2017, the calibration period was June-August 2017, while the validation period was September-November 2017. Once the model was calibrated, it was run again for the period 2012-2022 (only for the months from May to November of each year, since winter data were not available) in order to generate the simulated results that constitute the base of this analysis.

3.3 Sensitivity analysis, Model calibration and validation

Hydrologic models try to reproduce, conceptualize and aggregate the complex, spatially distributed and closely interconnected processes that occur in a watershed by means of mathematical equations, which determine the development of an aggregation process that leads to have model parameters that do not always constitute directly quantifiable elements and, for this reason, they must be estimated by using measurements of system inputs and outputs [57]. In this way, the parameters values are optimized in order to obtain a model behaviour that replicates, as closely as possible, the real hydrologic response of the watershed over a predefined period of time [57]. The described procedure is known as calibration. In fact, hydrologic models are usually characterized by large uncertainties mainly related to parameters, input data and conceptual design [58]. In this perspective, calibration represents a crucial step in model application, since it is necessary to generate reliable results, allowing a correct prediction of the catchment behaviour under specific circumstances [59]. Notably, in the majority of watershed models, calibration entails an iterative process involving the evaluation and refinement of parameters, achieved by comparing simulated and observed values of relevance [60]. The way to assure that a calibrated model is able to evaluate all the conditions and the variables that can have an impact on the outputs, is named validation [60]. This is basically an extension of the calibration process and it is use to verify that the calibrated model is able to forecast observation data for periods different from the calibration one [60]. In fact, validation consists in running the model with the parameters used in the calibration phase, but the estimations are compared to measured data that are not implemented in the calibration. This one can be manually or automatically performed [61].

Generally, calibration should adopt a process-oriented and spatially focused approach, considering uncertainties in inputs, models, and parameters, and should be performed at the subbasin or landscape level to efficiently capture the variability in the predominant processes that happen within each subbasin, which would not be assessed if a global analysis was considered [7]. Furthermore, in order to assess the goodness of model outputs, by comparing them with the observations, different statistical and graphical methods can be used, such as time series plots, Nash-Sutcliffe efficiency (NSE), root mean square error (RMSE) and percent bias (PBIAS), which will be better described in the following sections [62].
For a clear understanding of the calibration process, it it useful to take a look at the flowchart reported in figure 3.17, that explains how SWAT manual calibration works. The scheme shows the performance assessment criteria for each model component alongside with the parameters that should be adjusted for each of them. It clearly highlights the fact that streamflow, sediment and nutrients should be calibrated in sequence due to their interconnections related to shared transport processes, and that attention should be paid to the water balance components (ET, surface/base flow ratios, tile flow proportions, plant yield, and biomass) which affect the reasonability of the results [63] [64]. In this thesis, the calibration phase involved the steps of the flowchart until the one referring to total flow, since the provided observed data concerns channel streamflow and the main analysis of this study is the impact of urban and rural areas on surface runoff in the Haaganpuro catchment (that is basically why the curve number "CN" was one of the most important calibration parameters, as will be explained later).
Usually, the observed dataset is split into two different datasets: one for calibration and one for validation. The splitting is normally executed based on time periods, trying to produce two datasets that are not so substantially different, especially in terms of climate [65]. Datasets can be also spatially divided by having a calibration phase that involves all the data provided by a certain monitoring station, and a validation stage referred to the other gauges located in the basin [66]. This solution can be useful when time splitting procedures are not possible due to a limitation in the availability of data [7]. However, these are just some recommended approaches but they are not mandatory. In fact, there are multiple ways in which the SWAT model can be calibrated and validated and several techniques have been studied over the years. For the streamflow calibration operated in this study, the available measured dataset was limited to the period June-November 2017 with the consequence that the time interval accessible for both calibration and validation was not that large. However, a time splitting procedure was implemented, with the cut-off point placed on the last day of August 2017, defining, in this way, the months between June and August as the calibration period, and the ones between September and November as the validation period. This decision was taken in accordance with the thesis supervisor and due to the fact that normally, in Southern

Finland, the wettest months in terms of rainfall are the ones that go from July to October [67], allowing in this way to have similar climate characteristics with two wet months for each time split period. In particular, October appears to be the month with the most rain in Helsinki, with an average rainfall of 2.2 inches [21].

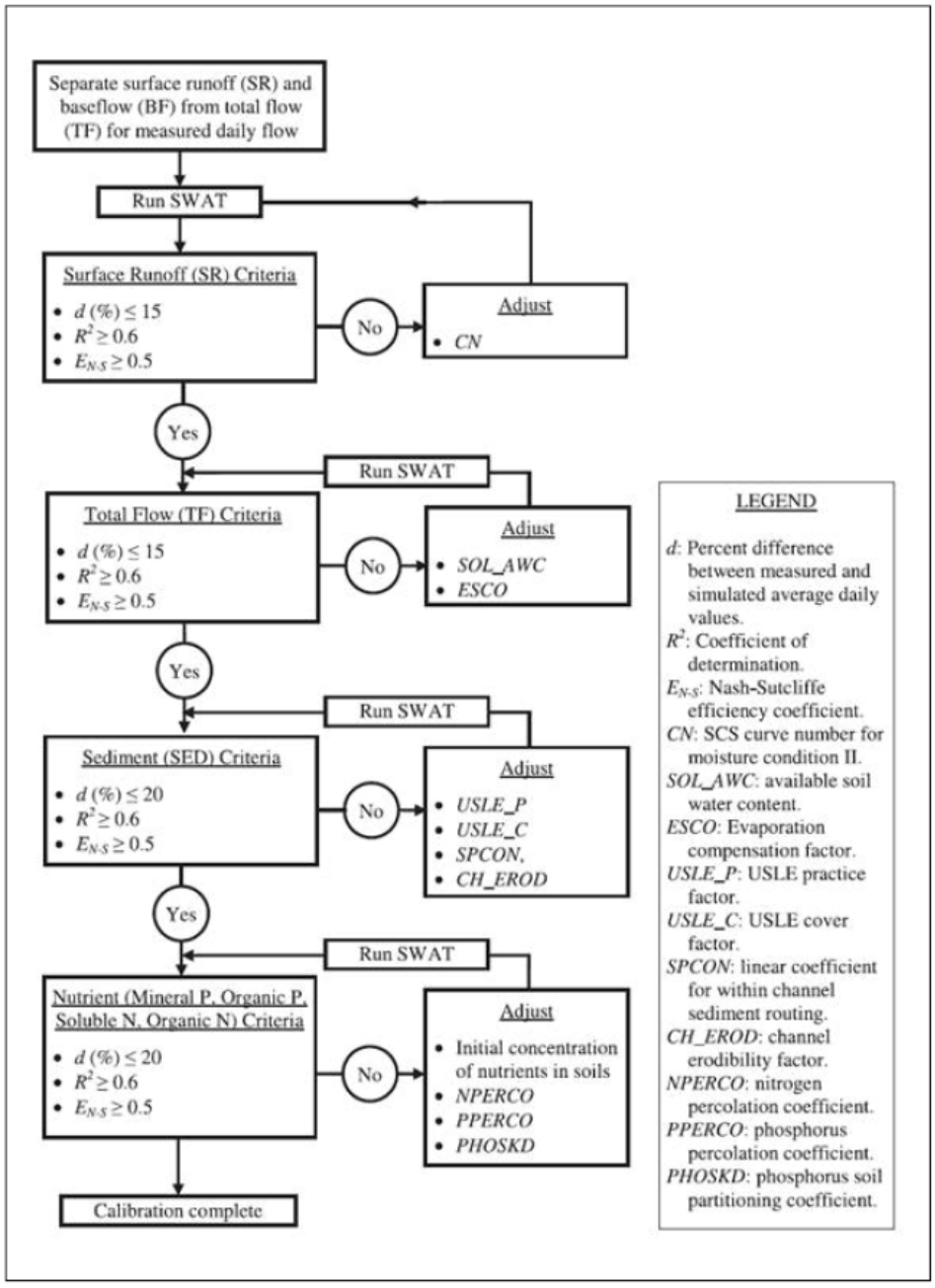

Figure 3.17: SWAT manual calibration flow chart [63]

The discussion presented above deals with a general overview of how model calibration and validation work. More detailed insights about their application in this case study are given in the next sections. Before going through them, it is worth to mention that both calibration and validation were carried out through a tool associated with SWAT+ named "SWAT+ Toolbox" (version 1.0.2), a free software enriched with features and functionalities essential to perform model analysis and calibration and whose characteristics are better described in the next section. The toolbox also allows to perform a sensitivity analysis, which is a fundamental step in the calibration process since it is able to detect the most sensitive parameters that require to be adjusted, and therefore calibrated, for a specific watershed (more details are given in section 3.3.2). In this way, from a selected set of potential parameters, the sensitivity analysis identifies those that are more influential on the model outputs and sorts them by means of a statistical index that gives insights on how large their impact is on the results. Anyhow, as already said, a deeper description of the sensitivity analysis phase will be provided in the related section, together with the method implemented to carry it out. For clearance purposes, it is useful to come up with a brief illustration of SWAT+ Toolbox, the software considered to perform the above cited steps.

3.3.1 SWAT+ Toolbox

As previously mentioned, the SWAT+ model is relatively new and, for this reason, there is still a need to develop more tools able to perform model analysis and calibration. Among the most recent ones, there is the SWAT+ Toolbox which is a free software written in C# and available for the moment only for the Windows operating system, that assists the user on uncertainty and calibration analysis, and model check [68] [69]. Its main interface is shown in figure 3.18.
Once downloaded, the SWAT+ Toolbox is integrated on the QGIS interface and a new project is created with the same directory as that of the SWAT+ Editor outputs (the so called "TextInOut" directory). This fact is particularly useful since it automatically correlates the run settings of the SWAT+ Toolbox with those of the SWAT+ Editor, which then will be used to run sensitivity analysis, manual and automatic calibration [68]. The run section is reported in figure 3.19. In this form, it is possible to set the simulation period, the warm-up period, the PET (Potential Evapotranspiration) method, the routing method and the required outputs. The simulation period goes from the beginning of June to November 2017 and is the same one used in the first run of the SWAT+ Editor to generate simulated values for calibration purposes. Generally, it is automatically set due to the aforementioned correlation related to the directory. The warm-up period constitutes an initial phase of the simulation where the model is permitted to adapt to its starting conditions and attain a stable state, moving to an optimal stage [70]

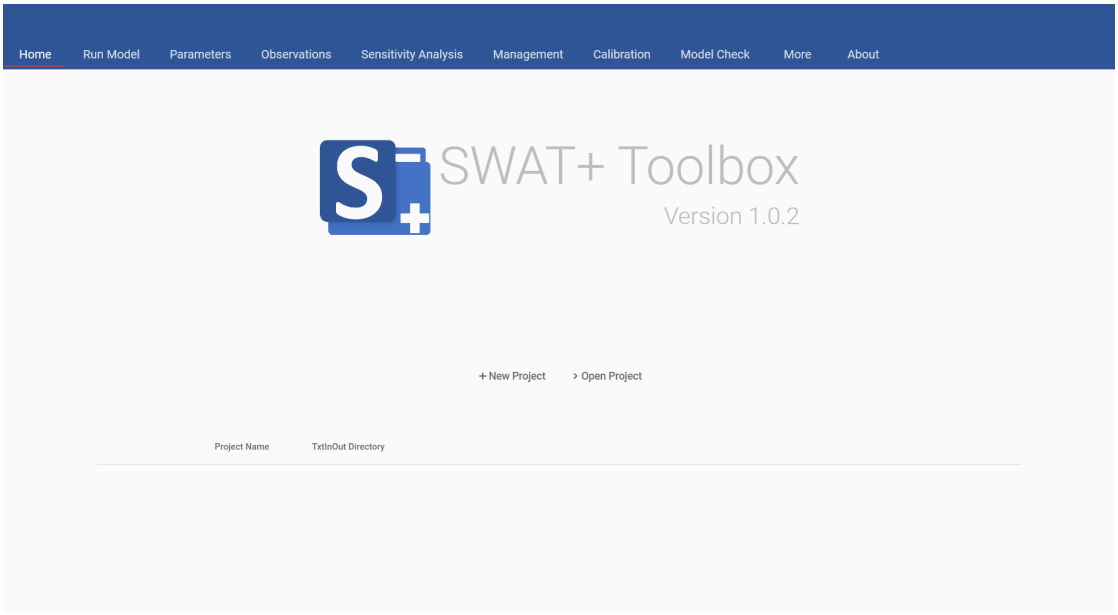

Figure 3.18: SWAT+ Toolbox main interface

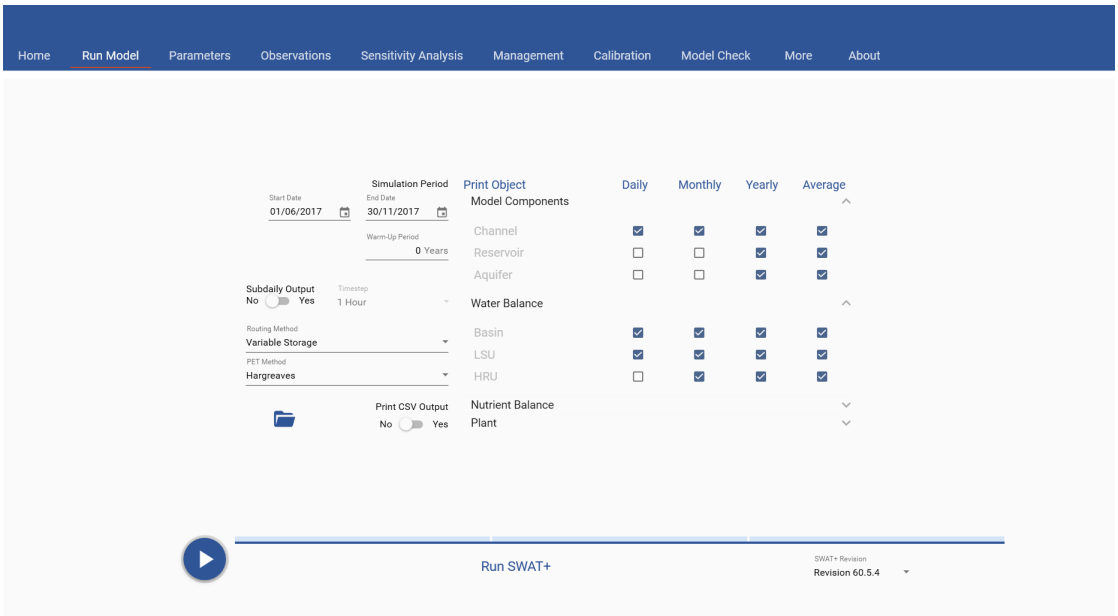

Figure 3.19: SWAT+ Toolbox run model interface

[71]. Its duration varies based on the particular simulation and the preferences of the user, but it typically spans over one or two years [70]. However, since the simulation of the warm-up period does not produce any results, in the case of

short datasets and periods (like the observed streamflow data and the respective calibration interval considered in this thesis), the warm-up period can be set to zero [72].
The PET method in SWAT represents the way through which the model is able to define the share of water that transpires and evaporates from a specific surface [73]. At first, SWAT estimates potential evapotranspiration by means of three possible methods: Penman-Monteith (PM), Hargreaves (HA) and Priestly-Taylor (PT) [55]. This thesis mostly concentrates on the first two.
The PM method integrates elements that consider the energy required for sustaining evaporation, the necessary mechanisms for water vapor removal, and terms related to aerodynamic and surface resistance [74] [75]. Its equation is reported below:

$$\lambda E = \frac{\Delta \cdot (H_{net} - G) + \rho_{air} \cdot c_p \cdot (e_z^0 - e_z) / r_a}{\Delta + \gamma \cdot (1 + r_c / r_a)} \tag{3.4}$$

where λE is the latent heat flux density (MJ/m^2 $\cdot$ d), E is the depth rate evaporation (mm/d), Δ is the slope of the saturation vapor pressure temperature curve de/dT (kPa/°C), H_{net} is the net radiation (MJ/m^2 $\cdot$ d), G is the heat flux density to the ground (MJ/m^2 $\cdot$ d), ρ_{air} is the air density (kg/m^3), c_p is the specific heat at constant pressure (MJ/kg°C), e_z^0 is the saturation vapor pressure of air at height z (kPa), e_z is the water vapor pressure of air at height z (kPa), γ is the psychrometric constant (kPa/°C), r_c is the plant canopy resistance (s/m), and r_a is the diffusion resistance of the air layer (aerodynamic resistance; s/m) [74] [75].
Concerning the HA method, the original version of its equation is the one implemented in SWAT:

$$\lambda E_0 = \alpha_{pet} \cdot \frac{\Delta}{\Delta + \gamma} \cdot (H_{net} - G) \tag{3.5}$$

where E_0 is the potential evapotranspiration (mm/d), α_{pet} is a coefficient and all the other variables have the same meaning as before [76].
A first fundamental distinction between the two methods refers to the amount of required inputs, as it is possible to see from their respective equations. The PM method involves all the weather data inputs that have been used in this thesis (relative humidity, solar radiation, wind speed, air temperature), while the HA equation requires only air temperature. In this study, initially, the Penman-Monteith method was considered for flow simulations. However, the unsatisfactory performance results, during the calibration phase, led to a change in the type of PET method adopted, with the consequence that the Hargreaves approach was implemented. The reason behind this choice will be discussed in detail in the "discussion" section to allow a better understanding while looking at the results. For now, just a brief theoretical background about the two approaches was given in order to have a clearer vision when their performance will be compared. The estimated PET is then used by SWAT to predict actual evapotranspiration by

taking into account both soil moisture and land use [73].
Lastly, the routing method constitutes a relevant instrument for SWAT since it simulates the water movement through the channel network of the basin and calculates the water amount arriving at the catchment's outlet [77]. In SWAT, it is possible to implement two types of routing approaches: the Muskingum Routing (MRM) method and the Variable Storage Routing (VSR) method. Their main difference is related to their characteristics of linearity. In fact, the first one is a linear method that considers a linear change in depth along the reach, while the second one is a non-linear approach where the outflow volume depends on the storage coefficient, the stored and flowing volume [78]. Specifically, the advantages of the VSR method concern the consideration of the non-linearity of the routing procedure, a storage coefficient obtained by a physical basis, an easy quantification and no assumptions regarding the prismatic channel cross-section for routing [78]. A study developed by Pati et al. (2018) compared the performance of the two methods in simulating discharge and found out that the VSR method allows a more realistic simulation of the results on a daily time step even if their level of accuracy is comparable to that of the MRM model [78]. In particular, a better reflection of the reality is explained by the fact that the VSR model is able to generate a stage hydrograph corresponding to the discharge hydrograph at any specified point along the routing reach, and that its sound physically based origin produces consistent advantages when data is limited [78]. Also, it was noted that the VSR method has a better performance in the validation stage if compared to the MRM one [78]. For all these reasons, the run of the SWAT model and the various iterations of both sensitivity analysis and calibration were executed by implementing the Variable Storage Routing method.
Now that a deeper explanation about the methods used to run the SWAT model has been given, it is possible to proceed with the next sections of the SWAT+ Toolbox. In particular, there are two specific interfaces dedicated to the uploading of the observations and the parameters that will be subjected to a sensitivity analysis and then to calibration. As stated throughout the thesis, the observations are composed by two datasets: the first one involves the measured flow values coming from Pakila, a urban area located in the North-East part of the Haaganpuro catchment, while the second one contains the measurements of the flow coming from the channel that acts as the outlet of the catchment. The parameters interface will be better analyzed in the next subparagraph. Most of the discussion made in the treated section was set to give an idea about how each run of the SWAT+ Toolbox works. The methods here described to understand what there is behind each run are the same ones implemented to run the SWAT+ Editor. Their description was reported in this subparagraph only for purposes of continuity with the next section.

3.3.2 Sensitivity analysis

Before going directly into the sensitivity analysis phase, it is necessary to take a look at the parameters section and identify a set of potential parameters that, based both on their definition and impact on the model outputs, could represent a collection prone to calibration. Obviously, since there are two sets of observations, one for an urban area and one for the whole basin, there is a need to split the parameters set into those that refer only to urban areas and those that will be calibrated on rural areas. This subdivision is essential because, at first, calibration of urban areas is performed and then, once completed, it is possible to proceed with the calibration of the whole Haaganpuro watershed. During the calibration of built up areas, the data coming from the Pakila district, in accordance with the thesis supervisor, were considered as representative of all the urban areas in the basin. This means that, at first, a set of parameters only applied to built up area was selected.
Before going into details, a map showing the basin division into the 33 landscape units (LSUs) identified by the model and another one reporting their distinction in urban and natural areas are provided (figure 3.20). The analysis of figure 3.20 clarifies how the majority of the built up areas are concentrated in the Eastern part of the basin (especially in the North-East), while the more natural ones are placed in the Western part (especially in South-West), defining, in this way, a non-negligible separation in two main regions. This differentiation was done based on the share of each land use in each LSU. If the predominant one got to be the urban category (most of HRUs classifed with an urban purpose), then the whole unit would be classified as urban. Same discussion for the natural regions. The results of the distinction process obtained with this approach were supported by a visual verification through Google Maps, by overlaying the delineated basin (subdivided in LSUs) on the Google Hybrid map for comparison (figure 3.21).
Figure 3.21 demonstrates the correspondence between the real land use (in orange) of each LSU and the supposed one (in blue and grey) implemented on the toolbox. In fact, the supposed urban areas are correlated to areas mostly composed of buildings and vice versa for the natural ones. Specifically, the urban areas of the catchment involve the Helsinki city's districts of Pakila, Pirkkola and Maunula, while the more natural regions include the parks of the Pirkkola and Maunulanpuisto areas, part of the Helsinki Central Park.
Since, as said earlier, the flow measures coming from the Pakila district are to be considered representative of all the urban areas in the catchment, it is important to highlight which landscape unit resembles most of that area. In this way, the observed urban flow is referred to the channel in which all the water coming from the considered LSU drains. In this analysis, the Pakila area coincides with LSU n. 320, located in the most North-Eastern part of the basin (figure 3.22).

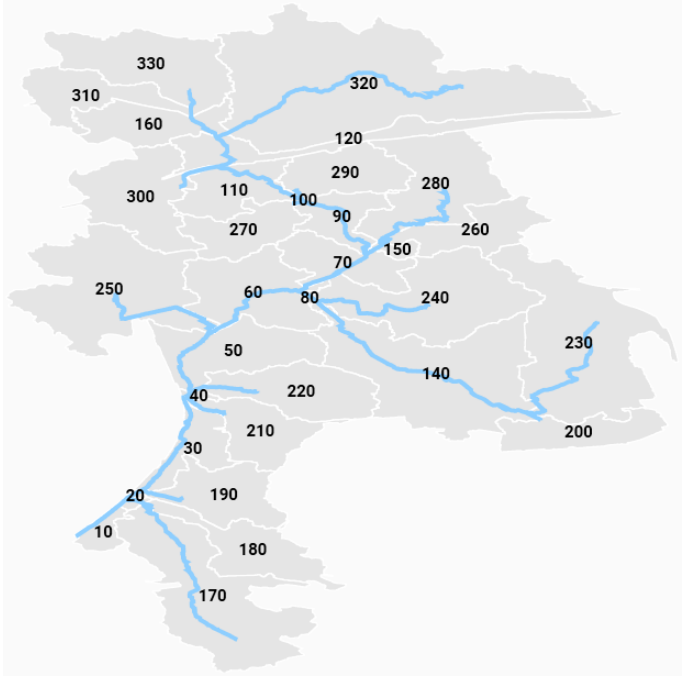

(a) *Subdivision of Hagaanpuro in LSUs*

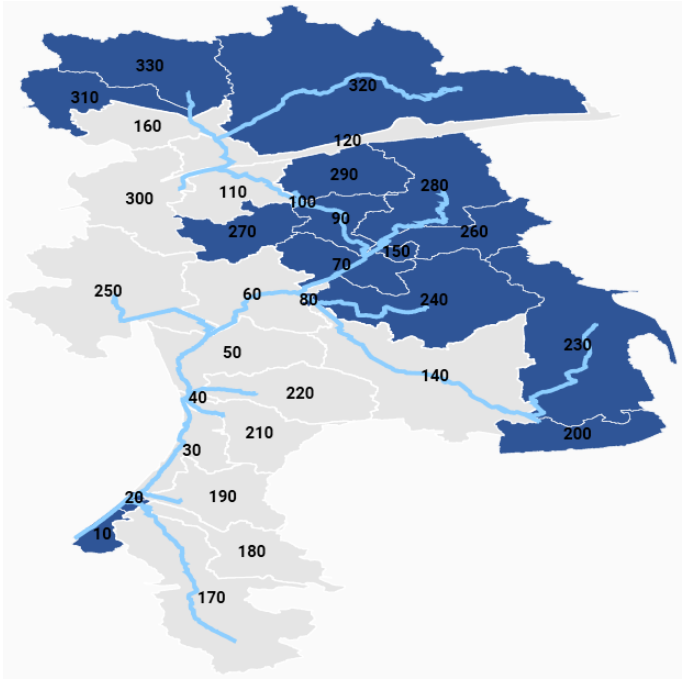

(b) *Distinction between urban (in blue) and non-urban (in grey) areas*

Figure 3.20: Haaganpuro basin map on SWAT+ Toolbox

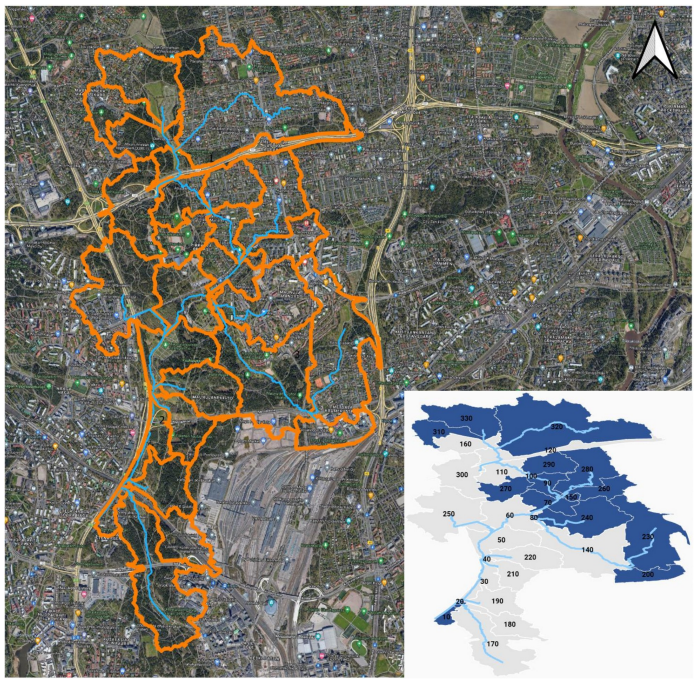

Figure 3.21: Haaganpuro basin divided in LSUs and overlaid on a Helsinki Google Hybrid map

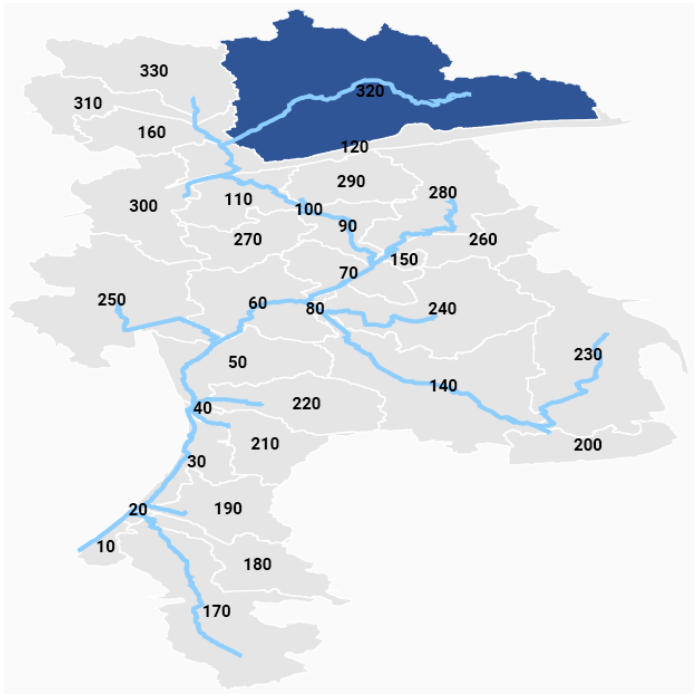

Figure 3.22: Location of the Pakila district in the Haaganpuro basin

The assumption behind the correspondence between Pakila and LSU n. 320 was always made based on visual inspection through Google Maps (figure 3.22).
At this point, it is time to identify which are the parameters that need to be calibrated in order to get a simulated flow trend that resembles the measured one. At first, a set of potential parameters was selected based on literature and impact on flow and surface runoff. Then, the same group was subjected to a sensitivity analysis in order to determine the most sensitive parameters for calibration. Each parameter was considered twice, once for urban areas and another time for rural areas. This means that the selected parameters collection was composed of two subsets, constituted by the same parameters, but related to two different kind of zones (urban and non-urban). To add a parameter on the SWAT+ Toolbox, it is necessary to choose the group from which it is taken (there are six main levels: HRU, soil, aquifer, routing, reservoir, SWQ) and settle its change type method, that defines the way through which its value is increased or decreased. On the software there are three options for the change type [68]:

- Percentage: alters the current value by a specified percentage, either increasing or decreasing it.
- Relative change: alters the current value by a specified fixed value.
- Replace: the specified value substitutes the existing parameter value.

It is important to notice that not all parameters can be changed with a replacement method, especially if they apply to all the objects in the model. An example of this situation is represented by the curve number (CN) which is a parameter that defines the ability of a surface to generate runoff based on its soil properties and its land use. If all CN values are replaced with the same one, then the parameter will lose its spatial variability and all land uses will acquire the same properties in producing surface runoff [68]. It is clear that this would not have any rational meaning since an urban surface does not have the same runoff characteristics as a vegetated surface (normally the CN is higher for urban areas rather than rural areas) and, consequentially, the same CN values for all land uses would generate a significant error in the results. This is why a special attention should be paid to the choice of the parameter change method.
Furthermore, an interval within which each parameter changes must be defined. In this way, a maximum and a minimum value is set depending on how large the user wants a parameter to change. The parameters section looks like figure 3.23. In this form, it is also allowed to apply a parameter to a specific object and it is through this function that the parameters were separated into those applied to urban areas and those applied to rural areas, in accordance with what has been reported in figure 3.20b.

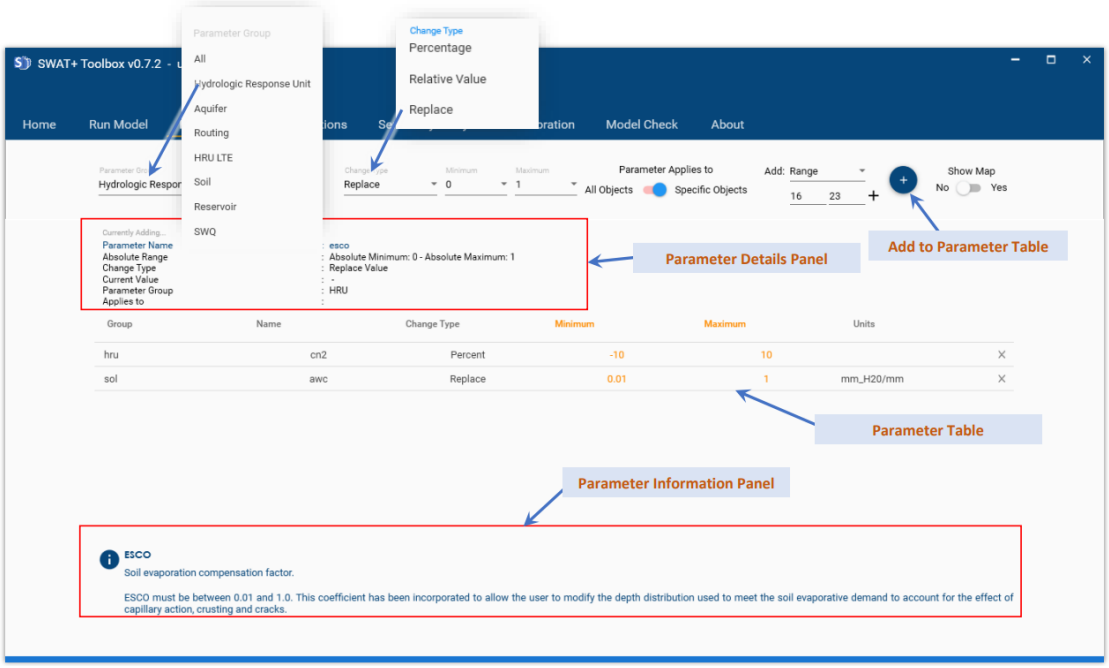

Figure 3.23: SWAT+ Toolbox parameters interface [68]

The analyzed parameters, their definition and the reasons behind their choice will be discussed in the "Results" chapter. For now, only a description of the methodology and its theoretical background is given to have a view of the procedure that leads to the results of this thesis.
In the observation section, instead, the measured flow values for Pakila and the whole basin are uploaded referring respectively to channel 32 (LSUs n. 320) and channel 1 (the catchment outlet). Their graph will be shown in the next chapter together with the simulated values.
Once the parameters are added and the observations are loaded, the sensitivity analysis tab becomes available. The SWAT+ Toolbox provides four methods to perform a sensitivity analysis [68]:

- Sobol
- Fourier Amplitude
- Random Balance Designs Fourier Amplitude
- Delta Moment-independent Measure

In the field of hydrology, the most common sensitivity analysis method is the Sobol one due to its accuracy, efficiency and ability to account for the existing dependence

between input variables. These constitute some of the main properties that led to the choice of the Sobol approach for the data of this study. Notably, the Sobol sensitivity analysis is a variance-based method that relies on the decomposition of the model output variance into components that represent the variances of input parameters at progressively higher dimensions, defining, in this way, their interaction and their contribution to the output variance [79] [80]. The method works within a probabilistic framework and is conceived to quantify how much of the variability in the model output each parameter is responsible for, whether it is due to a single parameter or an interaction between multiple parameters [81]. The input effect on the output is measured by means of some sensitivity indices. In particular, the first-order Sobol sensitivity index represents a measure of the direct impact of a parameter on the model output variance, and constitutes the evaluation element through which the parameters are sorted from the most sensitive to the least sensitive one [68] [82]. Instead, the effect of the interactions between different parameters is measured through indices of higher order. The sum between the mentioned indices gives the total Sobol sensitivity index [83]. However, it is worth mentioning that the Sobol approach is not able to identify the source that causes the input variability, but it was develop only to analyze its impact and its extent on the results [81]. A flowchart describing how Sobol sensitivity analysis works, is reported below:

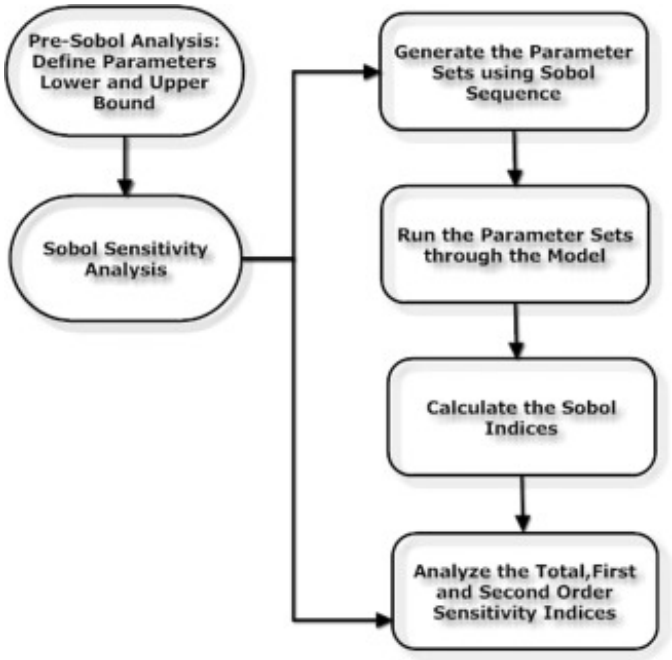

Figure 3.24: Steps in the implementation of a Sobol sensitivity analysis [81]

From figure 3.24, it is clear that there are a Pre-Sobol analysis phase and a Sobol sensitivity analysis phase. The first is related to the discussion concerning how the parameters are chosen, to which regions they are applied and how they are added on the SWAT+ Toolbox, that was done at the beginning of this subparagraph. The second one is the proper sensitivity analysis that has been debated in these last lines. Going more in detail, the flowchart shows how the Sobol sensitivity analysis is composed of four stages that can be read from figure 3.24. In particular, the first one uses a Sobol sequence, proposed by the Russian scientist I. M. Sobol, to generate the parameter sequence [84]. The Sobol sequence is a low-discrepancy sequence, also known as the "quasi-random sequence", that has the advantage to sample space more uniformly if compared with entirely random sequences [81]. The implementation of such kind of sequence allows the algorithm to have a superior convergence and the parameters sets, that are consequentially generated, are subsequently employed to simulate the model outputs [84] [85]. For more insights about the calculations of the Sobol sensitivity indices and the steps that constitute its implementation, it is suggested to take a look at the study elaborated by Zhang et al. (2015) [81].
A more detailed description of the theoretical background behind the Sobol method was given since it is the one implemented to perform the sensitivity analysis in this study. However, it is essential to briefly mention the other three approaches that can be chosen in order to properly understand the following discussion about the advantages of Sobol with respect to the other methods and why it was chosen.
The Fourier Amplitude sensitivity analysis (FAST) employs a periodic sampling technique along with a Fourier transformation to break down the variance of a model output into partial variances attributed to various model parameters [86]. The ratios between those partial variances and and the model output variance indicate how important the contribution of each parameter to the uncertainty in the results is. This contribution is determined by means of a integer characteristic frequency that is assigned to the periodic sampling of each parameter through a search function, causing, in this way, the development of an aliasing effect which may lead to a loss of information and an underestimation of the sensitivity indices [86] [87]. In addition to this limitation, another disadvantage is that the method considers the parameters to be independent and can be applied only to linear models since in case of the non-linearity it might not be suitable [88]. However, new approaches have been developed over the years in order to extend its applicability to non-linear models [87].
Some of these improvements led to the birth of the Random Balance Designs Fourier Amplitude (RBD-FAST) method which is a modified version of the FAST sensitivity analysis that is provided with a more efficient sampling scheme for the determination of the partial variances, improves FAST's computational efficiency and robustness and extends its use to more complex models [89]. The extension also

involves the estimation of the sensitivity indices, accounting for the interactions between the input parameters, as happens in the Sobol method. However, it remains limited to linear models and the accuracy of the results, even though bias correction methods have been implemented, remains lower then the Sobol one [90] [91].
The accuracy, in fact, was one of the main reasons why the Sobol method was preferred among the ones incorporated in the SWAT+ Toolbox. The other reasons are related to a series of advantages that characterizes the method if compared to the others. Always starting from accuracy, several studies have compared the one achieved with Sobol to that of the Fourier Amplitude method, and discovered various features in favor of Sobol. The main findings can be listed as follows:

- In the hydrology field, the results generated by the Sobol method have a higher level of accuracy than the ones produce by the Fourier Amplitude sensitivity analysis (FAST) [92] [86] [93] [94].
- The Sobol approach assumes the existence of a interconnection between the input variables, which is absent in the case of FAST, where the input parameters are considered to be independent from each other. The assumption of connection between the inputs plays an important role in hydrology since the variables are usually correlated [86] [95].
- The calculations of sensitivity indices of different order, allowed by the Sobol analysis, provides a larger overview on the model's behaviour, also accounting for interactions between parameters. This feature is absent in the FAST method since it takes into account only first-order effects [92] [96].
- The Sobol sensitivity analysis is not affected by the aliasing effect that happens in the FAST related to the use of integer characteristic frequencies, and can better predict the behaviour of non-linear models [81] [86].

The last possible method to be implemented for a sensitivity analysis is the Delta Moment-independent Measure (DMIM), useful for studying non-linear models due to its independence from the moments of the output distribution [97]. It is a variance-based method that relies on a sensitivity measure independent from moments and seeks to gauge the input variables' contribution to the probability density function (PDF) of the model output [97] [98]. Sensitivity indices are calculated through a density-based estimator, enabling the estimation of two types of indices: the distribution-based and moment-independent ones [98]. However, the implementation of this estimator can be computationally expensive [99]. In addition to this, a study elaborated by Gan et al. (2014) noticed how both Sobol and DMIM methods output similar values concerning first-order sensitivity, but the most accurate numbers for the indices of higher order are given by Sobol [93].

All the topics presented above justify the choice of using the Sobol sensitivity analysis. However, attention should be paid to its computational cost which, depending on the number of input parameters and the complexity of the model, can be very expensive. Usually, the larger the number of evaluations set, the higher the computational cost is [81]. Although there is no global consensus on the optimal number of iterations needed, Gan et al. (2014) suggested a minimum sample size of 1050 samples for the Sobol analysis to compute the first-order and the total sensitivity indices in a correct and efficient way [93]. More information about the sample size and the most sensitive parameters selected by the sensitivity analysis are given in the "Results" chapter.

3.3.3 Calibration and validation

The SWAT+ Toolbox was also used to carry out flow calibration and validation. As said earlier, the observed streamflow datasets (for both the Pakila area and the whole Haaganpuro basin) are referred to the period that goes from June to November 2017 and were divided by means of a time splitting procedure, with the cut-off point placed on the 31st of August, defining, in this way, the months from June to August as the calibration period, the ones from September to November as the validation period, and allowing to have two wet months for both the calibration and the validation periods (July and August for the first one, September and October for the second one). As it was discussed, the available observations do not extend over a large time interval (only six months are included) and, therefore, the time splitting procedure may show some limitations. However, the presence of two months with approximately similar rainfall characteristics for both the calibration and the validation periods, justifies the operated subdivision and grants the possibility of validating the model, an essential step in verifying that it is able to produce simulated values closer to the observed ones for periods different from the calibration one.
On the SWAT+ Toolbox, calibration can be performed in two ways: manually or automatically. The manual and automatic calibration interfaces are illustrated in figure 3.25. The values shown in the parameters form of the figure are just random numbers and are not the ones generated during the automatic calibration that was executed. Instead, in the panel related to indices performance for channel 1 and channel 32, the values of the Nash-Sutcliffe efficiency (NSE), root mean square error (RMSE) and percent bias (PBIAS) are the real ones obtained after the first run of the SWAT+ Editor, before any kind of calibration or sensitivity analysis was performed. Those indices values will be discussed more in details in the next chapter.
In the case of a manual calibration, the user can manually change the value of a parameter from the respective section under the tab "Value". Those parameters

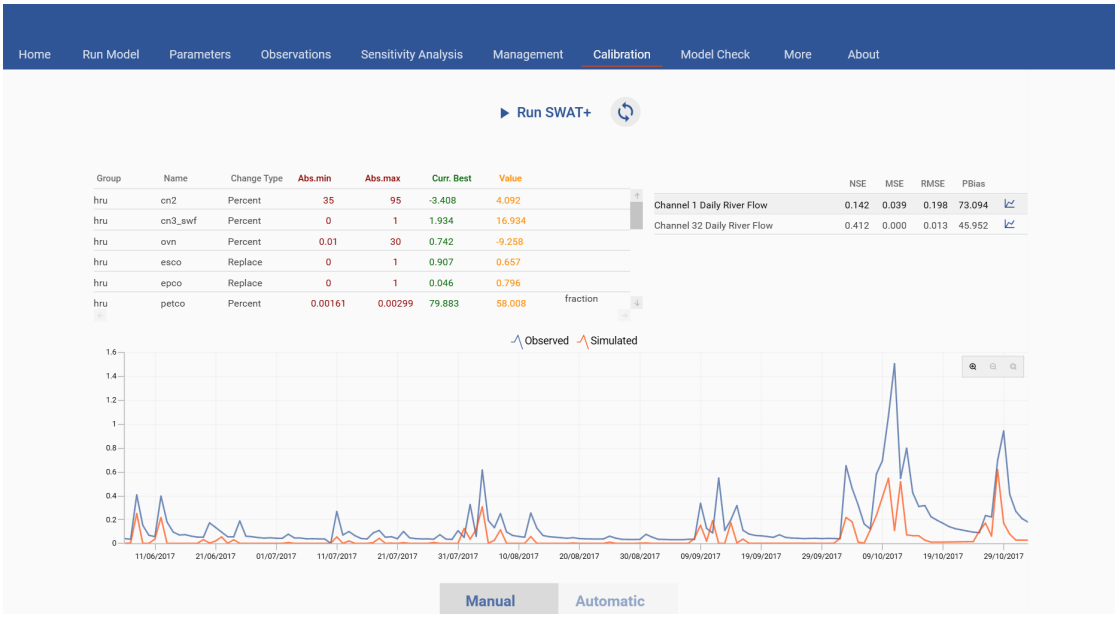

(a) *Manual calibration interface*

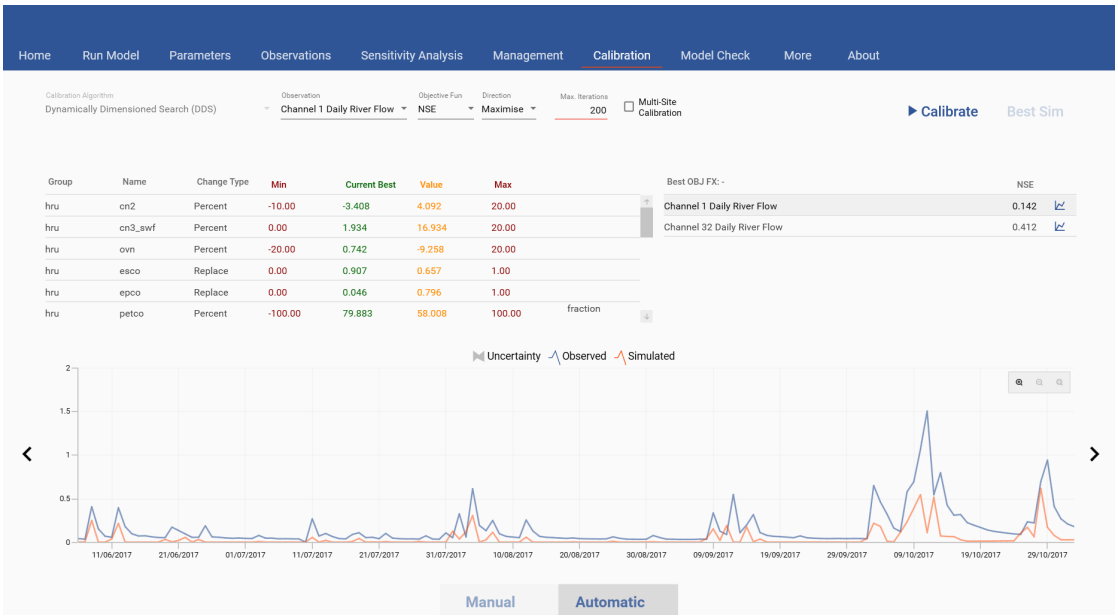

(b) *Automatic calibration interface*

Figure 3.25: SWAT+ Toolbox calibration interfaces

are the most sensitive ones, identified through the Sobol sensitivity analysis. The "Current Best" column reports the parameter value that currently has the best improvement effect on the model performance. After every change, the user can

always run the model and refresh the interface to see the new estimated performance indices. It is possible to go through these steps until satisfactory results are obtained. In this study, manual calibration was only used as a preliminary step for the automatic procedure to refine the extremes of the variation range of each parameter that, at first, were imposed based on a quantification of the increase or decrease related to the parameter's definition. By doing this, the parameters' variability ranges are narrowed, allowing the software to search the optimal value within a more restricted interval. Obviously, the change in the value of a parameter was imposed considering its impact on the simulated streamflow trend, and the more the performance indices improved, the more the ranges were circumscribed around the change value that produced that improvement.
The performance indices through which the SWAT+ Toolbox evaluates model performance are:

- The Nash-Sutcliffe efficiency (NSE)
- The Mean Squared Error (MSE)
- The Root Mean Square Error (RMSE)
- The Percent Bias (PBIAS)

The Nash-Sutcliffe efficiency (NSE) is a widely used statistical technique in the field of hydrology to assess how well a model is able to predict observations, evaluating the goodness of the fit between measured and simulated values [100]. It is a normalized statistic used to assess the proportion of residual variance (referred to as "noise") in relation to the variance of the measured data (referred to as "information") [101], and is computed by subtracting the ratio between the error variance of the modeled time-series and the error variance of the observed time-series from 1, as it can be seen from its formula:

$$NSE = 1 - \left[\frac{\sum_{i=1}^{n} \left(Y_i^{obs} - Y_i^{sim} \right)^2}{\sum_{i=1}^{n} \left(Y_i^{obs} - Y^{mean} \right)^2} \right] \tag{3.6}$$

where Y_i^{obs} is the ith observed value, Y_i^{sim} is the ith simulated value, Y^{mean} is the mean of the observed data and n is the number of observations [101]. The NSE ranges between $-\infty$ and 1, where NSE = 1 indicates a perfect fit between simulated and observed values, $0 < \text{NSE} < 1$ relates to acceptable levels of performance, NSE = 0 signifies that the model predictions are as precise as the mean of the observed data, and $\text{NSE} < 0$ refers to an unacceptable performance, indicating that the model predictions are worse than the mean of the observed data [102]

[103]. Several authors recommended the use of NSE to evaluate the performance of rainfall-runoff models due to its frequent implementation over the years, which extended its ability to provide information about reported values, and the fact that it constitutes the best objective function for representing the overall fit of a hydrograph, as found out by Sevat and Dezetter (1991) [103] [104] [104].
The Mean Squared Error (MSE) and the Root Mean Square Error (RMSE) are two error indices used to evaluate model performance, measuring the difference between predicted and actual values [103]. The RMSE is basically the square root of the MSE, represents the standard deviation of the residuals and its formula is given as follows:

$$RMSE = \sqrt{\frac{1}{n}\sum_{i=1}^{n}\left(Y_i^{obs} - Y_i^{sim}\right)^2} \tag{3.7}$$

where the symbols have the same meaning as before [105]. The lower the RMSE, the closer the fit is to the data and vice versa. The same discussion is valid for the MSE. Their application in hydrological modelling is favored by the fact that they are measured in the same unit as the analysed variable and that they are indices of simple interpretation, accessible to users without a solid statistical background [105]. However, it it important to highlight that the RMSE is sensitive to outliers, with a large impact on its value caused by large errors, and is scale-variant, meaning that the comparison of models through the RMSE is influenced by the scale of the data [106] [107].
The Percent Bias (PBIAS) quantifies the average tendency of the simulated data to either overestimate or underestimate their observed counterparts [108]. It measures the average difference between the predicted and the actual values, expressed as a percentage of the latter [109]. This is clearly visible in its equation:

$$PBIAS = \left[\frac{\sum_{i=1}^{n}\left(Y_i^{obs} - Y_i^{sim}\right)\cdot 100}{\sum_{i=1}^{n}\left(Y_i^{obs}\right)}\right] \tag{3.8}$$

The ideal PBIAS value is 0, with values of low magnitude suggesting accurate model simulation. Positive values signify that the model underestimates observations, while negative values identify model overestimation bias [108]. As the RMSE, the PBIAS is sensitive to outliers, but is not affected by the scale of the data, allowing the comparison of different models. Specifically, in the context of streamflow, a study conducted by Gupta et al. (1999) points out how the index is influenced by the adopted autocalibration method and this impact is more evident during dry periods rather than wet periods [108]. This fact should be taken into account when splitting the observed dataset into a calibration one and a validation one [103]. Furthermore, an aspect that should be highlighted is that, even if the PBIAS

gives an idea about the direction and the magnitude of the error, it has to be used in conjunction with other indicators to have a complete overview of the model performance [109].
From what has been described, it is evident that the SWAT+ Toolbox is provided with statistical indices that give the possibility to have a detailed recap about the goodness of the model and, from the interfaces shown in figure 3.25, it is understandable that a visual inspection is also allowed by the plot of the observed and simulated time series reported in the lower part of the form. This graph changes during each iteration of the automatic calibration as happens for the NSE.
The toolbox implements a Dynamically Dimensioned Search (DDS) algorithm to perform the automatic calibration. DDS is a single-solution-based and a stochastic-based heuristic global optimization algorithm that, at first, searches the optimal parameter value globally across the whole user-specified parameter interval and then, becomes more locally-based as the process continues [110] [111] [112]. It is designed to find good solutions quickly within the pre-specified maximum number of iterations, exhibits efficient scaling with both the number of dimensions and the model evaluations employed to explore the parameter space, and demands minimal parameter adjustment [112] [113]. It also shows a good efficiency in performing autocalibration of computationally expensive hydrologic models characterized by a significant number of parameters [112]. The steps through which the DDS operates are shown in figure 3.26.
This one highlights the presence of three operators incorporated in the algorithm: sampling operator, perturbing operator, and decision operator [114]. The sampling operator, governed by the probability of sampling criteria (P), chooses a subset of decision variables from the complete set of decision variables. The mentioned probability (P) is a function that steadily decreases with each iteration (i) and is subjected to a maximum number of function evaluations (m) as defined by the following relation [114]:

$$P = 1 - \frac{ln(i)}{ln(m)} \tag{3.9}$$

During each iteration, the sampling operator assigns a uniformly distributed random number between 0 and 1 to every decision variable [114]. It perturbs a decision variable if the assigned random number is less than the sampling criteria probability. In this way, it generates new candidate solutions (used to update the current best solution) in the search space by randomly selecting a point in the search space and perturbing it to create a new candidate solution [114].
The perturbing operator controls the size of the perturbation applied to the selected point by the sampling operator and introduces changes to the current best solution to create a candidate solution for a chosen decision variable selected by the previous operator [114]. For the others, the current best solutions remain the candidate ones.

Finally , the decision operator is responsible for deciding whether the new candidate solution should be used to update the current best solution or not [114]. This decision is essentially based on the evaluation of the objective function value that, if it is higher than the current best value, becomes the new best solution [114].

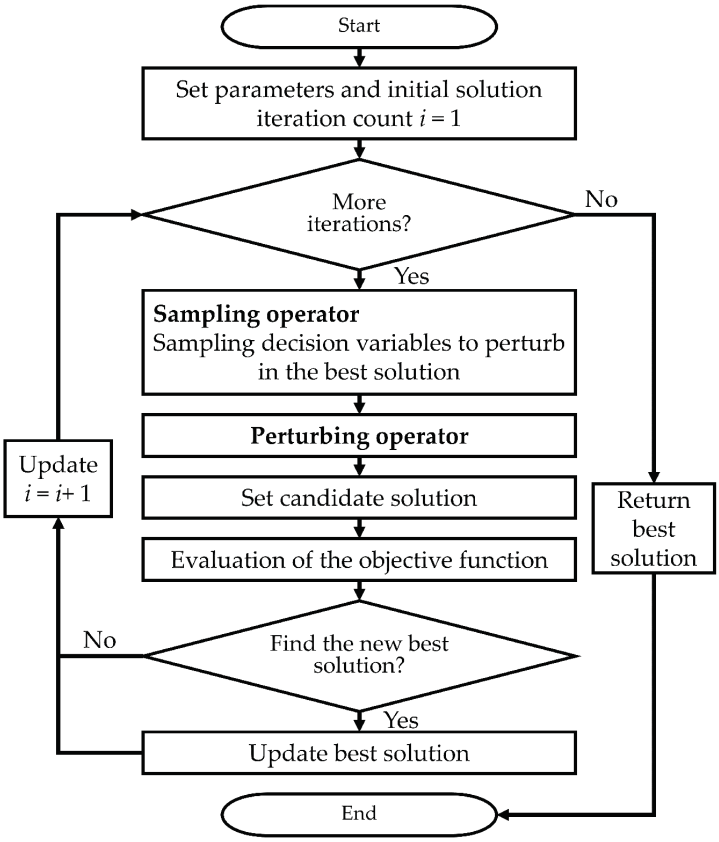

Figure 3.26: Steps in the DDS algorithm [114]

This is basically what happens during one iteration of the DDS algorithm. The objective function is the element through which the algorithm evaluates model performance and can be one of the three statistical indices: NSE, MSE and RMSE. Purpose of the DDS is to maximize (in the case of NSE) or minimize (in the case of MSE and RMSE) the objective function. In this study, the algorithm operates through the assessment of the NSE, so the process should maximize the results.
Various studies pointed out the robustness and the efficiency of the DDS, finding it to be more efficient and effective if compared with other optimization methods like the Adaptive Simulated Annealing (ASA), the Covariance Matrix Adaptation Evolution Strategy (CMAES) and the Shuffled Complex Evolution (SCE) algorithms [112] [115]. That is one of the main reasons why it is implemented on the SWAT+ Toolbox, even if future updates will probably conduct to the integration of additional

calibration methods.
Now that the way through which sensitivity analysis, calibration and validation were performed in this study, has been explained both from a theoretical and a practical point of view, it is possible to go through the results of all the simulations executed, discussing the outputs, assessing their accuracy and comparing them to the results of other studies elaborated in similar climate conditions as the Haaganpuro catchment.

Chapter 4

Results and discussion

The analysis of the study area (Haaganpuro catchment), the data necessary to build the SWAT model and the methods that allowed its setup and calibration was fundamental to really understand how the results, presented in this chapter, were obtained and how they were affected by all the assumptions made during the development of the model. In particular, this section presents, at first, the flow outputs generated by the first run of the SWAT+ Editor for the period June-November 2017 to allow their comparison with the streamflow observations that refer to the same time interval. Then, the report proceeds with an overview of what was done during the sensitivity analysis phase, from the choice of the potential calibration parameters to the selection of the most sensitive ones which are consequentially calibrated to guarantee a good fit between predictions and observations. Therefore, the results of the automatic calibration and validation stage will be presented, together with an assessment of the reached performance level, through an evaluation of the three statistical indices: NSE, RMSE, PBIAS. Once the model is calibrated and validated, the SWAT+ Editor is run again to generate surface runoff values for each year included in the decade 2012-2022, only considering the months form May to November and skipping winter months due to a lack of observed data for that period and the limited time to develop a snow model. The simulated runoff outputs for the mentioned period will be compared to the results of other hydrological studies conducted in Finland or in places with climate characteristics similar to the Finnish context. In this way, the accuracy of the SWAT model in predicting runoff in the Haaganpuro basin will be assessed, the contribution of stormflow to runoff generation will be quantified, and the runoff volume will be separated in the one coming from urban areas and the one coming from more natural areas, in order to compute the share of flow that originates from regions drained with a stormwater piping system against more natural park areas.

4.1 First SWAT+ run and comparison of model outputs to observations

The first run of the built SWAT+ model, set up according to the procedures explained in the previous chapter, was performed for the period June-November 2017 and generated the simulated daily streamflow values to be compared with the observed ones. The software calculated the flow for all the 33 channels flowing through all the 33 landscape units (LSUs) identified by the model. The observations, instead, reported the flow measurements only for channel 1, the catchment's outlet, and channel 32, assumed as representative of the Lansi-Pakila urban area. The comparison was adopted for these two channels in order to allow the selection of the most sensitive parameters affecting flow, the calibration of urban drained areas and the overall calibration of the whole basin. The graphs showing this comparison are reported in figure 4.1 for both channels. The figures also report the values of the performance indices (NSE, RMSE, PBIAS) used to evaluate the fitness of the data.

From their analysis, it is possible to understand how badly the first run of the model underestimates the observations in both cases, as it is testified by the large positive values assumed by the PBIAS: 73.1 % for the catchment's outlet, 45.9 % for Lansi-Pakila. These values highlight a performance that is even worse in the case of the basin's outlet, as it is also confirmed by a NSE close to 0 against a value of 0.412 for Pakila. In fact, as suggested by Santhi et al. (2001), a satisfactory fit between simulations and observations is reached when the NSE is higher than 0.500, so in both cases improvements are needed to increase the mentioned index [116]. However, a NSE value above 0.500 does not guarantee a good model performance since the PBIAS value must be also taken into account. Concerning this fact, Van Liew et al. (2007) consider as unsatisfactory an output characterized by a PBIAS > 25 %, with the consequence that an equal agreement between the two indices must be found [117].

The main problems depicted from figure 4.1 are related to the concepts of base flow and peak flow. The first one defines the contribution of groundwater to streamflow, while the second one identifies the maximum flow of a river developed as a response to a rainstorm event. Simulated base flow constitutes a common issue for both catchment's outlet and Pakila area, with a tendency to assume a null value for most of the days when there are not significant rainfall events. This discrepancy is highlighted by the trend of the measured base flow which, even during the drier days, assumes values different from zero. From this fact derives a necessity to increase this component in order to allow the simulation to replicate reality as close as possible.

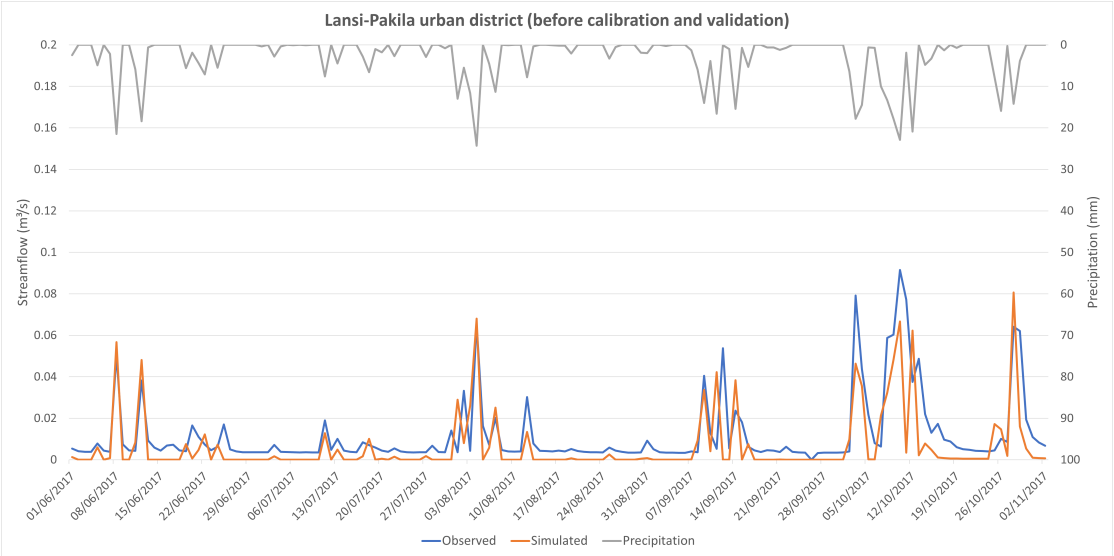

(a) *Streamflow from Lansi-Pakila*

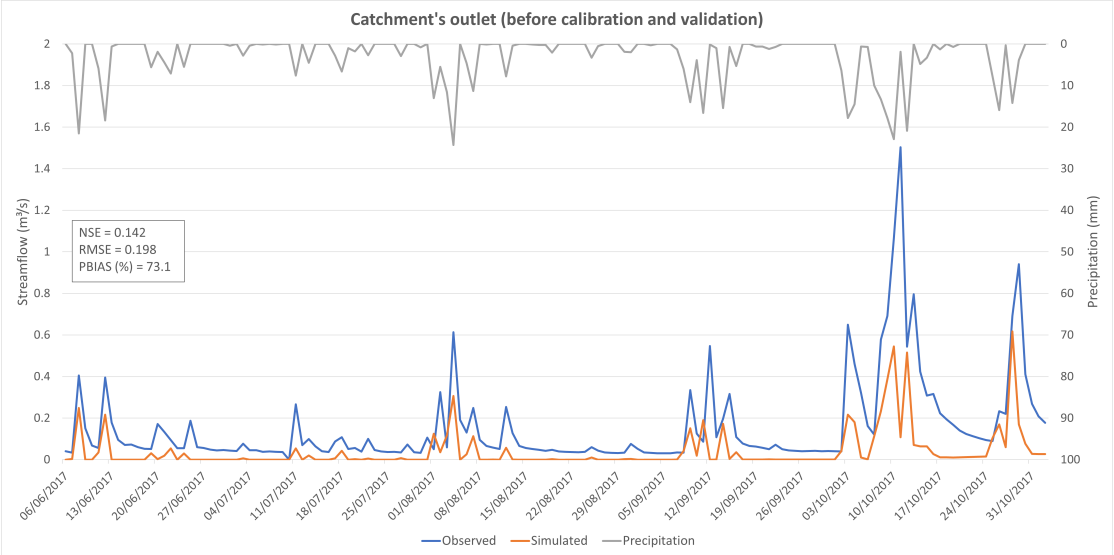

(b) *Streamflow from catchment's outlet*

Figure 4.1: Observed vs simulated streamflow for June-November 2017

The factors that can determine a low level of base flow are strictly related to groundwater storage and dynamics, as it is possible to understand from its definition. For example, a low groundwater recharge can produce a low base flow condition, due to a lower groundwater contribution to streamflow. This phenomenon is usually caused by low precipitation, human activities, land use changes and high evapotranspiration. Specifically, in the case of figure 4.1, the flow values are simulated for a period that covers summer months, when generally evapotranspiration levels are higher due to extended hours of sunlight, especially in the Nordic countries such as Finland that, during this season, experiences a prolonged daytime, with more time available for evapotranspiration to happen. In this way, the reduction in the groundwater storage and recharge is larger, if compared with winter months, since stormwater infiltrating into the soil and reaching the acquifer is lower and water losses are higher. Also, always looking at figure 4.1, in both plots the low base flow levels seem to coincide with the days characterized by low precipitation intensity which, together with the high summer evapotranspiration rates, deeply decreases the water available for groundwater recharge. From what has been said, a first idea for the execution of the sensitivity analysis could be referred to a consideration of the parameters affecting evapotranspiration to see if their change has an impact on groundwater and, consequentially, on base flow, confirming if the studied case is characterized by the existence of a link between the two.
Another factor impacting base flow is connected to a parameter named "ALPHA", defined as the base flow alpha factor and measured in units of inverse time (1/days) [55]. It regulates the rate of groundwater flow from the shallow aquifer to the stream channel and gives insights about groundwater flow reaction to alterations in recharge. It represents a fundamental parameter for modelling base flow and, for this reason, it was taken into account among the set of potential parameters subjected to sensitivity analysis. Probably, according to the results of figure 4.1, ALPHA should be increased since, regularly, a low value can lead to low base flow.
Concerning peak flow, the situation is not the same for the catchment's outlet and Pakila. For the latter (figure 4.1a), modelled peak flow resembles most of the peaks in the observed streamflow trend, even if some adjustments are needed for the ones that are underestimated. For the outlet (figure 4.1b), instead, peak flow is badly underpredicted and assumptions must be done to improve model performance. However, in both cases, the simulated peaks are placed in correspondence of the pinnacles registered in the precipitation trend that identify the strongest rainfall events. Also, even though in most cases there is an underestimation problem, the model outputs peak flows during the same day as the measured ones, as it can be seen from figure 4.1. This kind of agreement between simulated peak flow, observed peak flow and precipitation, indicates how SWAT+ is able to simulate peak flow at the right time and recognize that, to a rainstorm event of strong

intensity, corresponds a consistent contribution of stormflow to channels which determines a significant increase in their discharge, identified as peak flow.
In order to identify which can be the potential parameters linked to the mentioned underestimation of observed peak flow, it is useful to examine all the causes that can lead to a low modelled trend. A first possible reason can be related to low surface runoff volumes that can lead to reduced water amounts flowing over surfaces to water bodies. This fact can be related to a wrong set up of the SWAT parameter "CN2" (the curve number) which controls runoff generation in the various areas of a watershed. The CN2 should be set according to the land use of the considered region since not all areas act the same in terms of runoff production. This fact is extremely fundamental in this thesis, especially considering its purpose of separating the contribution of urban areas to surface runoff from that of more natural/park areas. It is evident that the two kind of land uses can not be characterized by similar curve number values since the processes involved in the development of runoff are different in the two cases. For a natural area, the surfaces are mostly permeable, allowing water to infiltrate and recharge groundwater, with a consequent smaller amount of runoff produced. Instead, a built up area is characterized by a large collection of impermeable surfaces that block or reduce infiltration rates, allowing more water to flow over them during a rainfall event. In this last case, runoff generation is higher and, sometimes, can reach extreme levels that might lead to flooding phenomena in an urban context with consequent inconvenience for the population, city's services and urban flow management. This overview gives a first input on the pressure that climate change is putting on stormflow urban management networks that was highlighted in the introduction to this thesis.
Generally, a low CN2 means low runoff potential, while a high CN2 indicates high runoff potential [43]. Following this principle, the CN2 adjustments should be made in the perspective of enhancing the parameter value for urban areas and reducing it in the case of more natural areas, if needed. The analysis of the model outputs shows that SWAT assigns a curve number value of around 55-75 to the basin's urban districts and a value between 45-65 for its natural areas. These results give a proof about the ability of the software to model built up areas with a higher curve number than natural areas, reflecting the data provided in the land use map and confirming the operated division of LSUs in urban and park areas mentioned in figures 3.20b and 3.21. However, some studies conducted by Zhang et al. (2019) and Koltsida et al. (2021) found that the proper urban curve number range is from 80 to 95 with an average value of 88-89, whereas the CN2 interval for natural areas goes from 30 to 80, based on the vegetation cover and soil types [42] [118]. From what has been said, it is clear that the assigned SWAT curve number values could be representative of the selected natural areas, but need to be increased in the case of built up areas. This description sets the basis for the curve number to be considered among the potential parameters interested in the sensitivity analysis

phase.
Other parameters crucial for peak flow estimations are "ALPHA" and "AWC". The first one was previously described concerning base flow, but it is considered effective also for peak flow since an increase in its value causes an increase in base flow, which in turn determines a consequent rise in peak flow levels. The second one is defined as the available water capacity of the soil layer and is measured in mm H20/mm soil [55]. It refers to the volume of water that a soil layer can retain for the purpose of nourishing plants and can affect peak flows in several ways. In fact, AWC has impacts on infiltration rates and soil moisture. A high AWC identifies a condition in which the soil is able to hold a greater amount of water, thereby increasing soil moisture content, minimizing surface runoff and promoting greater water infiltration into the soil. This fact leads to a larger water storage in the soil and a corresponding decrease in peak flow, justifying the need to reduce the parameter's value to produce a rise in the peaks that characterize the simulated flow curve.
The parameters, and the relative phenomena described above, are the first and most obvious ones that come to mind when talking about base flow and peak flow. They also are used to enrich the explanation of the processes that lead to an increase or a decrease in their rates and for this reason, they were presented in this paragraph. They were basically selected according to their definition and knowledge about how they work. In the next section, other additional potential parameters will be considered always based on their meanings, but also on suggestions derived from literature. Then, this potential set will be subjected to a sensitivity analysis that will circumscribe the collection to the most significant ones.

4.2 Parameter's sensitivity analysis, calibration and validation

4.2.1 Sensitivity analysis results

From what has been presented in the previous paragraph, the discussion clearly underlines that the initial run of the simulation represents a situation of low simulated base flow, low peak flow and high evapotranspiration. Abbaspour et al. (2015) analyzed a case with the same conditions and deduced the parameters and the action through which they should undergo to improve model performance in a context as the one generated by the first SWAT+ run [58]:

- For too little base flow: REVAP_CO (decrease), REVAP_MIN (increase), FLO_MIN (decrease)
- For too high evapotranspiration: ESCO (decrease)

- For too little peak flow: CN2 (increase), AWC (decrease)

All these parameters were taken into account in the potential set. Some of them, as CN2 and AWC, were described above, others are still to be deepened. However, it is already possible to notice how they basically rotate around the major spheres of evapotranspiration, soil, groundwater and surface runoff, and this is valid for all the additional parameters that still need to be mentioned.
As already said when discussing the methods, the algorithm applied to perform the sensitivity analysis was the Sobol one, for all the advantages testified by the discussed studies. This means that the parameters were classified according to a first-order sensitivity index, going from the one characterized by the highest index value to the one corresponding to the lowest. Table 4.1 reports a list of the potential parameters selected to undergo the Sobol sensitivity analysis which was performed for both Pakila (and the basin's urban areas) and the whole Haaganpuro basin (including forested/park areas). A total of 19 potential parameters belonging to three main groups: HRUs, soil (SOL) and aquifer (AQU), was considered. The table also reports, for each of them, their definition and the respective change method (which depicts the way through which they are increased or decreased).
Gan et al. (2014) suggested a minimum number of iterations equal to 1050 to compute the first-order sensitivity index in a correct and an efficient way [93]. For this reason, the Sobol sensitivity analysis was performed on the SWAT+ Toolbox by setting a sample size of 1200 samples for both Pakila and catchment's outlet. The most sensitive parameters were almost the same for both cases. As it was expected, parameters like CN2 and AWC ranked among the most sensitive ones. The collection also included the additional parameters controlling evapotranspiration, soil, elevation and lateral flow. The main difference between the relevant parameter sets for Pakila and the whole basin relates to the aquifer (AQU) group, which was found to be significant for the latter, but mostly irrelevant for the urban district. In order to deeply understand the link between the parameters and the relative processes, it is better to separate the discussion of the two cases.

Group	Parameter	Change Method	Description
HRU	CN2	Percent	Curve number
HRU	CN3_SWF	Percent	Pothole evaporation coefficient
HRU	OVN	Percent	Manning's "n" value for overland flow
HRU	SLOPE	Percent	Average slope steepness in HRU (m/m)
HRU	SLOPE_LEN	Percent	Average slope length for erosion (m)
HRU	ESCO	Replace	Soil evaporation compensation factor
HRU	EPCO	Replace	Plant uptake compesation factor
HRU	PETCO	Percent	Potential evapotranspiration
HRU	CANMX	Relative	Maximum canopy storage (mm H20)
HRU	LAT_LEN	Percent	Slope length for lateral subsurface flow
HRU	LATQ_CO	Percent	Lateral flow coefficient
SOL	K	Percent	Saturated hydraulic conductivity (mm/hr)
SOL	BD	Percent	Moist bulk density (Mg/m3)
SOL	Z	Percent	Depth from soil surface to bottom of layer (mm)
SOL	AWC	Percent	Available water capacity of the soil layer (mm H20/mm soil)
AQU	ALPHA	Replace	Baseflow alpha factor (1/days)
AQU	REVAP_CO	Replace	Groundwater "revap" coefficient
AQU	REVAP_MIN	Percent	Threshold depth of water in the shallow aquifer for "revap" or percolation to the deep aquifer to occur (mm H2O)
AQU	FLO_MIN	Percent	Minimum aquifer storage to allow return flow (m)

Table 4.1: Potential parameter set selected to undergo Sobol sensitivity analysis for Pakila urban district and the whole Haaganpuro basin

Lansi-Pakila and urban areas

The sensitivity analysis of the Lansi-Pakila district and the basin's urban areas was the first to be performed. The Sobol algorithm generated as the most significant parameters for streamflow, the ones controlling surface runoff, evapotranspiration, lateral flow and the hydraulic properties of the soil. Specifically, the curve number (CN2) was found to be the overall most sensitive parameter, indicating the need for an increase in its value that, as highlighted in the previous paragraph, should reenter in the range 80-95 defined by Zhang et al. (2019) and Koltsida et al. (2021). In this way, runoff contribution from urban areas to channels is increased, determining a consequent rise in the levels of peak flow. Always concerning parameters affecting surface runoff contribution to streamflow, the Manning's "n" value for overland flow (OVN), conceived to calculate the frictional resistance of water as it flows over the surface, did not rank among the relevant parameters as well as slope length (SLOPE_LEN), while slope steepness (SLOPE), lateral flow coefficient (LATQ_CO) and slope length for lateral subsurface flow (LAT_LEN) were identified as effective for the impact of lateral flow on channels' water amount. Lateral flow refers to the horizontal movement of water within the soil profile that enters the main channel during a given time step. This phenomenon takes place when the soil's moisture level surpasses its capacity to retain water [55]. The combined outputs of the Sobol algorithm and the manual calibration pointed out that an overall increase in lateral flow was essential to make both base flow and peak flow grow. In fact, a greater volume of later flow entails a larger water amount for both groundwater recharge and streams.
As said in the methods chapter, a manual calibration was done before going through an automatic procedure to identify the ranges of variation of each parameter and to clearly define their direction of change (increase or decrease), fundamental for the Dynamically Dimensioned Search (DDS) algorithm, applied to perform the automatic calibration, to find the optimal value in the shortest time and with the lowest computational cost possible. This means that the manual calibration was used as a sort of test to verify if the supposed ranges and change directions were correct or not.
Concerning evapotranspiration effects on the channels flowing through the Pakila district, and consequentially on all the urban streams, parameters like soil evaporation compensation factor (ESCO), plant uptake compensation factor (EPCO), potential evapotranspiration (PETCO) and maximum canopy storage (CANMX) were all individuated by the software as sensitive for streamflow and all required a decremented value to improve fit between predictions and observations, since the high evapotranspiration rates represented one of the main drivers in the low base flow and peak flow levels. It is interesting to notice from table 4.1 that ESCO and EPCO are some of the few parameters for which a replace change was

adopted, while CANMX was the only one subjected to a relative change. Another evapotranspiration parameter that was considered in the potential set is the pothole evaporation coefficient (CN3_SWF) but it resulted to be not as sensitive as the others.
The soil parameters considered as sensitive by the Sobol algorithm are saturated hydraulic conductivity (K), moist bulk density (BD), depth from soil surface to bottom of layer (Z) and available water capacity of the soil layer (AWC). The reasons why the latter was presumed to be relevant were already explained in the previous section. As said, this parameter has to be decreased to increment peak flow, but attention should be paid to the effect on base flow because a lower AWC implies lower infiltration and less water retain capacity of the soil layer, leading to an increase in the water amount available for runoff production and a reduction in the one able to recharge groundwater storage. This last impact determines less water for base flow generation which can be critical for drier days when the simulated base flow is already zero. This means that a sort of balance in the AWC value should be found to account for both effects. The other soil parameters were also decreased except for K which was subjected to a slight increase. This one is also related to the reduction of the moist bulk density (BD) which can increase the porosity of the soil (and therefore, infiltration) and its hydraulic conductivity, with a following higher groundwater recharge and subsequent rise in base flow, as pointed out by a study elaborated by Andrade (1971) [119].
As previously mentioned, the aquifer parameters were found to be irrelevant in the case of Lansi-Pakila and the considered urban areas of the basin. The Sobol first-order sensitivity index showed a value equal or very close to zero for all of them, indicating no impact on the ability of the model to replicate observations. For the other discussed parameters, the index assumed a positive value, confirming their significance for the calibration phase.

Catchment's outlet

Once the Sobol sensitivity analysis was completed for the Pakila district, the same procedure was repeated, with the same potential parameters set of table 4.1 (now applied to the more natural areas of the Haaganpuro catchment), for the whole basin, focusing on its outlet (channel 1) through which all the water flowing through the watershed converges. The results were very similar to the Pakila case, except for the parameters included in the aquifer group that were found to be relevant only for natural areas. This means that the discussed parameters for urban areas resulted sensitive also for the more natural areas of the basin, with a few differences related to their direction of change, proved also by testing through manual calibration.
These main differences refer to the curve number (CN2) and the moist bulk density (BD). For CN2, an increase in its value was supposed when discussing Pakila and

urban areas, in order to increase their runoff potential generation and reenter in the ranges defined by Zhang et al. (2019) and Koltsida et al. (2021). Concerning natural/park areas, the combination of sensitivity analysis and manual calibration, together with an insight about their common curve number interval given by the same mentioned studies, suggested the need for a slight decrease in the CN2 value which was not too large due to the fact that the value, assigned by SWAT to each HRU, already satisfied the usual CN2 ranges, as discussed in the previous paragraph. However, a slight reduction was needed since the runoff results from natural areas, reported in the LSUs output file, were too large to be representative of the common Southern Finland's surface runoff values. This last topic will be better discussed in the last paragraph of this chapter, when talking about the runoff results generated by the final simulation of the SWAT+ model. The LSUs output file, for the moment, was used to check if the assumed change directions were meaningful or not. Then, it will be reconsidered to extract the needed runoff results.
Concerning BD, in this case, the tests done by means of a manual calibration showed a rising trend in its value for this particular case. However, all of the supposed directions of change must be confirmed by the automatic calibration.
Above all, an important fact to consider is the inclusion of the aquifer parameters among the sensitive set for natural/forested areas. These ones are base flow alpha factor (ALPHA), groundwater "revap" coefficient (REVAP_CO), threshold depth of water in the shallow aquifer for "revap" or percolation to the deep aquifer to occur (REVAP_MIN) and minimum aquifer storage to allow return flow (FLO_MIN). As said in the previous paragraph, ALPHA was one of the most influential parameters for base flow as it regulates the rate of groundwater flow from the shallow aquifer to the stream channel. Its values was assumed to be increased, since a higher ALPHA value causes a larger groundwater amount to be transferred to streams and be converted to base flow. Instead, the other aquifer parameters were decremented since an hypothetical increase in their values determines a rise in evaporation rates up to the potential evapotranspiration ones, with a consequent reduction in the base flow levels, as stated by Koltsida et al. (2021) [42].
From what has been depicted from the separated sensitivity analysis of urban and natural areas, it is clear that all the sensitive parameters identified by the Sobol algorithm, were found to be all valid for natural/forested areas, whereas for more urban regions, the parameters belonging to the aquifer category were identified as irrelevant for calibration purposes. The most sensitive parameters were CN2, AWC, ALPHA (only for natural areas) and the ones connected to evapotranspiration, as it was expected from the analysis of the first run of the SWAT+ model for the period June-November 2017. At this point, this significant collection will undergo through an automatic calibration procedure to verify the accuracy of the assumptions made in this paragraph and to find the best value for

each parameter, able to improve model performance until a satisfactory level. This phase is described in the following section.

4.2.2 Calibration and validation results

The automatic calibration was carried out through the use of the SWAT+ Toolbox, by implementing the only available method to perform it on the mentioned software. This calibration method, as said, is the Dynamically Dimensioned Search (DDS) algorithm that at first, searches the optimal parameter values across the whole variation range defined by the user, and then narrows the analysis around an hypothetical optimal restricted range, identified through the various iterations of the process. The maximum number of iterations was set around 150, since, as pointed out by other SWAT+ users, the DDS algorithm is quite efficient in finding the optimal parameter value and, for this reason, it does not need a high maximum limit of runs. This fact was also verified during the execution of the automatic calibration itself because, after a certain number of iterations, the value of the selected objective function, used to evaluate model performance, did not improve anymore, suggesting the achievement of the maximum performance level with the selected options. The objective function used in this case was the Nash-Sutcliffe efficiency (NSE) which was subjected to a maximization process to try to get its value as close as possible to 1, a number that indicates a perfect fit between predictions and observations. Besides NSE, the percent bias (PBIAS) was also taken into account to assess if the underestimation problems, highlighted in figure 4.1 from the first run of the SWAT+ Editor, were solved or not, quantify the eventual remaining underestimation gap and have a clearer overview about model performance, since NSE alone is not sufficient to evaluate the goodness of the fit between simulated and observed values because it does not provide detailed information about over or underestimation issues. That is why the PBIAS was also considered.
Calibration was performed for the period June-August 2017 starting from urban areas which were calibrated against the streamflow observations coming from the Lansi-Pakila neighbourhood. Then, once a good level of model performance for built up areas was reached, calibration was applied to the whole basin, including natural/park areas and considering the streamflow measurements coming from the outlet of the watershed. Lastly, the model was validated for the months between September and November of the same year for both cases. Calibration and validation results are respectively shown in figures 4.2 and 4.3 for Pakila and urban areas, and in figures 4.4 and 4.5 for the whole catchment, together with the related values of the performance indices.

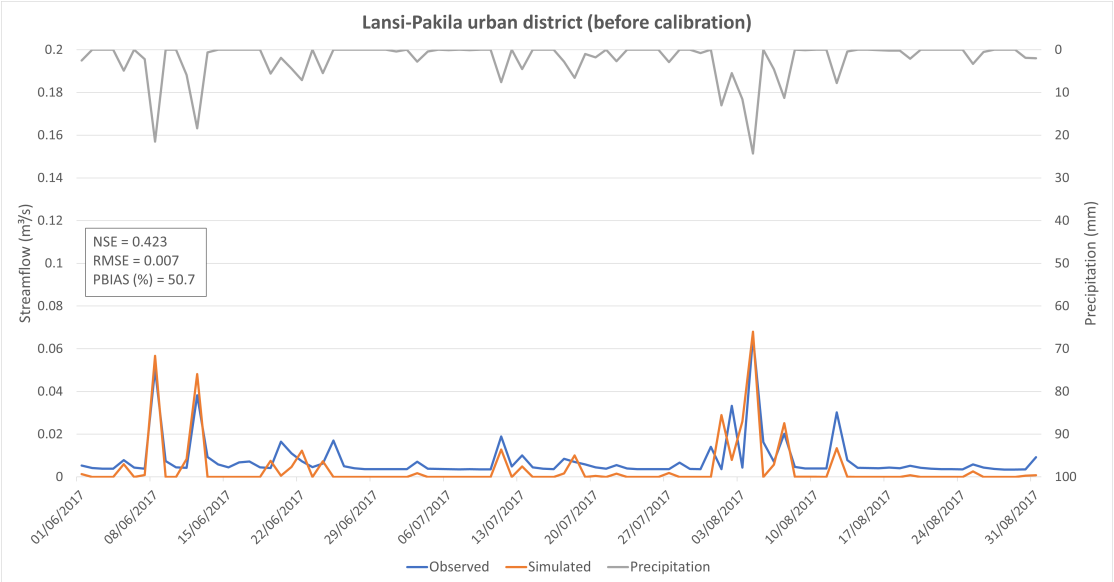

(a) *Before calibration*

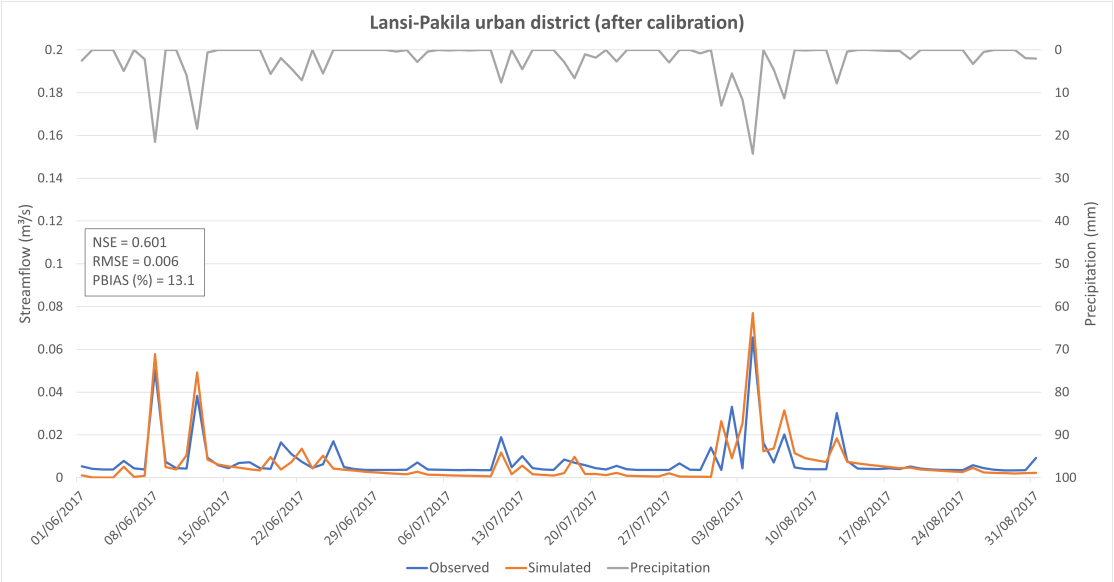

(b) *After calibration*

Figure 4.2: Calibration of basin's urban areas against streamflow coming from Lansi-Pakila (Calibration period: June-August 2017)

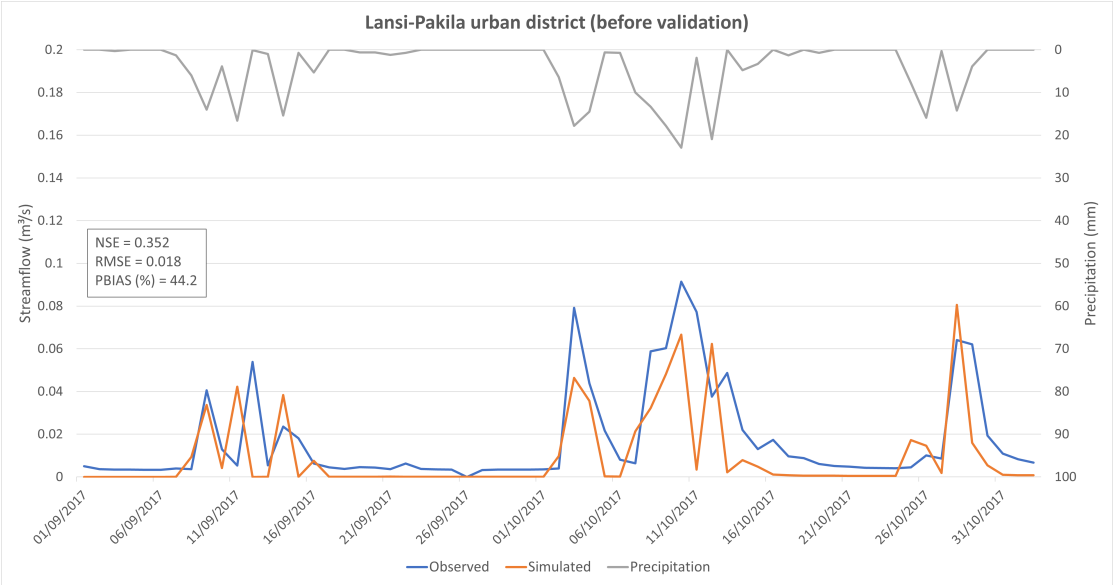

(a) *Before validation*

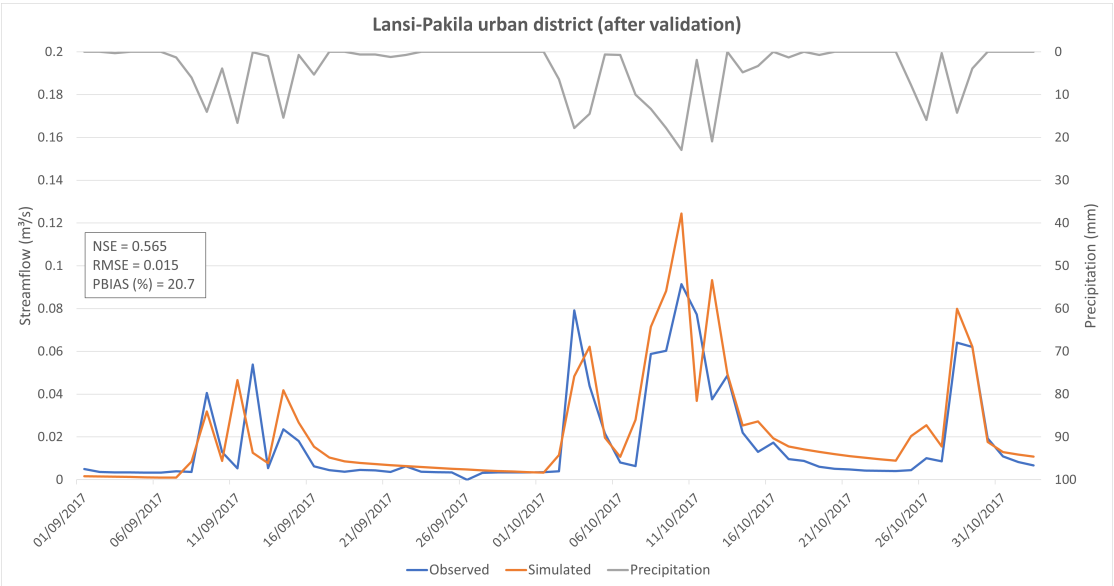

(b) *After validation*

Figure 4.3: Validation of basin's urban areas against streamflow coming from Lansi-Pakila (Validation period: September-November 2017)

Starting from the analysis of the calibration procedure applied to the basin's urban areas against the flow data coming from the Lansi-Pakila district, from figure 4.2 it is evident how the application of the DDS algorithm improved model performance both in terms of fitness of the data and in terms of underestimation issues. In fact, the NSE increased from a value of 0.423 to a value of 0.601, entering the satisfactory range for SWAT calibration defined by Santhi et al. (2001) and reached when NSE is higher than 0.500 [116]. This fact is also confirmed by Saleh et al. (2000), according to whom, the optimal NSE value obtained in this case has to be considered adequate since it falls in the interval included between 0.540 and 0.650 [120]. Concerning PBIAS, instead, its value is subjected to a significant drop, going from 50.7 % to 13.1 %, getting inside the range of good performance rating defined by Van Liew et al. (2007) when the percent bias is between 10 % and 15 % [117]. This drop in the PBIAS is a symptom of an improvement in the underestimation problems. In fact, even by looking at figure 4.2b, it is visible how the gap between observations and predictions related to base flow, which represented the main underprediction issue for the streamflow coming from Pakila, was reduced and the simulated trend better replicates the observed one. Nevertheless, a certain percentage of underestimation is still present, as it is testified by a reached PBIAS value of 13.1 % which, however, can be considered acceptable since it is included in the above mentioned good performance range provided by Van Liew et al. (2007) [117]. Referring to peak flow, the situation is more or less the same before and after calibration because, as said earlier, the model already reproduced peak flow quite well.
The validation of the basin's urban areas (figure 4.3) also shows acceptable levels of performance, even if they are lower if compared to the calibration ones. In this case, the NSE goes from a value of 0.352 to a value of 0.565, always reentering in the satisfactory ranges identified by both Santhi et al. (2001) and Saleh et al. (2000), while the PBIAS drops from 44.2 % to 20.7 %, indicating the achievement of a satisfactory performance in terms of underestimation, as suggested by Van Liew et al. (2007), who consider as satisfactory the PBIAS range between 15 % and 25 % [117]. As it is possible to notice, the validation phase is characterized by a higher underestimation if compared to calibration (PBIAS performance was considered good in this case) and by a higher discrepancy in the representation of the peaks, that sometimes are a little distorted. However, the comparison with the mentioned studies allows to assume an overall acceptable validation performance. The RMSE was reported for both calibration and validation, but its value did not improve so much and was always very close to 0 both before and after the DDS algorithm was applied. This condition is the same for the calibration of the whole Haaganpuro basin and, for this reason, the RMSE will not be analyzed anymore, but will only be shown in the respective graphs.

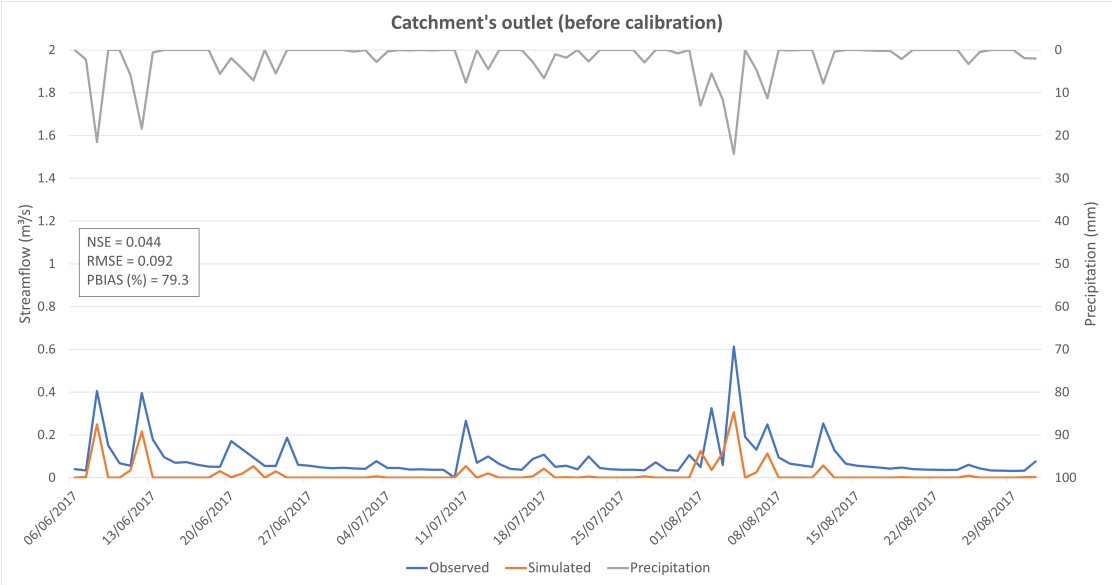

(a) *Before calibration*

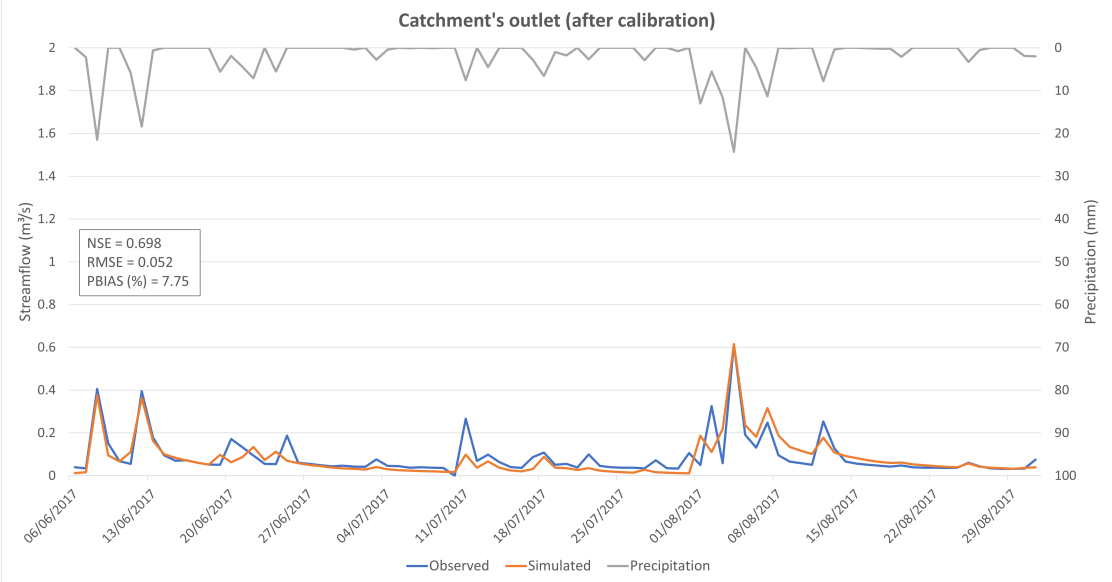

(b) *After calibration*

Figure 4.4: Calibration of the whole basin (including natural areas) against streamflow coming from catchment's outlet (Calibration period: June-August 2017)

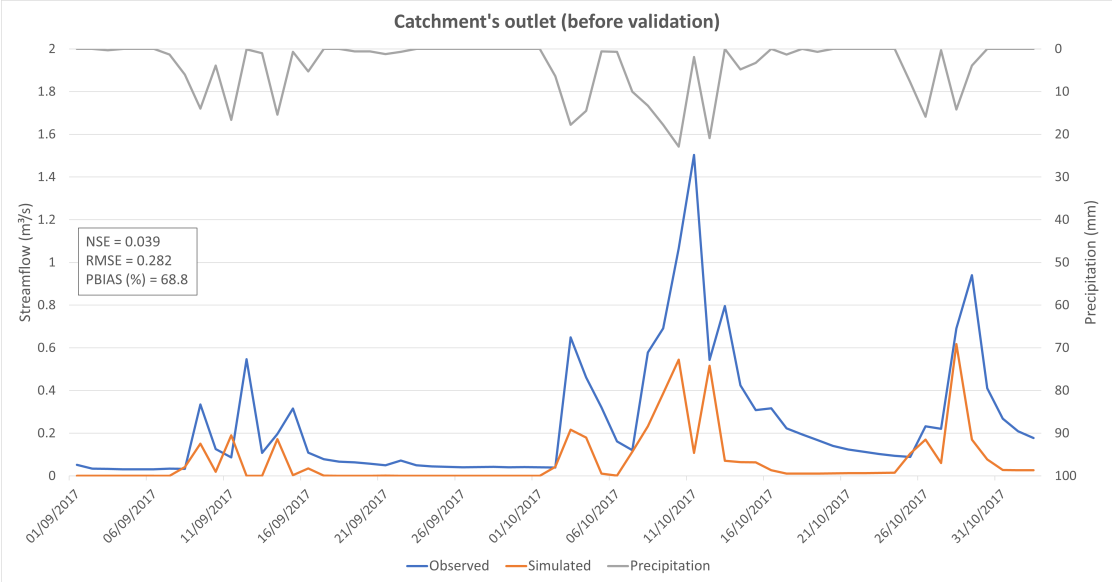

(a) *Before validation*

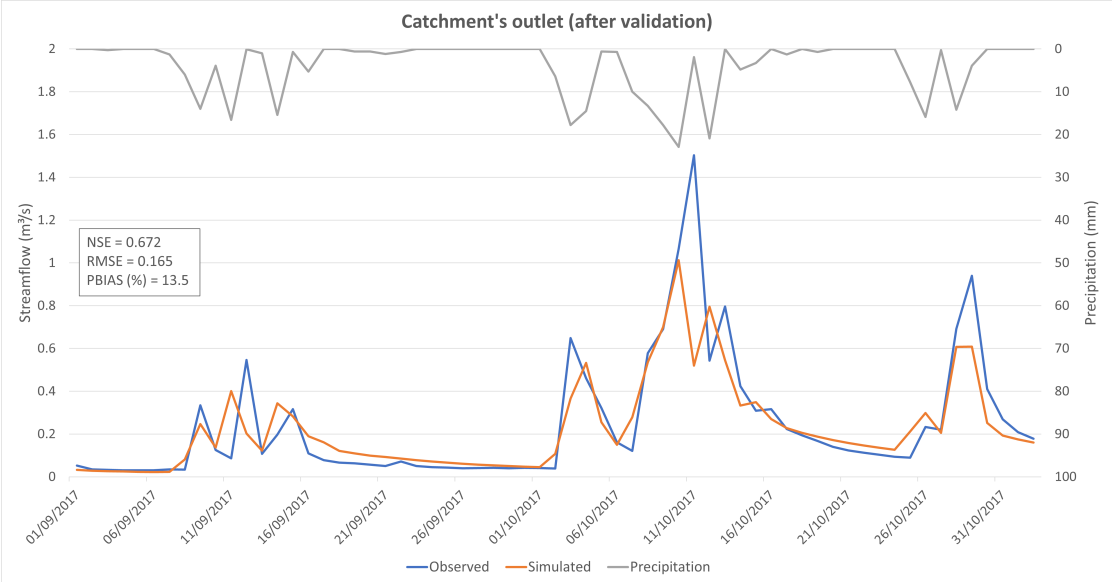

(b) *After validation*

Figure 4.5: Validation of the whole basin (including natural areas) against streamflow coming from catchment's outlet (Validation period: September-November 2017)

Once a good performance level was achieved with the calibration and validation of the basin's built up areas, it was possible to focus on its forested/park areas and consequentially complete the calibration of the whole Haaganpuro watershed. Concerning calibration phase, a significant improvement in the performance indices was registered with the implementation of the DDS algorithm and with the previously calibrated parameter values for urban areas. As it can be seen from figure 4.4, the NSE increased from 0.044 to 0.698, highlighting a very good performance rating due to a NSE value higher than 0.650, as pointed out by Saleh et al. (2000) [120]. The PBIAS dropped from 79.3 % to 7.75 %, a value indicating a very good underestimation level according to Van Liew et al. (2007) [117]. In fact, figure 4.4b shows how both the model reproduction of base flow and peak flow was successfully improved with the DDS algorithm and with the effects of the urban areas' calibration results. Now, both base flow and peak flow are predicted quite well for most of the calibration period, with some remaining underestimation gaps mainly in the month of July.
A similar discussion can be done for the validation phase (figure 4.5), during which the NSE rose from 0.039 to 0.672, and the PBIAS decreased from 68.8 % to 13.5 %, respectively indicating a very good and a good model performance, according to the same studies mentioned above. Even in this case, the model seemed to replicate base flow very well with only some underestimation issues related to peak flows, especially for the ones placed in the month of October that appear to be a little underpredicted.
The overall model performance for Lansi-Pakila and the catchment's outlet, after calibration and validation, for the observation period June-November 2017, is reported in figure 4.6. Concerning NSE, an overall value of 0.597 is identified for Lansi-Pakila, while, in the case of the catchment's outlet, the index assumes a value of 0.721, meaning that a very good fit between streamflow measurements and simulations has been reached, as it can also be visually verified by the plot of figure 4.6b. The goodness of the overall model performance is also testified by a low PBIAS value that, in the case of the basin's outlet, is 7.12 %, indicating that, with the optimal parameters values found by the DDS algorithm, the built SWAT+ model is now able to predict observations with minimal underestimation. The largest gaps between the observed and simulated datasets remain relegated to the month of October, as it was already pointed out. The PBIAS rotates around a similar value also for Lansi-Pakila (figure 4.6a) as it assumes a value of 10.6 %, almost at the border between a good and a very good percent bias. As mentioned above, in this case the NSE is 0.597, representing a satisfactory condition enhanced by a more than acceptable value of the PBIAS. The goodness of these improvements is appreciated even more by comparing figure 4.6 with figure 4.1 which reports the results from the first run of the SWAT+ model.

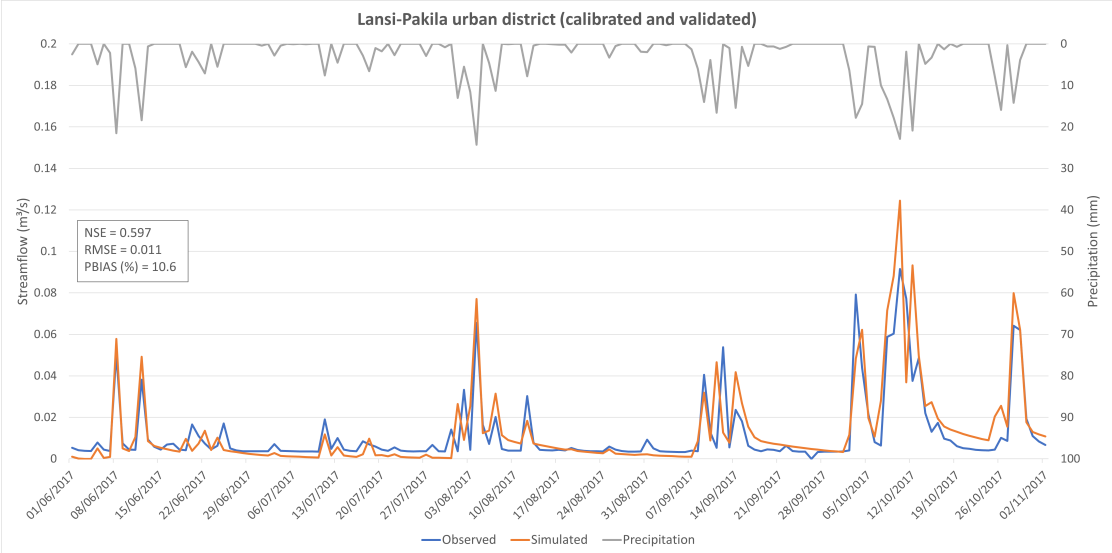

(a) *Lansi-Pakila*

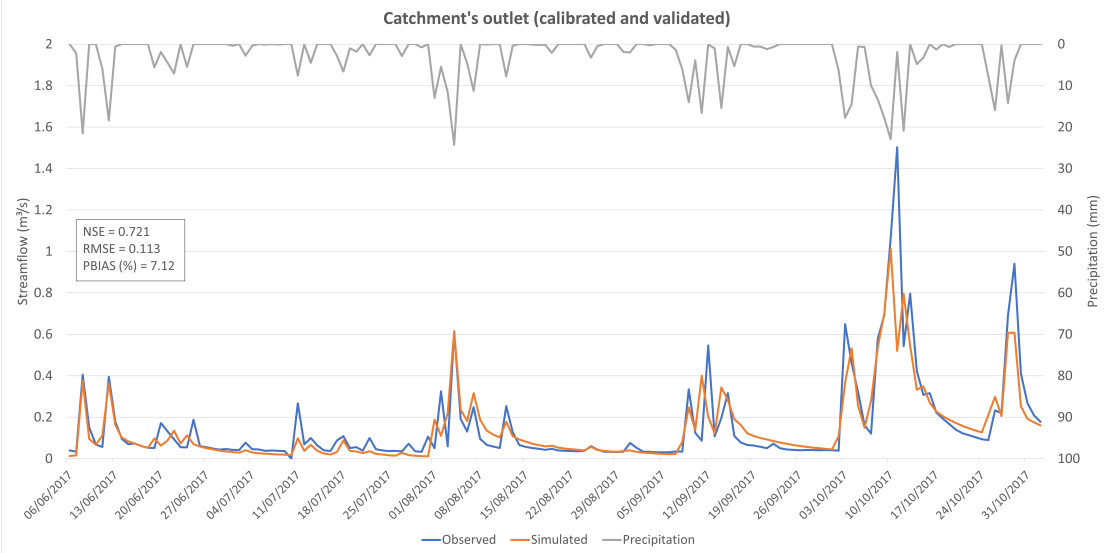

(b) *Catchment's outlet*

Figure 4.6: Calibrated and validated streamflow from Lansi-Pakila and catchment's outlet (Simulation period: June-November 2017)

From the mentioned comparison, it is evident how much the ability of the model in predicting streamflow observations has increased thanks to all the adopted methods and the hypothesis that has been done. In fact, all these insights give proof about the efficiency of the adopted calibration procedure, starting from the selection of the possible potential parameters, their identification through the Sobol sensitivity analysis, to the refinement of their variation range and the definition of their direction of change through manual calibration, and the implementation of the Dynamically Dimensioned Search (DDS) algorithm to perform automatic calibration. This collection of achievements also testifies the goodness of the SWAT+ Toolbox (through which all of these operations were performed) as an useful sensitivity analysis and calibration tool, even if updates are still needed to allow more functions and algorithms to be included in the automatic calibration phase.

Overall, the performance of the built SWAT+ model after calibration and validation is more than satisfactory. The main issues related to base flow and peak flow have been mostly resolved for both urban and natural areas. This resolution was also helped by a change in the PET method which, as discussed in the methods section related to the SWAT+ Toolbox, was shifted from the Penman-Monteith method to the Hargreaves approach. This adjustment was done based on suggestions provided by other SWAT+ users who highlighted an increase in the simulated base flow by adopting the Hargreaves PET equation (3.5). This increment was actually seen also in the case of this thesis even before calibration was performed, justifying the use of the Hargreaves method for the estimation of potential evapotranspirantion, since an almost null simulated base flow trend, and its discrepancy with the measured one, was one of the main problems in the context of this study.

Now that the model is able to replicate observations in a good way and that the optimal values of the sensitive parameters have been rationally chosen by taking into account the different land uses and characteristics of each area of the basin, it is possible to assume that the model is able to produce reliable surface runoff values that can be considered representative of the typical ones in the Helsinki area. However, to be sure about this fact, the runoff outputs will be compared with other hydrological studies from Finland and regions with similar climate properties, allowing an assessment of the reliability of the results and the efficiency of the calibrated SWAT+ model to simulate real runoff volumes.

4.3 Simulation of surface runoff volumes in the catchment's area

Since the beginning, the purpose of this thesis was to model and predict surface runoff (a component of the calibrated streamflow which also includes lateral and return flow) coming from all the various LSUs forming the Haaganpuro watershed, in order to quantify the share of water derived from precipitation that is directly converted to surface runoff. Particularly, this computation was implemented to study how the different land uses and soils, included in the basin, act as a reaction to intense rainfall events and, consequentially, what is their contribution to runoff generation based on their properties and their potential of producing runoff. To satisfy this objective, the LSUs were divided in two main categories: the urban and the forested/park units. The ones predominantly constituted by residential buildings, commercial activities, roads, etc... were assumed as urban, while the ones largely covered by trees, grassland, etc... were classified as natural. As already pointed out several times during this thesis, the impact of these two main groups of areas on runoff generation is totally different from each other, as it is mainly regulated by the curve number (CN2) which, as discussed in paragraph 4.1, assumes a specific range of values for the two cases.
The purpose of this section is to quantify this impact and separate it for the two categories in order to evaluate how large the contribution of stormflow in the two conditions is. This quantification is much more important for built up areas, as it is expected that they are the ones producing the highest runoff volumes, with the consequent need for a greater attention, mainly related to the eventual problem of urban flooding that is finding its way as one of the hottest issues to face and control in the context of climate change. Also, as mentioned in the introduction to this study, the whole Helsinki metropolitan area is experiencing a significant increase in the flooding risk, paving the way for a more detailed modelling of runoff amounts and climate projections, and the development of new solutions able to govern the more frequent extreme events of the future.
The absence of runoff measurements in the Haaganpuro region determines the need to assess the reliability of the reported surface runoff values, simulated through the built, calibrated and validated SWAT+ model, by comparing them with the results of other studies conducted in Finland and in countries with similar weather conditions as the Finnish context. The calibration and validation results showed that the model is now quite reliable in predicting streamflow, of which runoff is an essential contributor, but the validity of the calibrated streamflow can not be fully applied to surface runoff if not assessed through a comparison with other studies' outputs, especially in the absence of relative observations.
This is basically what will be done and discussed in the next paragraphs, starting

from a report of the Haanganpuro's runoff values generated by the SWAT+ model to the final statement about their integrity, supported by specific hydrological studies.

4.3.1 Surface runoff trends

This section presents the simulated surface runoff trends for the months going from May to November of each year included in the studied decade 2012-2022. Winter months were excluded due to a lack in flow observations for the season that were needed to calibrate the model also for that period, and due to a limited time for building a functioning snow model able to efficiently simulate and quantify snowmelt contribution to runoff. SWAT+ uses a temperature-index snowmelt method to predict the snowmelt component, but it needs to be calibrated with proper data in order to be taken as reliable.
All the materials, the methods, the tools, described in the previous chapters, were used to lead to the generation of the runoff trends reported in this section. Even calibration was done, not only by paying attention to streamflow, but also considering the eventual effects of the modified parameter values on surface runoff. In fact, as said in subparagraph 4.2.1, during this phase, runoff values were controlled by looking at the LSUs output file generated by SWAT, to verify if the operated changes produced some meaningless distortions in the numbers. This file is the same from which the runoff values, used to draw the trends reported below, are extracted for each simulation related to a different year in the study period.
The simulated surface runoff trends for the Haaganpuro watershed during the decade 2012-2022 are all reported in figure 4.7 with one plot for each year. In each graph the two contributions of urban and non-urban runoff are shown separately and a secondary axis is included to display precipitation, in order to assess if there is a correspondence between rainfall and runoff peaks, as done for streamflow during the calibration stage.
To enrich the following discussion about the results, table 4.2 shows the cumulative precipitation and runoff values over the months between May and November for each year, quantifying, in this way, the share of precipitation amount that turns into urban and non-urban runoff, and facilitating comparison between the two.

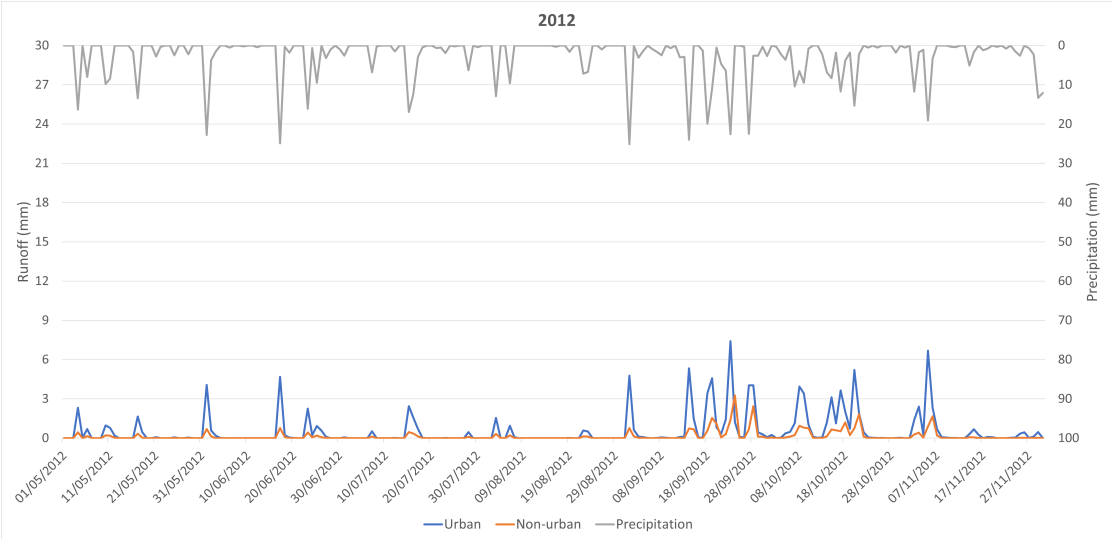

(a) *2012*

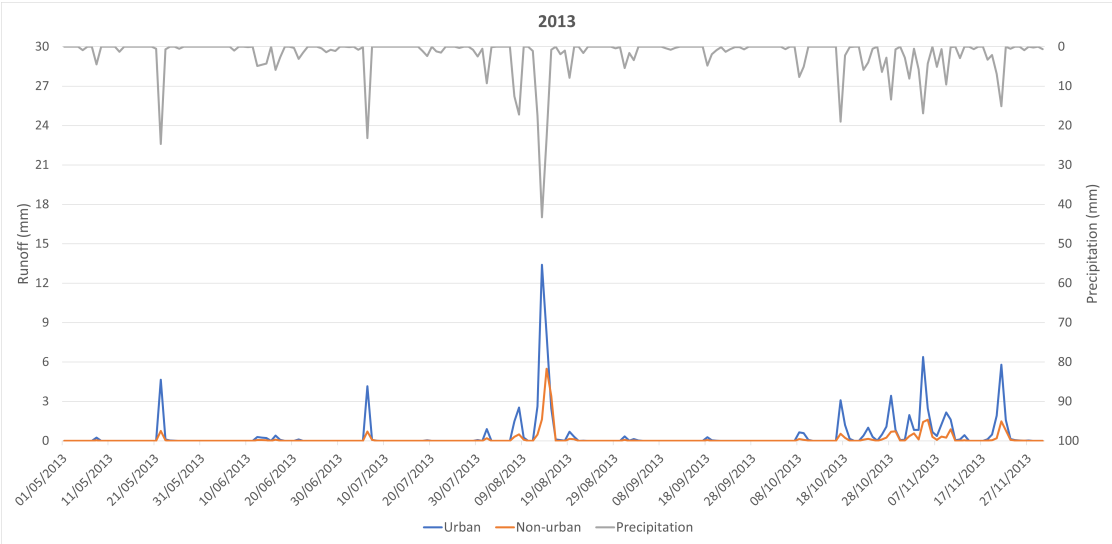

(b) *2013*

Figure 4.7: Simulated surface runoff for the months May-November of each year included in the decade 2012-2022

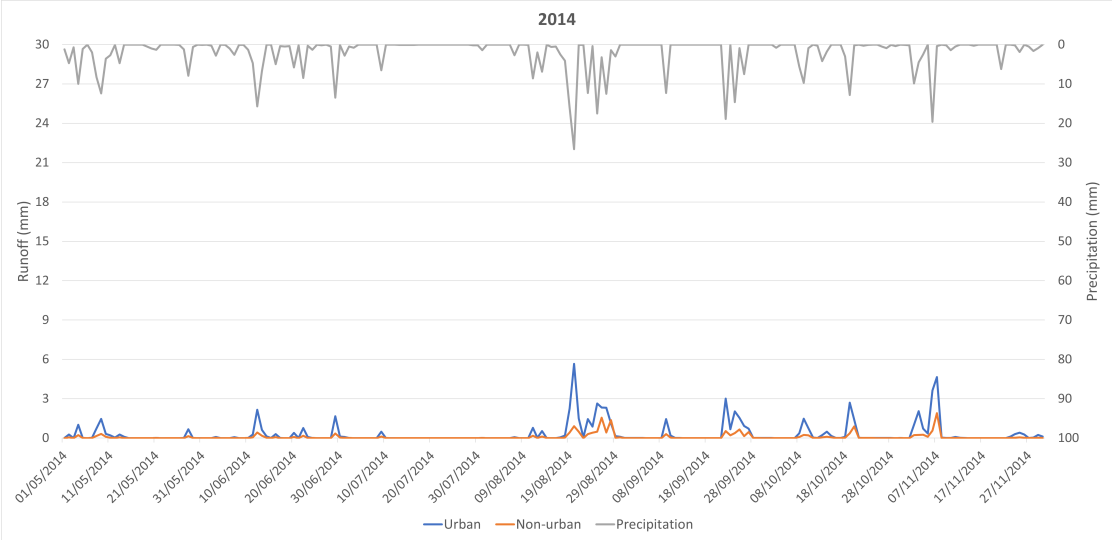

(c) *2014*

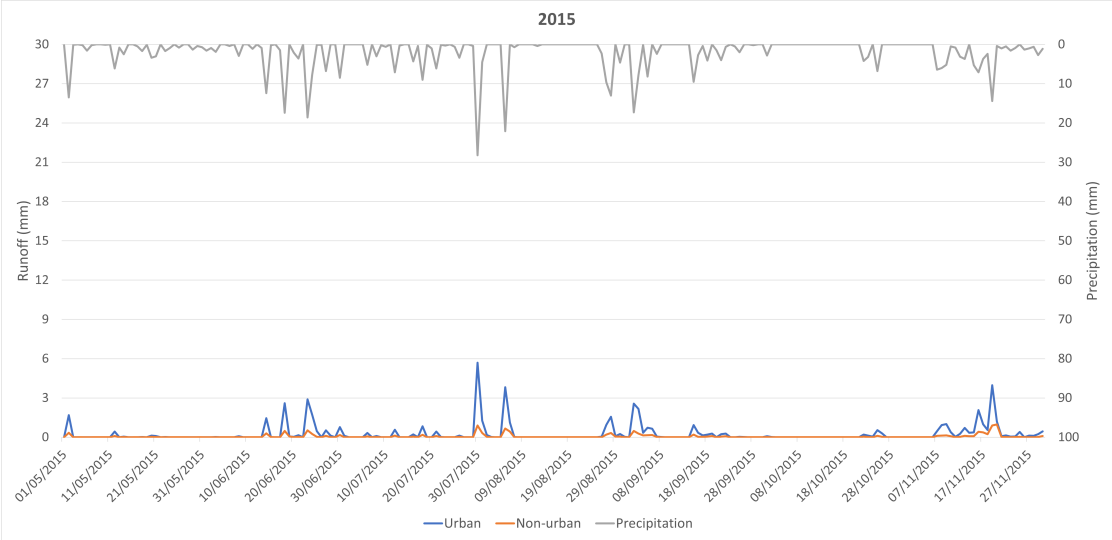

(d) *2015*

Figure 4.7: Simulated surface runoff for the months May-November of each year included in the decade 2012-2022

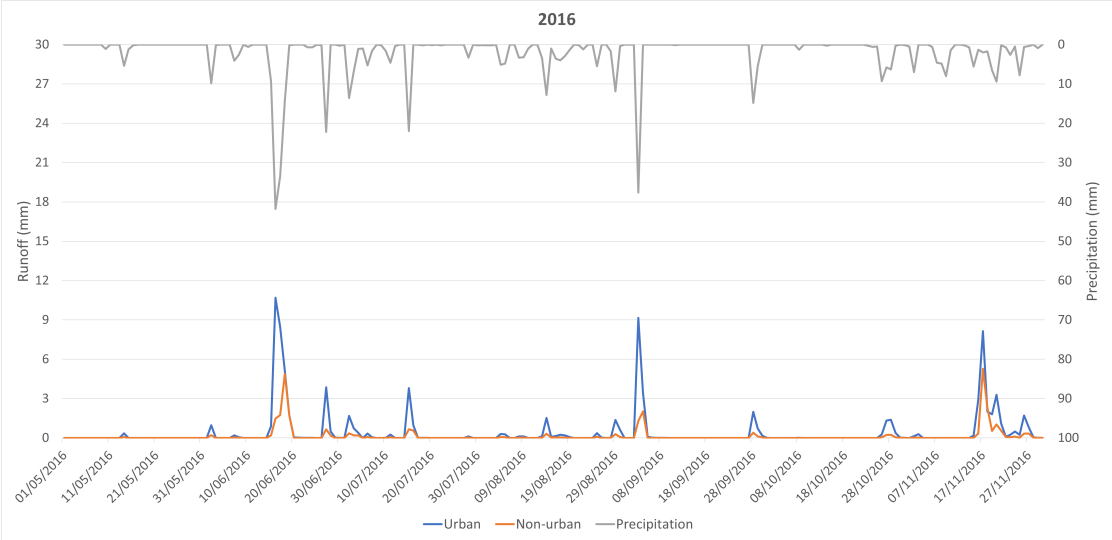

(e) *2016*

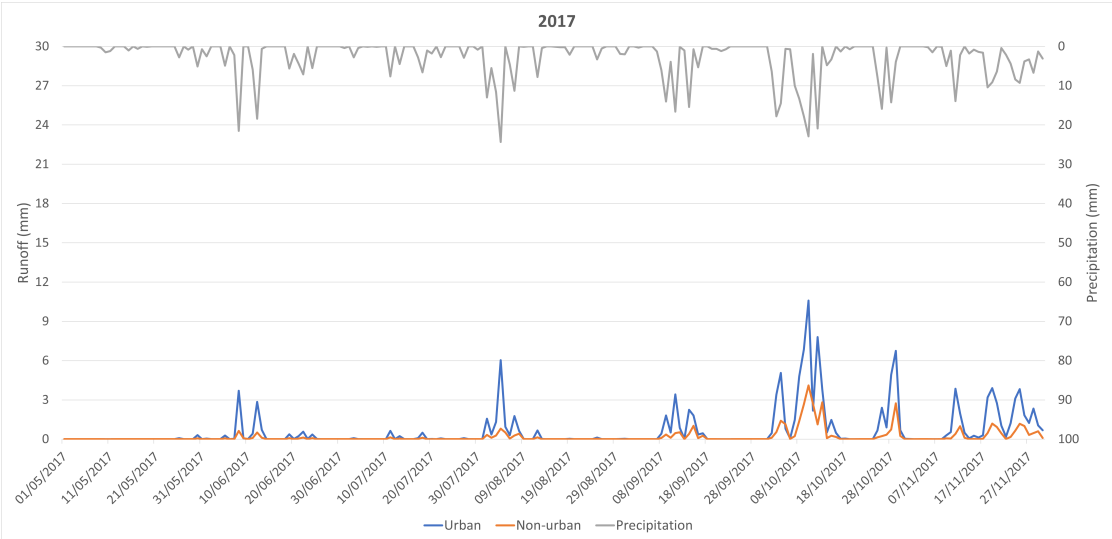

(f) *2017*

Figure 4.7: Simulated surface runoff for the months May-November of each year included in the decade 2012-2022

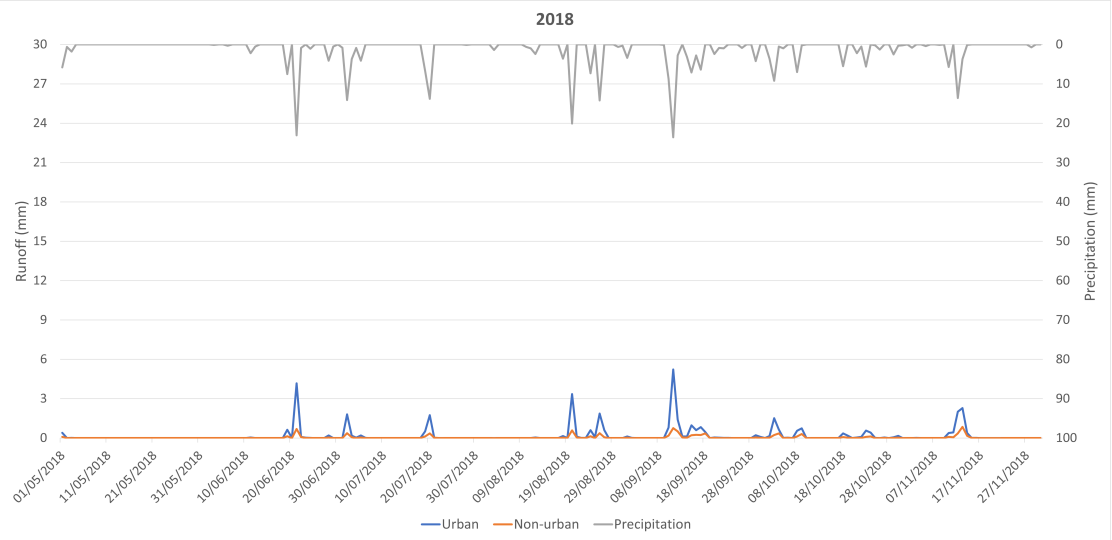

(g) *2018*

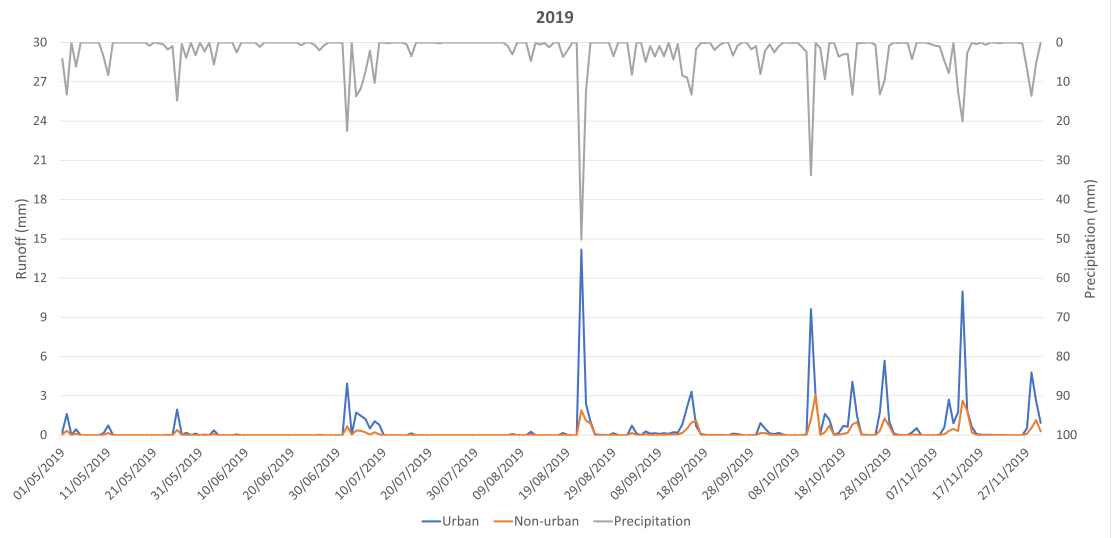

(h) *2019*

Figure 4.7: Simulated surface runoff for the months May-November of each year included in the decade 2012-2022

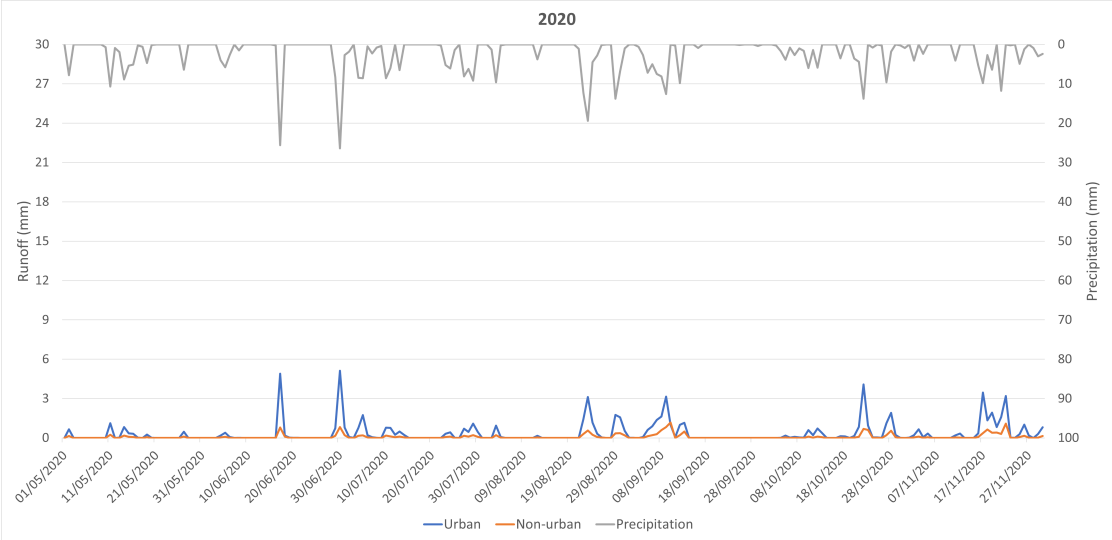

(i) *2020*

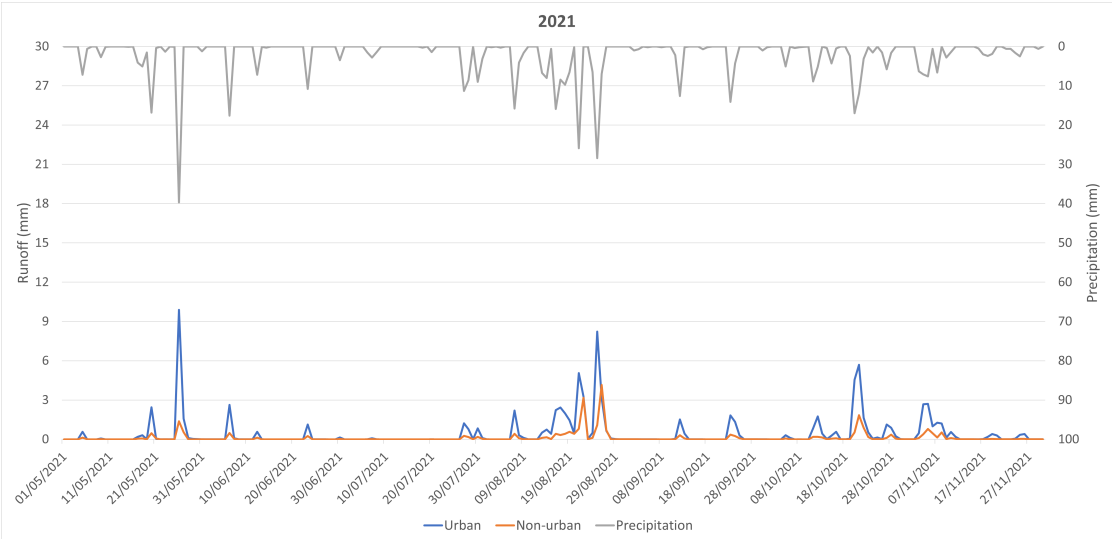

(j) *2021*

Figure 4.7: Simulated surface runoff for the months May-November of each year included in the decade 2012-2022

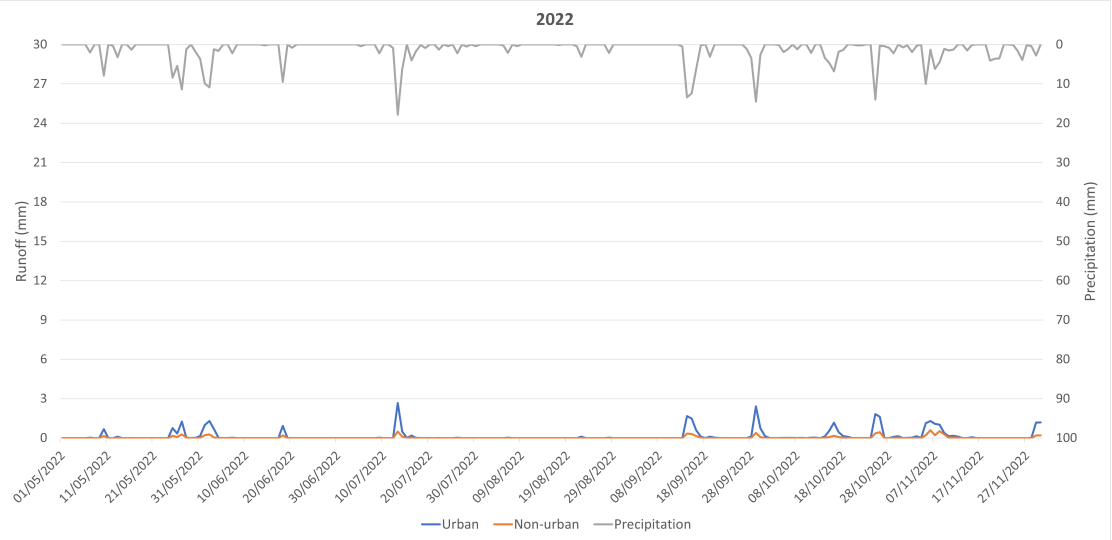

(k) *2022*

Figure 4.7: Simulated surface runoff for the months May-November of each year included in the decade 2012-2022

Year	Total precipitation (mm)	Total urban runoff (mm)	Total non-urban runoff (mm)	% of urban runoff	% of non-urban runoff
2012	579	119.2	32.8	20.6	5.7
2013	415	87.5	26.5	21.1	6.4
2014	417	66.9	17.7	16.0	4.2
2015	404	56.6	12.1	14.0	3.0
2016	429	89.5	29.9	20.6	7.0
2017	563	138.2	41.2	24.6	7.3
2018	277	39.0	8.9	14.1	3.2
2019	492	107.5	29.1	21.6	5.9
2020	467	76.6	17.9	16.4	3.8
2021	459	93.7	26.0	20.4	5.7
2022	281	32.8	7.3	11.7	2.6

Table 4.2: Cumulative precipitation and runoff values and shares of precipitation turning into urban and non-urban runoff

4.3.2 Discussion of runoff trends and assessment of their integrity

All the figures presented in this section are constructed based on the calculations done by means of the results shown in the previous subparagraph. These ones are here discussed more in depth, in order to achieve the purposes listed in the incipit of this paragraph, which, as said, constitute the heart of this thesis.
The first aspect to be verified is the supposed and rationally reasonable higher volume of runoff coming from urban areas with respect to the one generated by more natural areas. To do this, the daily values of the plots of figure 4.7 were accumulated for each year in order to calculate the total urban and non-urban runoff for the studied period. These cumulative values, as said, are reported in table 4.2, along with the shares of precipitation that turns into water flowing over the surfaces and are better visualized in the form of a bar graph in figure 4.8.

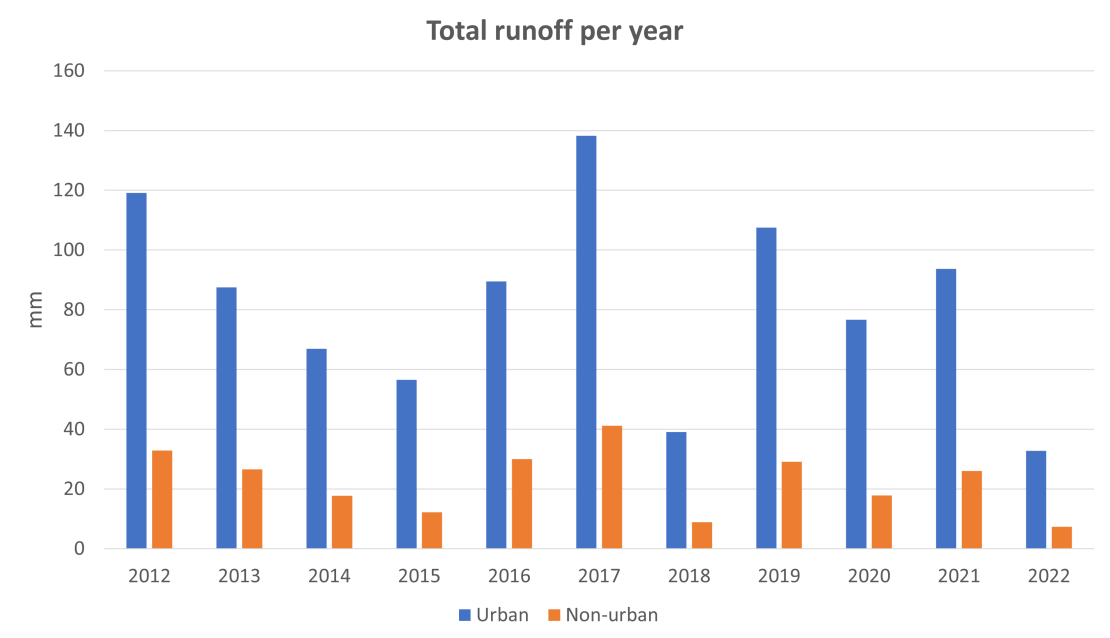

Figure 4.8: Urban runoff vs non-urban runoff for each year (considering only months from May to November)

The combination of the surface runoff trends of figure 4.7 and the relative total values displayed in figure 4.8 confirms that the calibrated SWAT+ model simulated an urban runoff amount larger than the natural one for both the daily time step and the cumulative volume. This achievement represents a first input for the assessment of the reliability of the analyzed outputs. The next step requires a deeper focus on the numbers.

From table 4.2, it is clear that urban runoff accounts for a mean share of around 20 % of the water amount coming from rainfall, while, in the case of non-urban stormflow, the share is around 5 % on average, almost four times lower than the urban one. These numbers seem to make sense according to the relationship between impervious cover and surface runoff described in the "Stream Corridor Restoration Handbook" published by the Federal Interagency Stream Restoration Working Group (FISRWG) in 1998 [121]. The document shows how the percentage of runoff in the water balance varies as a function of the imperviousness of the surfaces and, in the case of an impervious cover percentage between 35-50 %, it identifies a runoff share of 30 %. Based on the land use data described in table 2.2, the related map of figure 2.2 and the fact that nature is a significant component of Helsinki's urban regions (as it can be verified by focusing on each of the urban LSUs, that are always characterized by a consistent percentage of land covered by trees or grasslands), it is possible to assume that the share of impermeable surfaces does not go over 50 % for most of the basin's landscape units, deducing, in this way, that a value of 30 % in the share of surface runoff is representative of the urban districts of the Haaganpuro watershed. This means that the simulated overall runoff share of almost 25 % (including both urban and natural flow) can be considered acceptable and nearly indicative of the reality of stormflow processes in the catchment's area. This is even more accurate by considering that, in some of the studied years, the mentioned share is closer (as happens in 2012, 2013, 2016, 2019 and 2021) or higher than 30 % (as happens in 2017).
This last highlighted topic about the presence of years characterized by runoff shares higher than the average, gives a first insight on the different level of precipitation reached during the summer-autumn period of each year. In fact, during the decade 2012-2022, the years were marked by differences in the rainfall amounts, leading to the definition of wetter and drier years. To appreciate this variation, figure 4.9 shows the total precipitation trend over the years of the studied decade, together with the curves describing the two analyzed types of runoff.
From this analysis, it is possible to define as wet the years 2012, 2017, and 2019, with the first one being the wettest of the entire decade (total rainfall in 2012 was 579 mm as shown in table 4.2). Instead, the driest year is 2018 with 277 mm of precipitation registered in the months between May and November. Just above 2018, there is the last year of the decade with only 4 mm more, as pointed out in table 4.2. The other years are characterized by rainfall amounts that range around the decade's average of 435 mm and, for this reason, were not counted as extremes.
Figure 4.9 is also useful to assess the ability of the constructed and calibrated SWAT+ model to predict runoff based on precipitation measurements to see, for example, if the wettest year entails the generation of the highest stormflow volumes and vice versa. Form the figure, the shape of the cumulative runoff trends replicates more or less the one of the precipitation curve, evidencing the apparent existence of

a correspondence concerning the abundance of the amounts of the two hydrological components. In fact, the sequence of rainfall values appears to be reflected in the one of both urban and non-urban runoff, meaning that if a year is affected by a higher rain intensity than the following one, then the same thing is valid for runoff volumes.

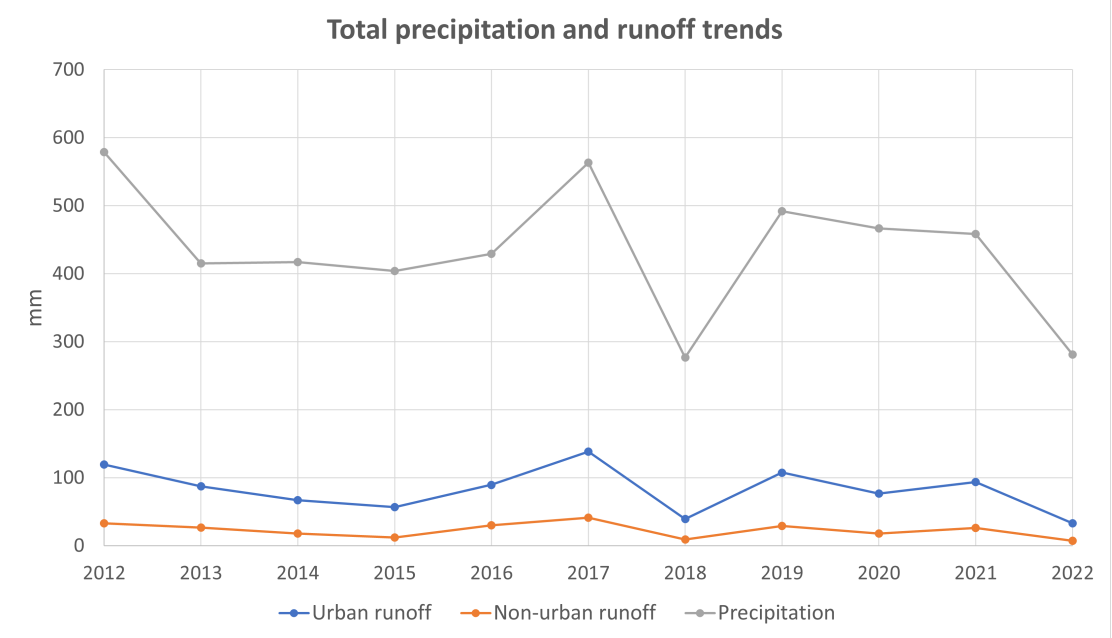

Figure 4.9: Total precipitation and runoff trends over the years (considering only months from May to November for each year)

Focusing on the identified extreme years, it is interesting to take a deeper look at their simulated runoff trends reported in figure 4.7. Concerning the wettest years (2012, 2017 and 2019), the model outputs the highest urban and natural stormflow amounts. The highest values are linked to 2017, with a total of 138 mm of urban flow and 41 mm of forested/park flow. This fact highlights a sort of discontinuity in what has been said above about the resemblance of the curves of figure 4.9. Based on that way of thinking, the year 2012, which, as seen, is the one characterized by the highest cumulative precipitation amount, should also present the highest volumes in terms of runoff. However, these peaks are generated for year 2017 which is affected by the second strongest precipitation intensity during the simulated months. This kind of distortion can happen because it is not sufficient to take into account only rainfall, but also air temperature and its impact must be assessed. In fact, the yearly oscillations in this variable can cause a warm year to be affected by a greater reduction in runoff volumes compared to a colder year, even if precipitation amounts for the warmer one are larger. This phenomenon is

mainly linked to the increased evaporation rates related to a higher air temperature, with a consequent decrement in the water available for surface runoff. This is predominantly what happens during the modelled months (from May to November), a period during which the absence of snow cover leads to assume that the effect of warmer temperatures can not be related to the development of snowmelt runoff, but only to an increase in evaporation levels and therefore, to a reduction in runoff volumes. For this reason, it is convenient to take look at the temperature annual average trends reported in figure 4.10.

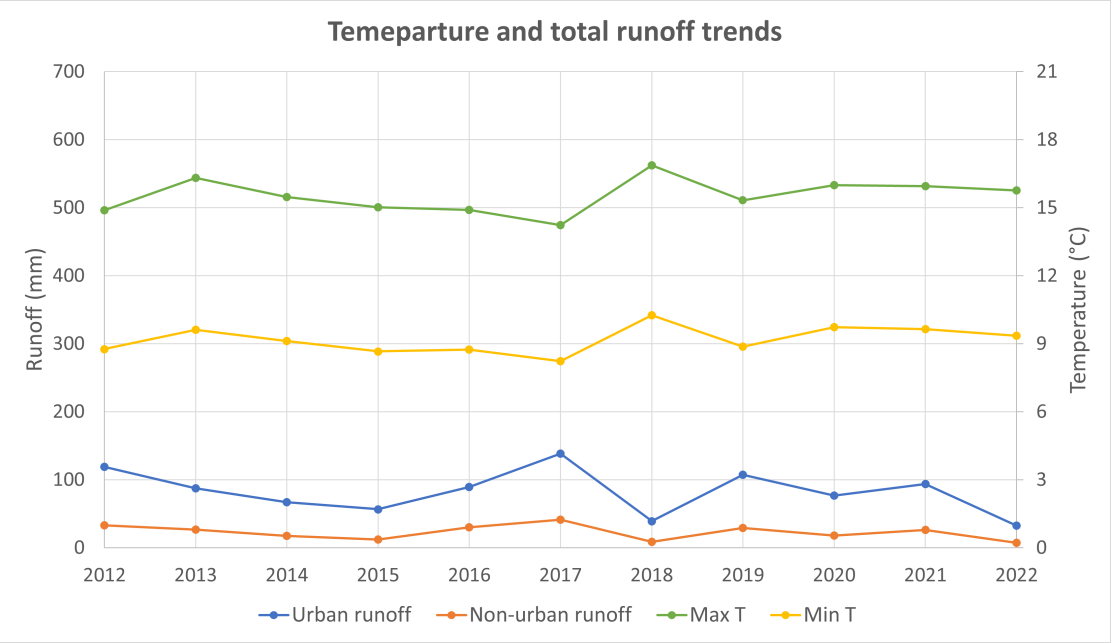

Figure 4.10: Max/Min temperature and total runoff trends over the years (considering only months from May to November for each year)

The scatter plot shows also the comparison with the same total runoff trends of figure 4.9, where they are set side by side with precipitation. If in that case, the curves had a very similar shape, in the context of figure 4.10 the temperature trends are almost specular with respect to the stormflow ones. In fact, the warmer years appears to be the ones characterized by the lowest runoff values (for example year 2018), while the coldest year (2017) of the studied decade is the one during which the peak in the runoff curves is reached. Therefore, figure 4.10 shows that 2017 has actually a lower maximum and minimum temperature then the year with the greatest rainfall event (2012), and this allows to assume that the production of a larger stormflow during 2017 is achieved thanks to the combined action of a lower average temperature and a consistent water quantity coming from precipitation, that is just 16 mm below the one accumulated during 2012 (the wettest year).

Hence, this example testifies the necessity of accounting for both rainfall and temperature to clearly understand the dynamics behind the modelled stormflow trends.
Going more in depth about the differences in the runoff trends generated by the model, the plots of figure 4.7 show how the various time series can change in terms of daily averages, location and quantification of daily peaks, and related frequency of occurrence, going from years distinguished by most of peak flow circumscribed in the summer season to years with a major number of pinnacles happening during autumn. Each of these graphs is now described separately in order to derive some general conclusions about the identification of runoff extremes, that are fundamental to be quantified since they might represent the starting point for the development of flooding phenomena. Also, once these "anomalies" are identified, it is interesting to evaluate how they evolved over time and if this evolution might be a symptom of the effects of climate change. All of the following discussion is based on what has been reported in figure 4.7.

Detailed analysis of runoff trends

Starting from 2012 (figure 4.7a), it was already pointed out that it is the year with the strongest total rainfall intensity. However, precipitation seems to assume a partly uniform trend with daily peaks of around 25 mm measured both in the summer and in the autumn season. Consequentially, peak flows are output for both periods with a higher concentration in the months of September-October, during the transient phase from summer to autumn. The urban peaks from September-October reach values around 5-8 mm, with the highest one arriving to 7.5 mm. As seen in figure 4.7a, autumn urban peaks are higher than the ones from June-July which never surpass 5 mm. Peaks in natural flow are simulated during the same days as the urban ones, but they never go over a value of 3.2 mm, the maximum one, whose occurrence happens in correspondence of the urban pinnacle.
During 2013 (figure 4.7b), there is a very particular day from the point of view of maximums in the runoff trends. This day is the 13th of August when a daily peak of 13.4 mm and 5.5 mm is reached in the urban and non-urban time series respectively. These values are generated by the model in correspondence of an intense amount of rainfall, measured around 43.3 mm. This observation is probably correlated to the occurrence of a strong thunderstorm event which, during summer, is frequent in Southern Finland and is usually responsible for the typical stormflow volumes developing over the season.
The situation is completely different in the following two years (2014 and 2015) which, as can be seen from figure 4.7, appear drier in terms of runoff if compared with the previous two. In fact, the highest daily peak flows never exceed a value of 6 mm for urban areas, and a value of 2 mm for the forested/park regions. Specifically,

a peculiarity that comes to the eye is the almost total absence of runoff for October 2015, mainly related to a greater lack in significant precipitation events during the 2015 autumn season. For both years, the main precipitation events happen during summer, with the strongest ones between the end of July and the end of August when the aforementioned peaks are reached.
This progressive fall in the runoff volumes is also testified by the total trends of figure 4.9 and the bar graph of figure 4.8 which show how the urban and natural cumulative flows go from values of 119.2 mm and 32.8 mm in 2012 to values of 56.6 mm and 12.1 mm in 2015, with a drop of nearly 53 % and 63 % respectively. Over these first four years, air temperatures ranged around an average maximum of 15.4 °C and an average minimum of 9 °C which are both very close to the decade's means of 15.5 °C and 9.2 °C. The only exception is year 2013, especially for a maximum mean temperature of 16.3 °C, almost 1 °C more than the four years' average. This situation is better visualized in figure 4.10 which, combined with figure 4.9, helps to assume that the highlighted significant decrease in the simulated runoff trends, in this case, is mostly due to a consistent drop in daily precipitation amounts over the first four years of the studied decade.
This falling tendency takes a reverse direction starting from 2016, when an increase in both measured rainfall and predicted runoff volumes is registered. Specifically, focusing on the runoff trends (figure 4.7e), it is possible to point out the presence of three distinctive peaks happening on June 16th, September 3rd and November 17th. The first one is characterized by an urban value of 10.7 mm, correlated to the observed rainfall peak of 41.8 mm, and a natural flow of 4.9 mm, shifted of two days to June 18th, probably due to the persistence of a significant amount of rain until June 18th when the measured precipitation is still around 33.5 mm. The second runoff peak, on September 3rd, is the one distinguished by the highest difference between the urban and natural maximums, with a distance of about 80 % between the urban value of 9.2 mm and the natural one of 2 mm. The peculiarity of these first two peaks is that they occur in correspondence of the two highest registered summer rainfall pinnacles, probably related to thunderstorm events which are very typical in Southern Finland in the months between May and September. The last mentioned peak flow is output on November 17th and, as can be seen from figure 4.7e, is not connected to a specific predominant rainfall peak, but more to a series of smaller pinnacles that range around 7-10 mm. There is no sufficient support to identify the real cause behind this simulation result. Until now, in all the plots of the described years, the highest runoff peaks have been reported in correspondence of the peaks of the observed rainfall trend, highlighting the ability of the SWAT+ model to predict runoff peaks as a response to the precipitation ones. However, some outliers can be possible, and a feasible reason behind the stormflow peak of November 17th may concern the progressive saturation of the soil due to antecedent precipitation events that may increase runoff volumes due to a gradual reduction

in the ability of stormwater to infiltrate into the soil.
The accumulated runoff volumes increase even more in 2017 when they reach the highest values of the decade. This year is also the second largest in terms of precipitation amounts, with most of them occurring between September and October. It is also in these months that the greatest runoff peaks are reached, with the largest one happening on October 10th for both urban flow (10.6 mm) and natural flow (4.1 mm). Then, the rest of the autumn season is characterized by the recognition of several runoff pinnacles during the same days as the rainfall ones, as can be verified from figure 4.7f. An interesting fact about this year, apart from the occurrence of the principle stormflow peaks during autumn instead of summer, is the almost null runoff quantity during May. This distinctive trait is identifiable also in 2018 (figure 4.7g), when the mentioned dry period is extended until the first half of June. This approximately null stormflow is caused by a quasi-total absence of rainfall events in the considered time interval, especially for 2018 when no precipitation is registered even for one month, from May 4th to June 3rd. If compared with the other plots of figure 4.7, this kind of behaviour is only restricted to these two years, especially for 2018, and, for this reason, can be considered as an unusual phenomenon. This drought affecting May and the beginning of June 2018 is, in reality, identifiable throughout the whole simulated period until November 2018. In fact, as shown in figures 4.8 and 4.9 and in table 4.2, year 2018 is the driest in terms of precipitation and the second driest in terms of surface runoff (only behind 2022). This fact is clearly reflected in the modelled trend of this last hydrological component which, as reported in figure 4.7g, is characterized by peaks even lower that the ones simulated for 2014 and 2015, with the urban highest ranging around 5 mm and the natural largest around 1 mm. They mainly occur between August and September, with some cases detected also between the end of June and the beginning of July.
A new rise, both in terms of measured precipitation and modelled runoff, is underlined for 2019 (the third largest for both variables) whose stormflow trend (figure 4.7h) presents some interesting maximum points. The highest one occurs on August 22nd as a response to an intense rainfall event of 50.2 mm, the largest observed in the decade 2012-2022 for the studied months (May-November). On this day, urban flow reaches 14.2 mm, its highest value during the analyzed time period, while natural flow is at 2 mm. The other stand out runoff peaks are concentrated in the autumn, with values of 9-11 mm for urban stormflow, and values around 2-3 mm for the natural one. The highest frequency of significant runoff peaks in this season is related to a more frequent occurrence of consistent rainfall events during autumn rather than summer.
In the last three years of the decade (2020, 2021 and 2022), both precipitation and its stormflow share are lower if compared to 2019. During 2020 (figure 4.7i), the simulated runoff quantity is approximately uniformly distributed over the reported

months, with the main pinnacles happening at the end of June, marked by values similar to the ones predicted for the 2018 peaks. Year 2020 is wetter than 2018, but the reason behind the mentioned similarity of the peak flows is represented by the discussed homogeneity that affects the 2020 stormflow trend.
Concerning 2021 (figure 4.7j), relevant peaks in runoff trends are distributed over the second halves of the months of June, August and October, with values between 5-10 mm for urban flow and values between 2-4.5 mm for natural flow, deriving from peaks in the precipitation amount of around 20-40 mm, depending on the event. In contrast to the common drier May of the six years before, the same month in 2021 is the month of May with the greatest rainfall and stormflow volumes in the whole decade 2012-2022. In fact, the highest peak in both variables, during this year, are reached on May 26th, an uncommon phenomenon if compared to the rest of the analyzed decade.
A significant drop in precipitation levels, similar to the one affecting 2018, is registered for 2022, the last year of the decade of interest. As said before and as reported in table 4.2 and figures 4.8 and 4.9, this is the year with the second lowest total precipitation and with the overall smallest cumulative stormflow (driest year in terms of runoff). As can be seen from their trends in figure 4.7k, all the rainfall peaks are below 20 mm, while the runoff ones are below 3 mm for urban areas and below 1 mm for forested/park area, marking the lowest possible peak values of the entire decade for both hydrological components. The lack in relevant precipitation events is the main reason behind the simulation of a so restricted runoff trend, which poses itself as a sort of outlier, especially by looking at the dryness affecting the weeks from the end of July to the beginning of September when, in most of the previous years, there was the occurrence of remarkable thunderstorm events and the consequent modelling of consistent peak flow volumes. This condition, and the fact that is so distant from what was typical during the years before, can be taken as a symptom of one of the several climate change impacts, that is an increment in the frequency of extreme drought events, whose recurrence is tending to increase as also highlighted in the case of flooding phenomena.
From what has been discussed during the analysis of the runoff trends of figure 4.7, it is possible to extract some important points. First of all, the calibrated SWAT+ model appears to be able to output peaks in the stormflow trend in correspondence of the ones observed in the precipitation curve, recognizing the existence of a correlation between the two. However, sometimes, some outliers can be possible, as the one modelled on November 17th 2016 which, as said, is not connected to a specific rainfall pinnacle as happens for all the other described peaks.
Concerning rainfall, some peculiarities in its trend over the years have been identified. At first, two significant decreases in the total precipitation amounts occur for the years 2018 and 2022, which also present the lowest runoff volumes. Focusing more on their trends, it was noticed how the period between the end of July and

the beginning of September 2022 is affected by a drought, considered uncommon since, usually, summer months are the ones during which thunderstorm events take place in Southern Finland, leading to the production of relevant rainfall amounts and stormflow volumes. In fact, this kind of behaviour was observed for most of the years of the studied decade, with the highest precipitation and runoff peaks concentrated during summer. However, sometimes, the largest collection of pinnacles referred to the autumn season, as happens for 2012, 2017 and partially for 2019, when, in any case, the highest overall peak in both rainfall and runoff occurs during summer and, as pointed out, represents the decade's highest peak both in terms of precipitation and urban runoff. The lowest peaks, instead, are related to 2022, with the whole year predominantly affected by a drought condition, that leads to have runoff values even lower than the 2018 ones. During the latter, a relevant drought period impacts the whole month of May, as partially happens for 2017, determining the simulation of approximately null stormflow volumes. In contrast, the situation is totally different for 2020 which presents the wettest May of the entire decade and constitutes the only year with the greatest rainfall and runoff peaks located in this month. The runoff trend of this year shows a sort of homogeneity throughout the modelled months, a property that is partially visible also for 2012 and explains the lower maximum stormflow values of 2020 if compared with other years characterized by a similar total rainfall amount.
Taking a deeper look at the simulated runoff values, form what has been reported and highlighted, it is possible to derive a table reporting the maximum urban and natural values predicted for each year of the decade 2012-2022, during the modelled months (from May to November) (table 4.3). This table gives a summary and a clear overview about the runoff maximums discussed above, and represents the starting point of the following discussion about the integrity of the results since peak values will be one of the sources of comparison with other studies' findings.

Year	Max urban runoff (mm)	Max non-urban runoff (mm)
2012	7.4	3.3
2013	13.4	5.5
2014	5.7	1.9
2015	5.7	1.0
2016	10.7	5.3
2017	10.6	4.1
2018	5.2	0.9
2019	14.2	3.1
2020	5.1	1.2
2021	9.9	4.2
2022	2.7	0.6

Table 4.3: Maximum urban and non-urban runoff for each year of the decade 2012-2022, from May to November

Assessment of the integrity of runoff results

The whole discussion about the surface runoff trends of figure 4.7, simulated by the built SWAT+ model for the Haaganpuro watershed during the considered study period, has identified the shares of precipitation turning into urban and natural runoff, the relationship between these two hydrological components and the relative ability of the model in predicting it, the additional impact of temperature on runoff calculations, the location and quantification of the peaks in stormflow trends, the eventual presence of outliers and uncommon phenomena, and the differences in the comparison between the various years. Now, to evaluate as accurate all these results and the interesting reported findings, it is necessary to go through a last step, which consists in assessing their accuracy in order to take them as approximately representative of the reality of runoff dynamics and volumes in the analyzed basin. Normally, to do that, it is useful to have measurements of stormflow amounts in the area of interest to allow the comparison with the simulated ones and finally assess the integrity of the model. However, that is not the case of this thesis. The absence of runoff observations for the analyzed period determines the need to compare the outputs to the results of other hydrological studies about runoff. It is important to notice that these studies must be conducted in catchments located in Southern Finland or in regions with similar climate properties as the Finnish context, to allow a meaningful comparison with the findings of this thesis. Otherwise, the discussion would not make any sense and the accuracy of the built and calibrated SWAT+ model would remain questionable.
In this perspective, some studies were selected, starting from the ones focused on watersheds located in Southern Finland. The runoff values reported or modelled by these papers commonly refers to a period that covers at maximum the first years of the one considered in this thesis, since studies about more recent years were not available (with some exceptions related to the runoff observations provided by the Finnish Environmental Institute for 2023). However, this fact did not represent a problem, since the order of magnitude of runoff values is approximately the same over the years despite climate change effects, which did not produce drastic modifications in the magnitude of runoff volumes, but were more linked to the production of circumscribed extreme events in a particular day or month of a year. This fact is testified by the results of the selected studies that give insights both on total seasonal and daily peak runoff.
Starting from total runoff volumes, a study elaborated by Lindgren et al. (2017) reports seasonal stormflow values, provided by the Finnish Environmental Institute (SYKE) and simulated though its Watershed Simulation and Forecasting System (WSFS), for the years between 1962 and 2014 (covering the first three years of the decade considered in thesis) [122]. The data implemented in the mentioned paper refer to 6172 subbasins in Finland, including transboundary watersheds in Norway,

Sweden, and Russia. The runoff dataset was split in four seasons, of three months each. Since the simulated period of this thesis mainly covers summer and autumn, the same division operated by Lindgren et al. (2017) was adopted, considering the months from June to August as summer and the ones from September to November as autumn. The runoff plots of the article show the average total runoff trend from 1962-2014 surrounded by a range in which values for individual subbasins vary [122]. To allow the comparison, the simulated total seasonal runoff volumes for the Haaganpuro basin were calculated for the first three years of the decade of interest, summing the seasonal amounts coming from urban and natural areas. The calculations generated the following runoff values:

- For summer: 28 mm in 2012, 52.6 mm in 2013 and 37.7 mm in 2014.
- For autumn: 115.3 mm in 2012, 55.5 mm in 2013 and 40.6 mm in 2014.

These simulated runoff volumes all reenter in the mentioned variation range of the plots of the article, with some of them closer to the average total runoff trend. For example, the autumn results seem to resemble the ones constituting the paper's autumn mean stormflow curve that assumes values of around 125 mm in 2012, 60 mm both in 2013 and 2014, mostly close to the ones computed based on the outputs of the calibrated SWAT+ model, confirming also the higher autumn runoff amount simulated for 2012. In fact, for both simulation and the study's results, between 2012 and 2013 there is a difference of approximately 60 mm in autumn runoff.
Concerning summer, instead, the outputs of the SWAT+ model are very close or almost close to the ones reported for 2013 and 2014, with the paper's values being around 50-60 mm for both years. A larger difference can be highlighted for 2012, for which the model generates a total summer runoff of 28 mm against the mean one of around 100 mm reported by Lindgren et al. (2017). However, this does not mean that the SWAT summer stormflow for 2012 is wrong since several differences in the circumstances and in the considered factors between this thesis and the mentioned study must be taken into account. In fact, as it was already pointed out, the study elaborated by Lindgren et al. (2017) is referred to 6172 subbasins placed all over Finland, with some of them located in neighbour countries like Sweden, Norway and Russia, therefore covering an area of approximately 390 000 km^2 with a subbasin size median of 42 km^2 and with a majority of more natural regions included in the basins. The modelled Haaganpuro catchment area was 7.2 km^2 out of the original 10.8 km^2, almost 80 % less than the article's mean basin size, and is mostly located in an urban region. This fact would allow to think that the runoff coefficient is lower for the watersheds considered by Lindgren et al. (2017) with respect to Haaganpuro, but Lindgren's runoff values also include other hydrological components such as later flow and return flow that represent an

additional contribution to the total volumes. In the case of the modelled stormflow amounts of this thesis, only the surface runoff component was extracted from the outputs, therefore excluding other flow components. This circumstance might be a reason behind the higher runoff values reported by Lindgren's article. Also, other factors related to the different weather events and the differences in the land use and in the soil types must be considered as well, especially due to the enormous area covered by forest or grasslands in Lindgren et al.'s study. In fact, a difference in the total summer precipitation is highlighted for 2012, when the summer rainfall is around 180 mm while the total average one for the same season is approximately 250 mm in the considered study, almost the same distance in mm between the runoff volumes, pointing out even more the development of stormflow as a direct response to intense precipitation events.
Unfortunately, total runoff values covering the rest of the years included in the decade 2012-2022 are not available, but the positive findings from the comparison operated for the first three years with Lindgren et al.'s study allow to assume that the stormflow volumes for the following years are included in the respective variation ranges, with some of them probably close to the seasonal average trend. At least, by looking at the whole trend from 1962-2014, it is possible to say that the order of magnitude of the simulated runoff seasonal volumes is correct and that the alteration between years characterized by higher summer runoff volumes and others affected by larger autumn amounts is feasible as happens for several years between 1962-2014, meaning that it constitutes a normal situation.
Focusing more on daily runoff trends, as the simulated ones reported in figure 4.7, the found studies cover only selected years of the modelled period or show the most recent measurements. The only available daily runoff observations are the ones registered by the Finnish Environmental Institute (SYKE) that reports those measured for different Finnish watersheds during the last year on its map service website [123]. This means that the runoff values visible on the site go from November 2022 to November 2023 and can be used to assess the order of magnitude of the peaks included in the simulated runoff trends of figure 4.7. Specifically, some of the available catchments close to the location of the Haaganpuro one were selected, taking into account that they mostly cover a larger area and that they extend mostly outside urban areas, meaning that water losses due to infiltration in forested soils or in grasslands have a consistent effect on the measured runoff values.
The catchments selected for runoff peaks comparison are: Myllymäki, Vanhakaupunki and Oulunkylä, that are three subbasins of the Vantaanjoki watershed, Mankinjoki and Espoonjoki watershed. They were chosen due to their proximity to the Haaganpuro basin (they are located in the Helsinki metropolitan area) and because they include some built up areas. The runoff peaks measured during May-November 2023 assume values around 5.5-7 mm, very similar for all the mentioned watersheds.

These 2023 pinnacles occur between the end of August and the first half of October and resembles most of the ones simulated by the SWAT+ model for Haaganpuro, during the same period, for each year of the decade 2012-2022, as can be seen from figure 4.7. Higher simulated runoff peaks, as the ones reported in table 4.3, identify occasional intense events, related, as said, to a stronger rainfall intensity, and, for this reason, they stand out from the typical values of 5-8 mm. Also, the semi-urban nature of the Haaganpuro watershed determines a higher runoff coefficient than the one of the selected catchments, therefore justifying the development of larger simulated stormflow peaks. This insight gives a significant contribution to the assessment of the validity of the model results and, together with the total runoff evaluation, represents a way to state that the simulated runoff trends for the decade 2012-2022 can be taken as representative of the reality of runoff volumes and dynamics in the Haaganpuro watershed.
This integrity is even more confirmed by the findings of other hydrological studies conducted in Finland, such as the one elaborated by the Finnish Environmental Institute (SYKE) that reports the runoff measurements for the Savijoki river basin, located in the South-West of Finland [124]. The stream has a catchment area of around 15 km^2, close to the Haaganpuro one of 10.8 km^2 and the double of the modelled one (7.2 km^2). Compared to other considered watersheds, the Savijoki basin is the one with an extension similar to the Haaganpuro one but, the main difference between the two is that the share of urban areas for Savijoki is only 4 %, meaning that it can not be even considered a semi-urban basin as Haaganpuro is. Therefore, even in this case, the impact of infiltration and forest/field hydrology on runoff must be taken into account. The Finnish Environmental Institute (SYKE) reports peak runoff values of around 3.5-7 mm for the ones measured during summer-autumn 2017, and an approximately dry autumn season for 2016, as it is simulated by the SWAT+ model for the same year in this thesis and as was pointed out and can be seen from figure 4.7e. Some simulated peaks during autumn 2017 are higher than 7 mm, but this fact does not compromise the goodness of the comparison since it is clear that a more urban basin can generate a higher runoff volume than a mostly natural one as the Savijoki catchment is. This additional comparison concerning other years inside the modelled decade, gives another proof about the accuracy of the SWAT+ model for Haaganpuro, especially considering that the Savijoki watershed is also located in Southern Finland.
Overall, it is possible to state that the calibrated SWAT+ model, set up for the Haaganpuro watershed, produced total and daily runoff results with an order of magnitude typical of the stormflow volumes occurring in reality. The seasonal amounts are very close to the ones characterizing the Finnish context and the daily peak values resemble most of the observations provided by the Finnish Environmental Institute (SYKE) for the considered years and months. Therefore, the comparisons and the findings of this section allow to assume that the runoff

outputs generated by the SWAT+ model are quite accurate and can be taken as representative of the stormflow volumes in the Haaganpuro catchment area.

Chapter 5

Conclusions

Hydrological modelling poses itself as a relevant and powerful tool to manage water resources. The constant increasing pressure through which they have been undergoing constitutes a significant incentive in expanding the boundaries of research in the field of hydrology, promoting the development of newer and more efficient models and the improvement of the already existing ones to integrate an always more accurate representation of reality and to simulate hydrologic processes with the highest level of details as possible. Specifically, in the context of urban stormwater management, hydrological models are used to predict and compute runoff volumes as a response to intense precipitation events, in order to provide a solid base for the correct dimensioning of the urban water collection systems whose effective functioning is required to deal with the more frequent extreme events, such as urban floods, and, therefore, to allow the continuous operability of cities without blocking the provision of their fundamental services to citizens.
In this perspective, a runoff modelling procedure was applied to a semi-urban watershed, located inside the city of Helsinki, Finland and referred to the Haaganpuro brook. The modelling was done by means of the Soil and Water Assessment Tool (SWAT) to test the ability of its restructured version (SWAT+) to simulate stormflow in the catchment area and separate the contribution of urban districts from the one of more forested/park areas to its generation. Runoff was modelled after the implementation of a sensitivity analysis, needed to identify the most sensible parameters for model calibration and validation. These last procedures were carried out though the use of the SWAT+ Toolbox, a software still subjected to a testing phase but practical in calibrating the model.
The input data implemented to set up the SWAT+ model included daily observations of precipitation, air temperature, relative humidity, wind speed and solar radiation, downloaded from the database of the Finnish Meteorological Institute and measured at the weather stations placed in Kaisaniemi and Kumpula, both

located in the city of Helsinki. The land use and soil maps were needed to characterize the whole basin and to define the so called "Hydrological Response Units (HRUs)", essential for SWAT+ to model the hydrological response of a certain area in the most precise way.
In fact, the setup of the model included three main stages. The first one is linked to the watershed delineation during which, the implementation of a digital elevation model (DEM) of the basin and the location of its outlet allowed QSWAT+ (a QGIS interface for SWAT+) to automatically draw the catchment's boundaries and the related streams and channels flowing through it. The software generated a simulated catchment area of 7.2 km^2 out of the original 10.8 km^2, with a 30 % loss in total area. The modelled region covers most of the real Haaganpuro basin, efficiently replicates its main river and incorporates the channels that predominantly contributes to the flow in the main stream. Probably, the presence of a shapefile reporting the existing stream network of the watershed would have helped improving its delineation by enlarging the simulated covered area, since it constitutes a reference for the number and the course of the streams and channels present in a basin.
The second phase is related to the creation of HRUs, lumping together similar responses of land use, soil and slope to enable the estimation of water loadings. In this stage, the land use and soil maps were converted in the respective SWAT format by means of two lookup tables reporting the corresponding SWAT codes/names and an additional file called "usersoil" for the identification of the geotechnical and hydraulic properties of the different soil types. Based on these data, the software generated a total of 2672 HRUs forming the 33 landscape units (LSUs), each of which represents a region of the basin draining into one of the 33 channels simulated by QSWAT+.
Once the model was built, the last step in its setup consisted in its import on the SWAT+ Editor to generate weather stations, upload climate data and finally run the model for the period June-November 2017, that is the one characterizing the streamflow observations used to calibrate the model. These measurements were divided into two datasets: the first referring to flow coming from Lansi-Pakila, an urban district in the North-East of the basin, taken as representative of all the urban areas in the catchment, and the second related to streamflow coming from the outlet of the catchment. The first run of the model underestimated streamflow observations in both cases, mainly due to a low prediction of components such as base flow and peak flow (especially for the catchment's outlet) and high evapotranspiration rates, therefore placing the need for an identification of calibration parameters through a sensitivity analysis.
The latter was performed through the use of the Sobol algorithm by computing the first-order sensitivity index for each parameter in the potential selected set. The sensitivity analysis reported as the most sensitive parameters, the curve number

(affecting runoff production) and the ones related to soil, evapotranspiration, elevation and lateral flow, for both Pakila and the basin's outlet. In this last case, also some of the aquifer parameters were found to be impactful on model outputs. The following automatic calibration phase, to which they were subjected, was performed by means of the Dynamically Dimensioned Search (DDS) algorithm, the only one available on the SWAT+ Toolbox. Its implementation produced acceptable calibration results, reducing the underestimation gap between simulations and observations and improving the goodness of their fit, as it is testified by the values assumed by the statistical indices (NSE and PBIAS), indicating a quite good improvement in model performance.
These facts give a proof about the goodness of the SWAT+ Toolbox, and the implemented algorithms, as an helpful free tool for performing sensitivity analysis and calibration, improving the fitness of the data with a rapid model execution and a simple printing of the results, and allowing the selection of a wide range of parameters controlling the main hydrological processes happening inside a watershed. However, some limitations in its use are related to the difficulty in finding a wide documentation and literature, its present availability only for the Windows system, and some bugs linked to the execution of a sensitivity analysis with a large number of iterations. Also, the choice of the calibration method, currently relegated only to one option, limits the possibility of exploring different types of algorithms, forcing the selection of the DDS one. However, efforts have been made to bring new calibration procedures to the toolbox, such as DREAM that, as it is discussed in its user manual, is currently in the testing phase [68].
Once all the sensitivity analysis and calibration operations were completed, the SWAT+ model was run again but, this time, for all the years in the decade 2012-2022, only considering the months from May to November for each year and excluding winter months due to a lack in streamflow observations needed for their calibration and the consequent necessity to build a proper snow model for estimating the snowmelt contribution to runoff, a procedure that surpass the boundaries of this thesis, mainly because of the increased time required to develop it. In reality, SWAT+ is provided with a temperature-index snowmelt method, but it was not efficient in predicting the snowmelt component without any calibration operated before.
From the output files generated by the model, the purpose of this study was to extract and analyze simulated daily surface runoff, dividing it in the urban and in the natural shares, with the latter found to be almost four times lower than the first one. The stormflow trends, produced for each year in the mentioned decade, showed a good correspondence between their peaks and the ones constituting the observed daily precipitation curve, with approximately 25 % of water coming from rainfall turning into runoff, a share in line with the 30 % one that has been reported by the Federal Interagency Stream Restoration Working Group (FISRWG) in the "Stream

Corridor Restoration Handbook" for areas characterized by an impervious cover percentage between 35-50 %, as various LSUs of the Haaganpuro basin are assumed to be, based on its land use map. A variability in runoff levels over the decade is identified by the results, with the wettest years being 2012, 2017, 2019, and the driest being 2018 and 2022, mostly reflecting the total precipitation amounts and the maximum and minimum temperature reached during all of the mentioned years. Specifically, the cumulative runoff trends appear to have a shape similar to the total rainfall one and to be specular to the temperature one.
Focusing more on the daily runoff trends for each year, for most of the decade, the highest stormflow and rainfall peaks are concentrated in summer, when commonly strong thunderstorms occur all over Southern Finland. Exceptions are represented by the wettest years of the decade which are characterized by larger rainfall and runoff amounts during autumn. The overall highest runoff peak happens in summer 2019, while the lowest pinnacles are simulated for 2022, a year mostly affected by a drought condition as happens for 2018. In fact, it is in these two years that the model identifies the two most relevant reductions in stormflow volumes of the decade.
In order to take these modelled runoff values as reliable and representative of the reality of stormflow volumes in the Haaganpuro watershed, the results were compared to the findings of other hydrological studies conducted in Southern Finland or in regions with similar climate characteristics. The comparison showed, for both total and daily runoff peaks, a good correlation with the ones reported by the considered studies for basins located in the Helsinki metropolitan area, in Southern Finland or in the neighbour countries. Especially, the order of magnitude of the model outputs resembled the ones of those studies' findings, and the peak flow values registered by the Finnish Environmental Institute for the catchments in the Helsinki area were very close to the ones predicted for the same months during each year included in the studied decade, apart from some occasional simulated intense events related to a stronger rainfall intensity.
Based on these insights, it was possible to state that the built and calibrated SWAT+ model was quite accurate in reproducing the typical runoff volumes occurring in the Haaganpuro catchment area, validating the integrity of the model outputs and highlighting its position as a reliable software for predicting stormflow over time. In fact, SWAT+ constitutes a valuable and robust tool for hydrological modelling and management of the water-related processes occurring in a catchment, thanks to a large availability of documentation, literature, studies, forums and groups supporting the users in the learning phase, and thanks to a bunch of properties and functionalities already included in it.
The QGIS interface, through which QSWAT+ operates, represents one of the strengths of the software, providing a simple procedure for the delineation of a watershed, an immediate visualization of its properties, and an easy modification

of the inputs. This flexibility in the input data loading allows SWAT+ to account for different soil types, land uses and climate conditions, and it is reflected in its ability to represent and robustly simulate the hydrological processes occurring in a certain basin, producing output files for different levels of analysis, going from the HRUs to the basin level in the case of spatial representation, and from the sub-daily to the annual time step in the case of temporal representation. Specifically, the feature related to the aggregation of similar land use, soil and slope responses into HRUs, and their consequent gathering into landscape units (LSUs), enables a more authentic prediction of the different hydrological components forming the water balance of a basin, which are then separated for each HRU or LSU, allowing the analysis of the behaviour of the different areas forming a watershed.
However, some weaknesses are still affecting SWAT+ as it is testified by the continuous development through which it is undergoing, as confirmed by Arnold et al. (2012) [7]. From what has been reported by the latter and from what has been depicted during the development of a SWAT+ model for this thesis, the required improvements concern a more detailed representation of HRUs, an intensified simulation of management practices and more complex hydrological processes to better reflect real World's dynamics, a greater level of stability in the related free calibration tool (SWAT+ Toolbox), an optimization of the current algorithms to reduce computational time (especially for larger and more complex basins), a better simulation of processes in urban areas and the related management practices, and an integration of methods able to quantify uncertainties affecting input data that can be transferred to model outputs. This last aspect is even more enhanced considering the high number of input parameters that must be taken into account for SWAT+ parameterization and calibration. In fact, the presence of observational errors in the input data, together with eventual flaws in the model's framework, may amplify inaccuracies in the results, leading to the presence of some outliers (as the ones pointed out during the discussion of runoff trends). In the future, a better quantification of this parameter uncertainty may be allowed by the inclusion of other observation variables, such as evapotranspiration and soil moisture, in the calibration process, that probably would have helped in resolving the underestimation problems identified for the first run of the model for the Haaganpuro basin, during which it was seen how the high evapotranspiration rates were one of the main causes behind a low base flow prediction [42].

Bibliography

[1] World Water Assessment Programme Unesco UN-Water. *The United Nations World Water Development Report 2023 : partnerships and cooperation for water*. UNESCO, Paris, 2023. ISBN: 978-92-3-100576-3 (cit. on p. 1).

[2] Chunyang He, Zhifeng Liu, Jianguo Wu, Xinhao Pan, Zihang Fang, Jingwei Li, and Brett Bryan. «Future global urban water scarcity and potential solutions». In: *Nature Communications* 12 (Aug. 2021). DOI: 10.1038/s41467-021-25026-3 (cit. on p. 1).

[3] Vijay Singh. «Hydrologic modeling: progress and future directions». In: *Geoscience Letters* 5 (Dec. 2018). DOI: 10.1186/s40562-018-0113-z (cit. on pp. 2, 3).

[4] K. Banasik, A. Krajewski, A. Sikorska, and L. Hejduk. «Curve Number Estimation for a Small Urban Catchment from Recorded Rainfall-Runoff Events». In: *Archives of Environmental Protection* 40.3 (2014), pp. 75–86 (cit. on p. 3).

[5] Martyn Clark et al. «The evolution of process-based hydrologic models: Historical challenges and the collective quest for physical realism». In: *Hydrology and Earth System Sciences Discussions* (Jan. 2017), pp. 1–14. DOI: 10.5194/hess-2016-693 (cit. on p. 3).

[6] Ezio Todini. «History and perspectives of hydrological catchment modelling». In: *Hydrology Research* 42 (Feb. 2011), p. 73. DOI: 10.2166/nh.2011.096 (cit. on p. 3).

[7] J. G. Arnold et al. «SWAT: Model Use, Calibration, and Validation». In: *Trans. ASABE, 55(4coper)* (2012), pp. 1491–1508 (cit. on pp. 3, 21–23, 25, 27, 43, 111).

[8] Philip Gassman, Manuel Reyes, Colleen Green, and Jeff Arnold. «Soil and Water Assessment Tool: Historical Development, Applications, and Future Research Directions, The». In: *Transactions of the ASABE* 50 (Mar. 2007). DOI: 10.13031/2013.23637 (cit. on p. 3).

[9] K. Bieger, J. G. Arnold, H. Rathjens, M. J. White, D. D. Bosch, P. M. Allen, M. Volk, and R. Srinivasan. «Introduction to SWAT+, A Completely Restructured Version of the Soil and Water Assessment Tool». In: *J. Am. Water Resour. Assoc. 53 (1)* (2017), pp. 115–130 (cit. on pp. 3, 28).

[10] Yle News. *Flooding in Finland is getting worse, new climate report says*. 2021. URL: https://yle.fi/a/3-12111938 (cit. on pp. 3, 4).

[11] Milla Mäenpää Anne-Mari Rytkönen Kirsi Mäkinen. *Shifting responsibilities for flood damages in Finland*. BASE: Bottom up Adaptation Strategies for a Sustainable Europe. URL: https://base-adaptation.eu/shifting-responsibilities-flood-damages-finland.html (cit. on p. 3).

[12] Yle News. *Heavy rain floods Helsinki streets, buildings*. 2023. URL: https://yle.fi/a/74-20047861 (cit. on p. 3).

[13] City of Helsinki. *The City of Helsinki Instructions on Prevention and Control of Floods*. 2013. URL: https://www.hel.fi/static/helsinki/julkaisut/Tulvaohje_eng_17062013.pdf (cit. on p. 4).

[14] Aleksi Teivainen. *Helsinki is planting trees to prepare for floods, heatwaves and other effects of climate crisis*. Helsinki Times. 2023 (cit. on p. 4).

[15] M. Kokkila, P. Paavilainen, O. Lintinen, A. Harju, L. Lahti, and J. Jalo. *Haaganpuron valuma-alueen hulevesiselvitys*. Helsinki: Helsingin kaupungin rakennusvirasto, 2016 (cit. on p. 6).

[16] M. Saikku. *Mätäpuro*. Helsinki: Virtavesien hoitoyhdistys ry, 2008 (cit. on p. 6).

[17] *Haaganpuro - Suomen urbaanein taimenpuro*. URL: https://haaganpuro.fi/ (cit. on p. 6).

[18] V. Tarvainen, E. Koho, A.-M. Kouki, and A. Salo. *Helsingin purot Millaista vettä kaupungissamme virtaa?* Helsinki: Helsingin Kaupungin Ympäristökeskuksen Julkaisuja, 2005 (cit. on p. 6).

[19] Daan van den Broek. *The Climate of Helsinki: What is the Typical Weather Like?* 2023. URL: https://www.daanvandenbroek.com/the-climate-of-helsinki-what-is-the-typical-weather-like/ (cit. on p. 9).

[20] *Climate elements*. Finnish Meteorological Institute. URL: https://en.ilmatieteenlaitos.fi/climate-elements (cit. on p. 9).

[21] *Climate and Average Weather Year Round in Helsinki*. Weather Spark. URL: https://weatherspark.com/y/91632/Average-Weather-in-Helsinki-Finland-Year-Round (cit. on pp. 9, 10, 44).

[22] *Finland's weather and light*. This is Finland. URL: https://finland.fi/life-society/finlands-weather-and-light/ (cit. on p. 10).

[23] T. Kilpeläinen, H. Tuomenvirta, and K. Jylhä. «Climatological characteristics of summer precipitation in Helsinki during the period 1951–2000». In: *Boreal Env. Res. 13* (2008), pp. 67–80 (cit. on p. 14).

[24] H. Nevanlinna. *Ilmatieteen laitoksen historialliset lämpötilahavainnot Helsingissä*. Ilmatieteen laitos, Havaintopalvelut (cit. on pp. 14–17).

[25] H. Nevanlinna. *Kaisaniemestä Kumpulaan - tutkimusta, havaintoja ja ihmisiä Ilmatieteen laitoksessa*. Ilmatieteen laitos, Yliopistopaino, 2005 (cit. on p. 14).

[26] L. Järvi et al. «The urban measurement station SMEAR III: Continuous monitoring of air pollution and surface–atmosphere interactions in Helsinki, Finland». In: *Boreal Env. Res. 14 (suppl. A)* (2009), pp. 86–109 (cit. on pp. 18, 19).

[27] P. Hari et al. «Air pollution in eastern Lapland: challenge for an environmental measurement station». In: *Silva Fennica 28* (1994), pp. 29–39 (cit. on p. 18).

[28] P. Hari and M. Kulmala. «Station for Measuring Ecosystem–Atmosphere Relations (SMEAR II)». In: *Boreal. Env. Res. 10* (2005), pp. 315–322 (cit. on p. 18).

[29] L. Järvi. *Turbulent vertical fluxes and air quality measured in urban air in Helsinki*. 2009 (cit. on pp. 18, 19).

[30] *SMEAR III*. University of Helsinki. URL: `https://www.atm.helsinki.fi/smear/index.php/smear-iii` (cit. on p. 20).

[31] J. G. Arnold, J. R. Williams, and Maidment D.R. «Continuous-time water and sediment-routing model for large basins». In: *Journal of Hydraulic Engineering 121(2)* (1995), pp. 171–183 (cit. on p. 21).

[32] S. L. Neitsch, J. G. Arnold, J. R. Kiniry, and J. R. Williams. *Soil and Water Assessment Tool: Theoretical Documentation*. Ed. by Soil Grassland and Water Research Laboratory - Agricultural Research Service - Blackland Research Center - Texas AgriLife Research. Version 2009. College Station, Texas 77843-2118: Texas Water Resources Institute - Texas AM University System, 2011 (cit. on pp. 21, 23–28).

[33] R. A. Leonard, W. G. Knisel, and D. A. Still. «GLEAMS: Groundwater loading effects on agricultural management systems». In: *Trans. ASAE 30(5)* (1987), pp. 1403–1418 (cit. on p. 22).

[34] W. G Knisel. «CREAMS: A field-scale model for chemicals, runoff, and erosion from agricultural management systems». In: *Conservation Research Report No. 26. Washington, D.C.: USDA National Resources Conservation Service* (1980) (cit. on p. 22).

[35] J. R. Williams, J. G. Arnold, J. R. Kiniry, P. W. Gassman, and C. H. Green. «History of model development at Temple, Texas». In: *Hydrol. Sci. 53(5)* (2008), pp. 948–960 (cit. on p. 22).

[36] X. Wang, N. Kannan, C. Santhi, S. R. Potter, J. R. Williams, and J. G. Arnold. «Integrating APEX output for cultivated cropland with SWAT simulation for regional modeling». In: *Trans. ASABE 54(4)* (2011), pp. 1281–1298 (cit. on p. 22).

[37] J. G. Arnold, P. W Gassman, and M. J. White. «New developments in the SWAT ecohydrology model». In: *Proc. 21st Watershed Technology Conf.: Improving Water Quality and Environment* (2010) (cit. on p. 22).

[38] L. C. Brown and T. O. Barnwell Jr. *The enhanced stream water quality models QUAL2E and QUAL2E-UNCAS: Documentation and user manual*. EPA/600/3-87/007. Athens, Ga.: U.S. EPA, Environmental Research Laboratory, 1987 (cit. on p. 22).

[39] A. R. Kemanian, S. Julich, V. S. Manoranjan, and J. G. Arnold. «Integrating soil carbon cycling with that of nitrogen and phosphorus in the watershed model SWAT: Theory and model testing». In: *Ecol. Modelling 222(12)* (2011), pp. 1913–1921 (cit. on p. 22).

[40] W. H. Green and G. A. Ampt. «Studies on soil physics: 1. The flow of air and water through soils». In: *J. Agric. Sci. 4(1)* (1911), pp. 11–24 (cit. on p. 22).

[41] M. Kalcic, I. Chaubey, and J. Frankenberger. «Defining Soil and Water Assessment Tool (SWAT) Hydrologic Response Units (HRUs) by Field Boundaries». In: *International Journal of Agricultural and Biological Engineering* (2015), pp. 69–80 (cit. on p. 23).

[42] Evgenia Koltsida, Nikos Mamassis, and Andreas Kallioras. «Hydrological modeling using the SWAT Model in urban and peri-urban environments: The case of Kifissos experimental sub-basin (Athens, Greece)». In: (Oct. 2021). DOI: 10.5194/hess-2021-482 (cit. on pp. 23, 68, 74, 111).

[43] United States Department of Agriculture. *Urban hydrology for small watersheds*. Technical Release 55 (TR-55) (Second ed.) Natural Resources Conservation Service, Conservation Engineering Division, 1986 (cit. on pp. 26, 68).

[44] S. Soil Conservation Service. «National Engineering Handbook». In: Washington DC, USA: Hydrology, Department of Agriculture, 1972. Chap. 4 (cit. on p. 26).

[45] MeinR.G. and C. L. Larson. «Modeling Infiltration during a Steady Rain». In: *Water Resour. Res.* (1973), pp. 384–394 (cit. on p. 26).

[46] J. R. Williams and H. D. Berndt. «Sediment yield prediction based on watershed hydrology». In: *Trans. ASAE 20(6)* (1977), pp. 1100–1104 (cit. on p. 27).

[47] J. R. Williams and R. W. Hans. «HYMO, a problem-oriented computer language for building hydrologic models». In: *Water Resour. Res. 8(1)* (1973), pp. 79–85 (cit. on p. 27).

[48] Y. T. Dile, P. Daggupati, C. George, R. Srinivasan, and J. G. Arnold. «Introducing a new open source GIS user interface for the SWAT model». In: *Environmental Modelling Software* (2016), pp. 129–138 (cit. on p. 28).

[49] Y. Dile, R. Srinivasan, and C. George. *QGIS Interface for SWAT+: QSWAT+*. 2022 (cit. on pp. 28, 29, 33, 35, 36).

[50] I. Kakarndee and E. Kositsakulchai. «Comparison between SWAT and SWAT+ for simulating streamflow in a paddy-field-dominated basin, northeast Thailand». In: *E3S Web of Conferences 187, 06002* (2020) (cit. on p. 28).

[51] *SWAT+ Documentation, Watershed Configuration: Spatial Objects*. Texas AM University. URL: `https://swatplus.gitbook.io/io-docs/` (cit. on pp. 28, 29).

[52] M. M. Kalcic, I. Chaubey, and J. Frankenberger. «Defining Soil and Water Assessment Tool (SWAT) hydrologic response units (HRUs) by field boundaries». In: *Int J Agric Biol Eng 8(3)* (2015), pp. 69–80 (cit. on p. 33).

[53] Michael J. White et al. «Development of a Field Scale SWAT+ Modeling Framework for the Contiguous U.S.» In: *JAWRA Journal of the American Water Resources Association* 58.6 (2022), pp. 1545–1560. DOI: `https://doi.org/10.1111/1752-1688.13056`. eprint: `https://onlinelibrary.wiley.com/doi/pdf/10.1111/1752-1688.13056`. URL: `https://onlinelibrary.wiley.com/doi/abs/10.1111/1752-1688.13056` (cit. on p. 33).

[54] United States Department of Agriculture, Natural Resources Conservation Service, and National Soil Survey Center. *Soil Survey Geographic (SSURGO) Data Base: Data Use Information*. 1995 (cit. on p. 35).

[55] J. G. Arnold, J. R. Kiniry, R. Srinivasan, J. R. Williams, Haney E. B., and S. L. Neitsch. *Soil and Water Assessment Tool: Input/Output Documentation*. Ed. by Soil Grassland and Water Research Laboratory - Agricultural Research Service - Blackland Research Center - Texas AgriLife Research. Version 2012. College Station, Texas 77843-2118: Texas Water Resources Institute - Texas AM University System (cit. on pp. 39, 47, 67, 69, 72).

[56] *SWAT+ Editor Documentation, Climate*. Texas AM University. URL: https://swatplus.gitbook.io/docs/user/editor/inputs/climate (cit. on pp. 40, 41).

[57] K. K. Yilmaz, J. A. Vrugt, H. V. Gupta, and S. Sorooshian. «Model Calibration in Watershed Hydrology». In: *NASA Technical Reports Server (NTRS)* (2009) (cit. on p. 42).

[58] K.C. Abbaspour, E. Rouholahnejad, S. Vaghefi, R. Srinivasan, H. Yang, and B. Kløve. «A continental-scale hydrology and water quality model for Europe: Calibration and uncertainty of a high-resolution large-scale SWAT model». In: *Journal of Hydrology* 524 (2015), pp. 733–752. ISSN: 0022-1694. DOI: https://doi.org/10.1016/j.jhydrol.2015.03.027. URL: https://www.sciencedirect.com/science/article/pii/S0022169415001985 (cit. on pp. 42, 69).

[59] I. W. Jung. «Comparison of global optimization approaches for robust calibration of hydrologic model parameters». In: *AGU Fall Meeting Abstracts*. Dec. 2015, GC53B-1205 (cit. on p. 42).

[60] A. Donigian Jr. «Watershed Model Calibration and Validation: The HSPF Experience». In: *Proceedings of the Water Environment Federation* (Jan. 2002), pp. 44–73. DOI: 10.2175/193864702785071796 (cit. on p. 42).

[61] A. Van Griensven and W. Bauwens. «Application and evaluation of ESWAT on the Dender basin and the Wister Lake basin». In: *Hydrological Processes* 19.3 (2005), pp. 827–838. DOI: https://doi.org/10.1002/hyp.5614. eprint: https://onlinelibrary.wiley.com/doi/pdf/10.1002/hyp.5614. URL: https://onlinelibrary.wiley.com/doi/abs/10.1002/hyp.5614 (cit. on p. 42).

[62] R. K. Goktas, U. Tezel, P. G. Kargi, T. Ayvaz, I. Tezyapar, B. Mesta, and E. Kentel. «Effect of Using Extreme Years in Hydrologic Model Calibration Performance». In: *AGU Fall Meeting Abstracts*. Vol. 2017. Dec. 2017, H43B-1620, H43B–1620 (cit. on p. 43).

[63] Bernard Engel, Dan Storm, Mike White, Jeff Arnold, and Mazdak Arabi. «A Hydrologic/Water Quality Model Applicati11». In: *JAWRA Journal of the American Water Resources Association* 43.5 (2007), pp. 1223–1236. DOI: https://doi.org/10.1111/j.1752-1688.2007.00105.x. eprint: https://onlinelibrary.wiley.com/doi/pdf/10.1111/j.1752-1688.2007.00105.x. URL: https://onlinelibrary.wiley.com/doi/abs/10.1111/j.1752-1688.2007.00105.x (cit. on pp. 43, 44).

[64] C. Santhi, J. G. Arnold, J. R. Williams, W. A. Dugas, R. Srinivasan, and L. M. Hauck. «VALIDATION OF THE SWAT MODEL ON A LARGE RWER BASIN WITH POINT AND NONPOINT SOURCES1». In: *JAWRA Journal of the American Water Resources Association* 37.5 (2001), pp. 1169–1188. DOI: https://doi.org/10.1111/j.1752-1688.2001.tb03630.x. eprint: https://onlinelibrary.wiley.com/doi/pdf/10.1111/j.1752-1688.2001.tb03630.x. URL: https://onlinelibrary.wiley.com/doi/abs/10.1111/j.1752-1688.2001.tb03630.x (cit. on p. 43).

[65] Thian Yew Gan, Enoch M. Dlamini, and Getu Fana Biftu. «Effects of model complexity and structure, data quality, and objective functions on hydrologic modeling». In: *Journal of Hydrology* 192.1 (1997), pp. 81–103. ISSN: 0022-1694. DOI: https://doi.org/10.1016/S0022-1694(96)03114-9. URL: https://www.sciencedirect.com/science/article/pii/S0022169496031149 (cit. on p. 43).

[66] Michael W. Van Liew and Jurgen Garbrecht. «HYDROLOGIC SIMULATION OF THE LITTLE WASHITA RIVER EXPERIMENTAL WATERSHED USING SWAT1». In: *JAWRA Journal of the American Water Resources Association* 39.2 (2003), pp. 413–426. DOI: https://doi.org/10.1111/j.1752-1688.2003.tb04395.x. eprint: https://onlinelibrary.wiley.com/doi/pdf/10.1111/j.1752-1688.2003.tb04395.x. URL: https://onlinelibrary.wiley.com/doi/abs/10.1111/j.1752-1688.2003.tb04395.x (cit. on p. 43).

[67] *Climate and Average Weather Year Round in Helsinki*. Weather Spark. URL: https://weatherspark.com/y/91632/Average-Weather-in-Helsinki-Finland-Year-Round (cit. on p. 44).

[68] C. J. Chawanda. *SWAT+ Toolbox User Manual*. 2021 (cit. on pp. 45, 52–54, 109).

[69] Giuseppe Pulighe, Flavio Lupia, Huajin Chen, and Hailong Yin. «Modeling Climate Change Impacts on Water Balance of a Mediterranean Watershed Using SWAT+». In: *Hydrology* 8.4 (2021). ISSN: 2306-5338. DOI: 10.3390/hydrology8040157. URL: https://www.mdpi.com/2306-5338/8/4/157 (cit. on p. 45).

[70] Kue Bum Kim, Hyun-Han Kwon, and Dawei Han. «Exploration of warm-up period in conceptual hydrological modelling». In: *Journal of Hydrology* 556 (2018), pp. 194–210. ISSN: 0022-1694. DOI: https://doi.org/10.1016/j.jhydrol.2017.11.015. URL: https://www.sciencedirect.com/science/article/pii/S0022169417307692 (cit. on pp. 45, 46).

[71] Donizete Pereira, Andre Almeida, Mauro Aparecido, and David. «Impacts of deforestation on water balance components of a watershed on the Brazilian East Coast». In: *Revista Brasileira de Ciência do Solo* 38 (Sept. 2014), pp. 1350–1358. DOI: 10.1590/S0100-06832014000400030 (cit. on p. 46).

[72] K. C. Abbaspour. *SWAT-CUP: SWAT Calibration and Uncertainty Programs - A User Manual*. 2015 (cit. on p. 47).

[73] Jalel Aouissi, Sihem Benabdallah, Zohra Lili Chabaâne, and Christophe Cudennec. «Evaluation of potential evapotranspiration assessment methods for hydrological modelling with SWAT—Application in data-scarce rural Tunisia». In: *Agricultural Water Management* 174 (2016). Sustainable Water Resources Management: Theory and Case Studies Part I Overseen by: Dr. Brent Clothier, pp. 39–51. ISSN: 0378-3774. DOI: https://doi.org/10.1016/j.agwat.2016.03.004. URL: https://www.sciencedirect.com/science/article/pii/S0378377416300804 (cit. on pp. 47, 48).

[74] John L Monteith. «Evaporation and environment». In: *Symposia of the society for experimental biology*. Vol. 19. Cambridge University Press (CUP) Cambridge. 1965, pp. 205–234 (cit. on p. 47).

[75] Richard G. Allen et al. «A recommendation on standardized surface resistance for hourly calculation of reference ETo by the FAO56 Penman-Monteith method». In: *Agricultural Water Management* 81.1 (2006), pp. 1–22. ISSN: 0378-3774. DOI: https://doi.org/10.1016/j.agwat.2005.03.007. URL: https://www.sciencedirect.com/science/article/pii/S037837740500154X (cit. on p. 47).

[76] George Hargreaves and Zohrab Samani. «Reference Crop Evapotranspiration From Temperature». In: *Applied Engineering in Agriculture* 1 (Jan. 1985). DOI: 10.13031/2013.26773 (cit. on p. 47).

[77] L. Briley. *Configuring and Running the SWAT Model*. 2010. URL: https://swat.tamu.edu/media/116389/swatsetup.pdf (cit. on p. 48).

[78] Ashutosh Pati, Sumit Sen, and Muthiah Perumal. «Modified Channel-Routing Scheme for SWAT Model». In: *Journal of Hydrologic Engineering* 23 (June 2018). DOI: 10.1061/(ASCE)HE.1943-5584.0001657 (cit. on p. 48).

[79] S. Tarantola A. Saltelli and K. P.-S. Chan. «A Quantitative Model-Independent Method for Global Sensitivity Analysis of Model Output». In: *Technometrics* 41.1 (1999), pp. 39–56. DOI: 10.1080/00401706.1999.10485594. eprint: https://www.tandfonline.com/doi/pdf/10.1080/00401706.1999.10485594. URL: https://www.tandfonline.com/doi/abs/10.1080/00401706.1999.10485594 (cit. on p. 54).

[80] Ilya M. Sobol. «Sensitivity Estimates for Nonlinear Mathematical Models». In: 1993. URL: https://api.semanticscholar.org/CorpusID:115460399 (cit. on p. 54).

[81] X. Y. Zhang, M. N. Trame, L. J. Lesko, and S. Schmidt. «Sobol Sensitivity Analysis: A Tool to Guide the Development and Evaluation of Systems Pharmacology Models». In: *CPT: pharmacometrics systems pharmacology* 4(2) (Feb. 2015), pp. 69–79. DOI: 10.1002/psp4.6 (cit. on pp. 54–57).

[82] I. M. Sobol. «On sensitivity estimation for nonlinear mathematical models». In: *Matem. Mod.* 2 (1990), pp. 112–118 (cit. on p. 54).

[83] Liu D., Li L., Rostami-Hodjegan A., Bois F. Y., and Jamei M. «Considerations and Caveats when Applying Global Sensitivity Analysis Methods to Physiologically Based Pharmacokinetic Models». In: *The AAPS journal* 22(5) (July 2020), p. 93. DOI: 10.1208/s12248-020-00480-x (cit. on p. 54).

[84] I. M. Sobol. «Distribution of points in a cube and approximate evaluation of integrals». In: *U.S.S.R Comput. Maths. Math. Phys.* 7 (1967), pp. 86–112 (cit. on p. 55).

[85] Ishaan Dalal, Deian Stefan, and Jared Harwayne-Gidansky. «Low Discrepancy Sequences for Monte Carlo Simulations on Reconfigurable Platforms». In: Aug. 2008, pp. 108–113. ISBN: 978-1-4244-1897-8. DOI: 10.1109/ASAP.2008.4580163 (cit. on p. 55).

[86] C. Xu and G. Gertner. «Understanding and comparisons of different sampling approaches for the Fourier Amplitudes Sensitivity Test (FAST)». In: *Computational statistics data analysis* 55(1) (2011), pp. 184–198. DOI: 10.1016/j.csda.2010.06.028 (cit. on pp. 55, 56).

[87] Chonggang Xu and George Zdzislaw Gertner. «A general first-order global sensitivity analysis method». In: *Reliability Engineering System Safety* 93.7 (2008). Bayesian Networks in Dependability, pp. 1060–1071. ISSN: 0951-8320. DOI: https://doi.org/10.1016/j.ress.2007.04.001. URL: https://www.sciencedirect.com/science/article/pii/S0951832007001342 (cit. on p. 55).

[88] Thomas Henkel, Heike Wilson, and Wilfried Krug. «Global sensitivity analysis of nonlinear mathematical models — An implementation of two complementing variance-based algorithms». In: *Proceedings of the 2012 Winter Simulation Conference (WSC)*. 2012, pp. 1–12. DOI: 10.1109/WSC.2012.6465065 (cit. on p. 55).

[89] Bo Gao, Qiang Yang, Zujun Peng, Weihua Xie, Hua Jin, and Songhe Meng. «A direct random sampling method for the Fourier amplitude sensitivity test of nonuniformly distributed uncertainty inputs and its application in C/C nozzles». In: *Aerospace Science and Technology* 100 (2020), p. 105830. ISSN: 1270-9638. DOI: https://doi.org/10.1016/j.ast.2020.105830. URL: https://www.sciencedirect.com/science/article/pii/S1270963819320784 (cit. on p. 55).

[90] Thierry Alex Mara. «Extension of the RBD-FAST method to the computation of global sensitivity indices». In: *Reliability Engineering System Safety* 94.8 (2009), pp. 1274–1281. ISSN: 0951-8320. DOI: https://doi.org/10.1016/j.ress.2009.01.012. URL: https://www.sciencedirect.com/science/article/pii/S095183200900026X (cit. on p. 56).

[91] Thierry A. Mara Stefano Tarantola Debora Gatelli. «Random balance designs for the estimation of first order global sensitivity indices». In: *Reliability Engineering and System Safety* 91 (6) (2006), pp. 717–727. DOI: 10.1016/j.ress.2005.06.003 (cit. on p. 56).

[92] Anqi Wang and Dimitri P. Solomatine. «Practical Experience of Sensitivity Analysis: Comparing Six Methods, on Three Hydrological Models, with Three Performance Criteria». In: *Water* 11.5 (2019). ISSN: 2073-4441. DOI: 10.3390/w11051062. URL: https://www.mdpi.com/2073-4441/11/5/1062 (cit. on p. 56).

[93] Yanjun Gan, Qingyun Duan, Wei Gong, Charles Tong, Yunwei Sun, Wei Chu, Aizhong Ye, Chiyuan Miao, and Zhenhua Di. «A comprehensive evaluation of various sensitivity analysis methods: A case study with a hydrological model». In: *Environmental Modelling Software* 51 (2014), pp. 269–285. ISSN: 1364-8152. DOI: https://doi.org/10.1016/j.envsoft.2013.09.031. URL: https://www.sciencedirect.com/science/article/pii/S1364815213002338 (cit. on pp. 56, 57, 70).

[94] E. Ryan, O. Wild, A. Voulgarakis, and L. Lee. «Fast sensitivity analysis methods for computationally expensive models with multi-dimensional output». In: *Geoscientific Model Development* 11.8 (2018), pp. 3131–3146. DOI: 10.5194/gmd-11-3131-2018. URL: https://gmd.copernicus.org/articles/11/3131/2018/ (cit. on p. 56).

[95] Maysoun Ayad Hameed. *Evaluating Global Sensitivity Analysis Methods for Hydrologic Modeling over the Columbia River Basin*. 2015 (cit. on p. 56).

[96] R. Confalonieri, G. Bellocchi, S. Bregaglio, M. Donatelli, and M. Acutis. «Comparison of sensitivity analysis techniques: A case study with the rice model WARM». In: *Ecological Modelling* 221.16 (2010), pp. 1897–1906. ISSN: 0304-3800. DOI: https://doi.org/10.1016/j.ecolmodel.2010.04.

021. URL: https://www.sciencedirect.com/science/article/pii/S0304380010002371 (cit. on p. 56).

[97] Wei P., Lu Z., and Song J. «Moment-independent sensitivity analysis using copula». In: *Risk analysis : an official publication of the Society for Risk Analysis* 34(2) (Feb. 2014), pp. 210–22. DOI: 10.1111/risa.12110 (cit. on p. 56).

[98] *Delta Moment-Independent Method*. GlobalSensitivity.jl. URL: https://docs.sciml.ai/GlobalSensitivity/dev/methods/delta/ (cit. on p. 56).

[99] Chris Turnadge, Dirk Mallants, and L. Peeters. «Sensitivity and uncertainty analysis of a regional-scale groundwater flow model featuring coal seam gas extraction». In: (Mar. 2018). DOI: 10.13140/RG.2.2.16198.37443 (cit. on p. 56).

[100] Richard McCuen, Zachary Knight, and A. Cutter. «Evaluation of the Nash–Sutcliffe Efficiency Index». In: *Journal of Hydrologic Engineering - J HYDROL ENG* 11 (Nov. 2006). DOI: 10.1061/(ASCE)1084-0699(2006)11:6(597) (cit. on p. 59).

[101] J.E. Nash and J.V. Sutcliffe. «River flow forecasting through conceptual models part I — A discussion of principles». In: *Journal of Hydrology* 10.3 (1970), pp. 282–290. ISSN: 0022-1694. DOI: https://doi.org/10.1016/0022-1694(70)90255-6. URL: https://www.sciencedirect.com/science/article/pii/0022169470902556 (cit. on p. 59).

[102] L. Duc and Y. Sawada. «A signal-processing-based interpretation of the Nash–Sutcliffe efficiency». In: *Hydrology and Earth System Sciences* 27.9 (2023), pp. 1827–1839. DOI: 10.5194/hess-27-1827-2023. URL: https://hess.copernicus.org/articles/27/1827/2023/ (cit. on p. 59).

[103] Daniel Moriasi, Jeff Arnold, Michael Van Liew, Ron Bingner, R.D. Harmel, and Tamie Veith. «Model Evaluation Guidelines for Systematic Quantification of Accuracy in Watershed Simulations». In: *Transactions of the ASABE* 50 (May 2007). DOI: 10.13031/2013.23153 (cit. on p. 60).

[104] Eric Servat and Alain Dezetter. «Selection of Calibration Objective Functions in the Context of Rainfall-Runoff Modeling in a Sudanese Savannah Area». In: *Hydrological Sciences Journal* 36 (Aug. 1991), pp. 307–330. DOI: 10.1080/02626669109492517 (cit. on p. 60).

[105] J. Frost. *Root Mean Square Error (RMSE)*. Statistics By Jim. URL: https://statisticsbyjim.com/regression/root-mean-square-error-rmse/ (cit. on p. 60).

[106] Robert Pontius, Olufunmilayo Thontteh, and Hao Chen. «Components of information for multiple resolution comparison between maps that share a real variable». In: *Environmental and Ecological Statistics* 15 (June 2008), pp. 111–142. DOI: 10.1007/s10651-007-0043-y (cit. on p. 60).

[107] C. Willmott and K Matsuura. «On the use of dimensioned measures of error to evaluate the performance of spatial interpolators». In: *International Journal of Geographical Information Science* 20 (Jan. 2006). DOI: 10.1080/13658810500286976 (cit. on p. 60).

[108] Hoshin Gupta, Soroosh Sorooshian, and Patrice Yapo. «Status of Automatic Calibration for Hydrologic Models: Comparison With Multilevel Expert Calibration». In: *Journal of Hydrologic Engineering - J HYDROL ENG* 4 (Apr. 1999). DOI: 10.1061/(ASCE)1084-0699(1999)4:2(135) (cit. on p. 60).

[109] Matthew Smith, Amy Then, Catarina Wor, Gina Ralph, Kenneth Pollock, and John Hoenig. «Recommendations for Catch-Curve Analysis». In: *North American Journal of Fisheries Management* 32 (Aug. 2012). DOI: 10.1080/02755947.2012.711270 (cit. on pp. 60, 61).

[110] Yun Wu, Junfeng Liu, and Dingfang Li. «Chaotic Dynamically Dimensioned Search Algorithm». In: *IEEE Access* 8 (2020), pp. 152474–152499. DOI: 10.1109/ACCESS.2020.3017210 (cit. on p. 61).

[111] Bryan Tolson and Christine Shoemaker. «Dynamically Dimensioned Search Algorithm for Computationally Efficient Watershed Model Calibration». In: *Water Resources Research - WATER RESOUR RES* 43 (Jan. 2007). DOI: 10.1029/2005WR004723 (cit. on p. 61).

[112] B. A. Tolson and C. A. Shoemaker. «The Dynamically Dimensioned Search (DDS) Algorithm as a Robust Optimization Tool in Hydrologic Modeling». In: *AGU Fall Meeting Abstracts*. Vol. 2006. Dec. 2006, H41I-07, H41I–07 (cit. on pp. 61, 62).

[113] Ali Behrangi, Behnaz Khakbaz, Jasper Vrugt, Qingyun Duan, and Soroosh Sorooshian. «Comment on 'Dynamically Dimensioned Search Algorithm for Computationally Efficient Watershed Model Calibration' by Bryan A. Tolson and Christine A. Shoemaker». In: *Water Resources Research - WATER RESOUR RES* 44 (Dec. 2008). DOI: 10.1029/2007WR006429 (cit. on p. 61).

[114] Youngkyu Jin, Sangho Lee, Taeuk Kang, and Yeulwoo Kim. «A Dynamically Dimensioned Search Allowing a Flexible Search Range and Its Application to Optimize Discrete Hedging Rule Curves». In: *Water* 14.22 (2022). ISSN: 2073-4441. DOI: 10.3390/w14223633. URL: https://www.mdpi.com/2073-4441/14/22/3633 (cit. on pp. 61, 62).

[115] Richard Arsenault, Annie Poulin, Pascal Côté, and François Brissette. «A Comparison of Stochastic Optimization Algorithms in Hydrological Model Calibration». In: *Journal of Hydrologic Engineering* 19 (July 2014), pp. 1374–1384. DOI: 10.1061/(ASCE)HE.1943-5584.0000938 (cit. on p. 62).

[116] C. Santhi, Jeff Arnold, J.R. Williams, W.A. Dugas, R. Srinivasan, and L.M. Hauck. «Validation of the SWAT Model on a Large River Basin with Point and Nonpoint Sources». In: *JAWRA Journal of the American Water Resources Association* 37 (Oct. 2001), pp. 1169–1188. DOI: 10.1111/j.1752-1688.2001.tb03630.x (cit. on pp. 65, 78).

[117] Michael Van Liew, T.L. Vieth, David Bosch, and Jeff Arnold. «Suitability of SWAT for the Conservation Effects Assessment Project: Comparison on USDA Agricultural Research Service Watersheds». In: *Journal of Hydrologic Engineering* 12 (Mar. 2007). DOI: 10.1061/(ASCE)1084-0699(2007)12:2(173) (cit. on pp. 65, 78, 81).

[118] Dejian Zhang, Qiaoyin Lin, Xingwei Chen, and Tian Chai. «Improved Curve Number Estimation in SWAT by Reflecting the Effect of Rainfall Intensity on Runoff Generation». In: *Water* 11.1 (2019). ISSN: 2073-4441. DOI: 10.3390/w11010163. URL: https://www.mdpi.com/2073-4441/11/1/163 (cit. on p. 68).

[119] Rafael Luiz Barboza de Andrade. «The Influence of Bulk Density on the Hydraulic Conductivity and Water Content-Matric Suction Relation of Two Soils». In: 1971. URL: https://api.semanticscholar.org/CorpusID:127735918 (cit. on p. 73).

[120] Ali Saleh, Jeff Arnold, Philip Gassman, L. Hauck, W. Rosenthal, J. Williams, and A. McFarland. «Application of SWAT for the Upper North Bosque Watershed». In: *Transactions of the ASAE* 43 (Sept. 2000), pp. 1077–1087. DOI: 10.13031/2013.3000 (cit. on pp. 78, 81).

[121] FISRWG (10/1998). *Stream Corridor Restoration: Principles, Processes, and Practices*. By the Federal Interagency Stream Restoration Working Group (FISRWG)(15 Federal agencies of the US gov't), 1998 (cit. on p. 93).

[122] Ville Lindgren, Joseph H. A. Guillaume, Timo A. Räsänen, Juho Jakkila, Noora Veijalainen, and Matti Kummu. «Spatiotemporal Hydroclimate Variability in Finland: Past Trends». In: *Journal of Hydrometeorology* 18.6 (2017), pp. 1765–1782. DOI: https://doi.org/10.1175/JHM-D-16-0278.1. URL: https://journals.ametsoc.org/view/journals/hydr/18/6/jhm-d-16-0278_1.xml (cit. on pp. 102, 103).

[123] *Hydrological maps: Runoff*. Finnish Environmental Institute (SYKE). URL: https://wwwi2.ymparisto.fi/i2/90/qrxx2/tanaan_en.html (cit. on p. 104).

[124] *Hydrology*. Finnish Environmental Institute (SYKE). URL: https://www.syke.fi/download/noname/%7B69BE771C-C841-4D7E-8515-BD0E8CC8E1D6%7D/135960 (cit. on p. 105).